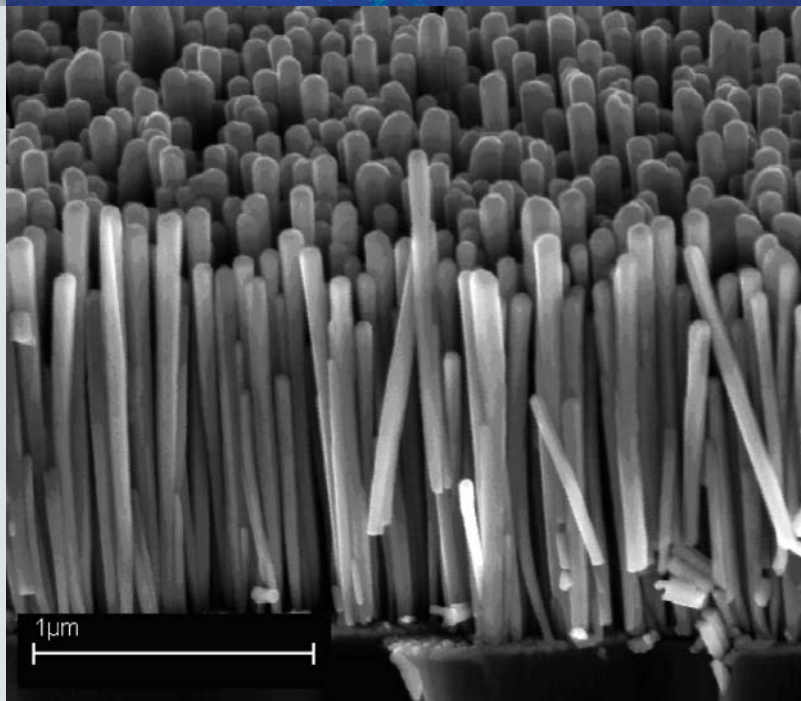
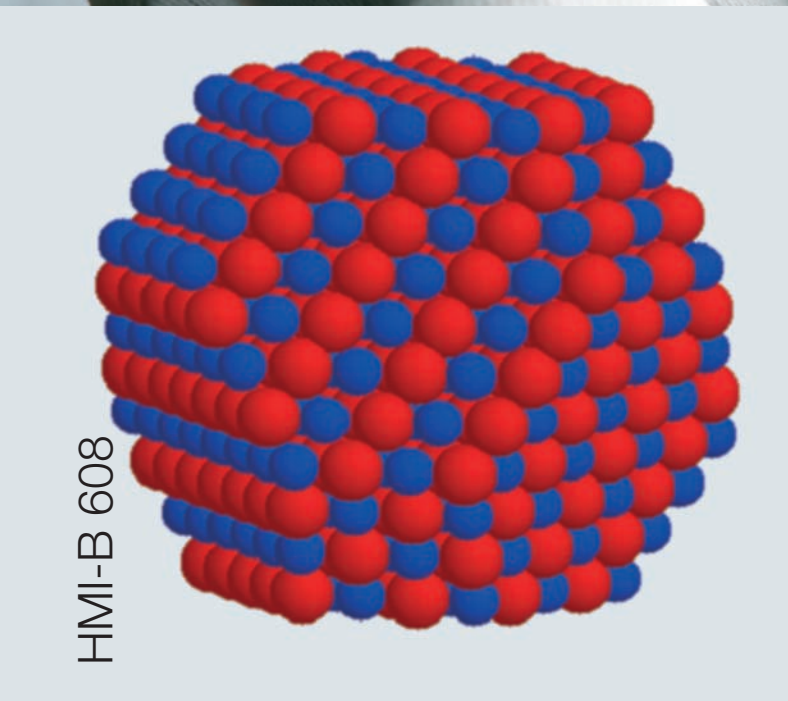
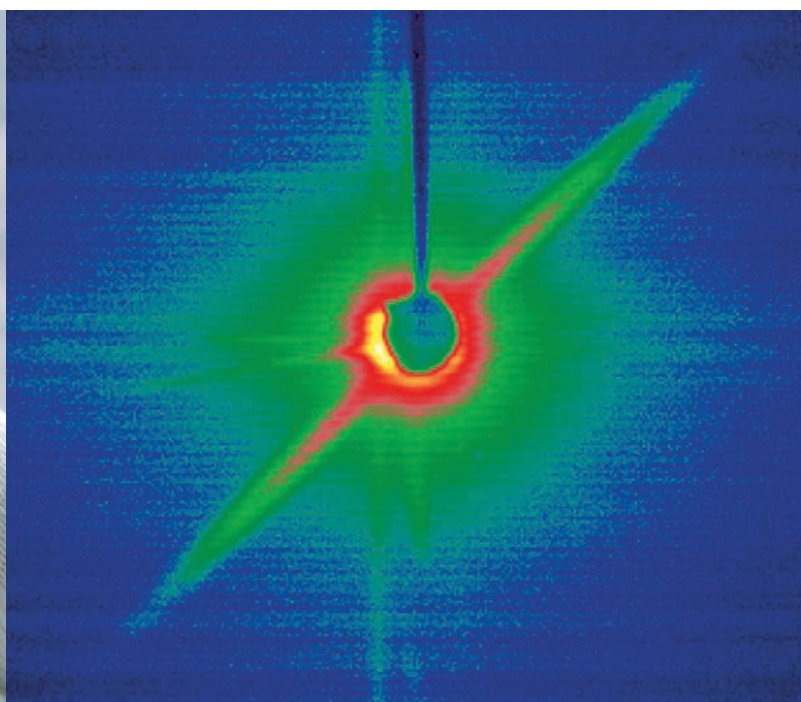
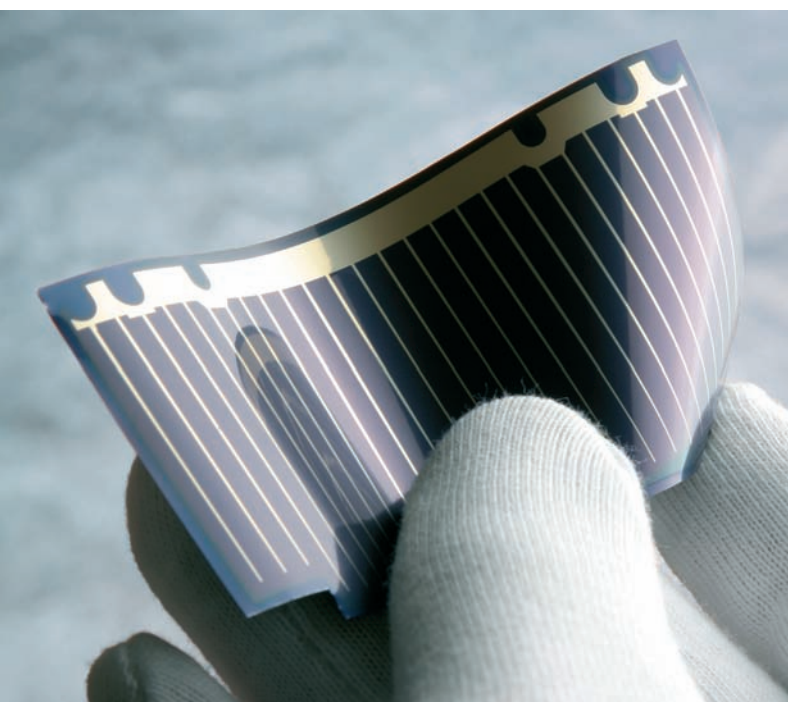


# Annual Report 2005

## Selected Results



HMI-B 608

**Legend to Cover Figures:**

- top left:** Flexible solar cell developed at the Hahn-Meitner-Institut
- top right:** SAXS (Small Angle X-Ray Scattering) image of glass with nano-sized silver clusters induced by ion irradiation
- bottom left:** Snapshots of an ordered 807-atom (around 2.5 nm size) platinum/cobalt nano-particle (blue spheres stand for cobalt atoms and red spheres for platinum). These particles have been investigated at a HMI beamline at the synchrotron source BESSY.
- bottom right:** ZnO-Nanorods grown on Sapphire/ZnO-Substrate

# Annual Report 2005

## Selected Results

Hahn-Meitner-Institut  
Berlin, 2006

# Table of contents

4	<b>Foreword</b>
6	<b>HMI in brief</b>
8	<b>News and Events 2005</b>
10	■ <b>People</b>
10	■ Dr. Ulrich Breuer becomes new administrative director of the Hahn-Meitner-Institut
11	■ Bella Lake becomes head of junior research group at the Hahn-Meitner-Institut
12	■ <b>New Neutron Guide Hall II</b>
14	■ <b>Meetings and Workshops</b>
14	■ Meetings and Conferences
15	■ First International Summer Academy on Photovoltaics
16	■ PIANO 05: French-German Summer School on Physics with ions
17	■ Discussing novel instrumentation
18	■ <b>Events</b>
18	■ Insights for the public: The Hahn-Meitner-Institut participated in the annual <i>Lange Nacht der Wissenschaften</i>
20	■ The school lab is in town
21	■ PhD students meet at the Hahn-Meitner-Institut
22	■ <b>Cooperations</b>
22	■ New partner for neutron autoradiography
22	■ Theory and experiment – a really interdisciplinary cooperation within the Helmholtz Association
23	■ Virtual institute to solve real problems
24	■ <b>Technology Transfer</b>
24	■ From laboratory to production – research meets market
25	■ Information day for the industry
26	■ <b>New Instruments</b>
26	■ The new neutron tomography instrument
28	■ First experiments using the new Small Angle X-ray Scattering Instrument at BESSY
29	■ The new 7 T high-field end station at the UE46-PGM beamline – a unique instrument for magnetic studies of ultrathin films and nanostructures
30	<b>User Service</b>
32	■ BENSCH Operation
35	■ NAA Laboratory and Irradiation Service at BER II
36	■ ISL Operations and Developments
38	<b>Scientific highlights Structural Research 2005</b>
40	■ <b>BENSCH User Service</b>
40	■ X-rays help find out how parts of historic organs were made
42	■ Magnetic field-induced antiferromagnetism in a cuprate high-temperature superconductor
44	■ Neutron diffraction studies of $R_2Fe_{17}$ (R=Y, Lu) intermetallics under pressure

46	■ NAA User Service
46	■ Use of arsenic isotopes for molecular imaging and endoradiotherapy
48	■ SF1 Methods and Instruments
48	■ Where are the limits of non-exponential relaxation?
50	■ Time scale of nuclear fission: fast or slow?
52	■ SF2 Magnetism
52	■ Probing magnetic complexity in cobalt nanoparticles
54	■ Climbing spin spirals: towards new magneto-electric materials
56	■ SF3 Materials
56	■ Characterization of Precipitates in Inconel 706 Superalloys by Three-Dimensional Atom Probe and Transmission Electron Microscopy
58	■ Stroboscopic neutron scattering investigations of dynamics in nanosized magnetic systems
60	■ SF4 Structure and Dynamics
60	■ Characterization of ion-beam induced nano-sized silver clusters in glass with synchrotron radiation
62	■ SF5 Theoretical Physics
62	■ Stochasticity in life: How microscopic fluctuations determine global behaviour of cells
64	■ SF6 Molecular Trace Element Research in the Life Sciences
64	■ The biological role of arsenic in the rat. Combined studies using tracer technique and biochemical methods.
66	■ Scientific highlights Solar Energy Research 2005
68	■ SE1 Silicon Photovoltaics
68	■ Origin of preferential (100) orientation of poly-Si films made by aluminium-induced layer-exchange process
70	■ Structural defects in crystalline silicon epitaxially grown at temperatures below 600°C
72	■ SE2 Heterogeneous Material Systems
72	■ Progress in Taking the CdS Layer out of Thin-Film Polycrystalline CuInS <sub>2</sub> Solar Cells
74	■ Optimising the interface between zinc-phthalocyanine films and the transparent indium-tin oxide anode in organic solar cells
76	■ On the CuGaSe <sub>2</sub> - CuGa <sub>3</sub> Se <sub>5</sub> solid state transition in CCSVT-grown CuGa <sub>x</sub> Se <sub>y</sub> thin films
78	■ SE3 Technology
78	■ Studying interdiffusion of CuInS <sub>2</sub> and CuGaS <sub>2</sub> by <i>in situ</i> diffraction
80	■ A flexible, Cu(In,Ga)Se <sub>2</sub> based, thin film solar cell module
82	■ SE4 Dynamics of Interfacial Reactions
82	■ Low band gap InP-based multi-junction solar cells
84	■ Binding geometry of phosphonic and carboxylic acid groups on rutile TiO <sub>2</sub>
86	■ Ultrafast electron transfer via a bridge-extended donor orbital
88	■ SE5 Solar Energetics
88	■ Photocurrent injection into TiO <sub>2</sub> nano particles utilizing WS <sub>2</sub> quantum sheets
90	■ Surface passivation of MoS <sub>2</sub> or WSe <sub>2</sub> for optimised photoconversion efficiencies
92	■ SE6 Electronic Structure of Semiconductor Interfaces
92	■ Electronic structure of epitaxial ZnO thin films grown by MOMBE
94	■ Organizational Chart
95	■ Imprint

# Foreword

The Annual Report 2005 of the Hahn-Meitner-Institut presents selected results of research activities obtained in that year. These highlights were selected from a large number and were not only achieved by our in-house researchers, but also by our guest researchers and external users of the large-scale facilities or in close collaborations of HMI scientists and partner institutions.

The HMI as a member of the Helmholtz Association acts in the framework of the so-called programme-oriented funding, and since 2005, the entire research activities of the HMI are funded according to this new scheme. One has to emphasise that the HMI researchers have succeeded in adjusting to this new frame and also to continuing their research under these new conditions. The stronger networking has turned out to be very positive and the enhanced competition within the Helmholtz Association stimulates our scientists.

The research programme of the department Trace Elements (SF6), participating in the Helmholtz Programme *Environmental Health* and the HMI eye tumour therapy activities (so-called Precision Proton Therapy) of the department SF4, participating in the Helmholtz Programme *Cancer* of the Helmholtz Research Area *Health* had their midterm evaluations in 2005. In these surveys carried out by members of HMI's Scientific Council supported by external experts, both activities received excellent evaluations and comments. The official reports will be given in 2006.

Concerning our ambitious future project at the Berlin Neutron Scattering Center BENSCH, the High Field Magnet (the former N25T-Project) which should reach magnetic fields for neutron scattering experiments of 25 Tesla and above, a feasibility study has demonstrated that pure superconducting technology is not yet ready to provide higher fields than about 22 T even when high- $T_c$  superconductors are used. Therefore at the end of 2005, we have decided to redesign our project and plan a hybrid system consisting of a superconducting part as an outer coil and a resistive part as an inner coil and in addition, to apply for additional money at the Helmholtz Association due to higher costs of this most promising but more complicated system.\*

At HMI and in particular at BENSCH, the research and the development programme associated with the scientific user service for the international community at our large-scale facilities is very important. We are pleased that in 2005 the number of proposals applying for beam time at our BENSCH instruments increased again after the shut-down of the research reactor BER II in 2004 due to the implementation of the neutron guides in our new Neutron Guide Hall II. The installation of the neutron guides and choppers, the moving of the instruments and the new instrumentation in the Neutron Guide Hall II proceeded in 2005 as planned. In addition, we are proud that the HMI beam line behind the 7T-Wiggler at BESSY and

\*By the time of printing (July 2006), the funding of the High Field Magnet has been assured.

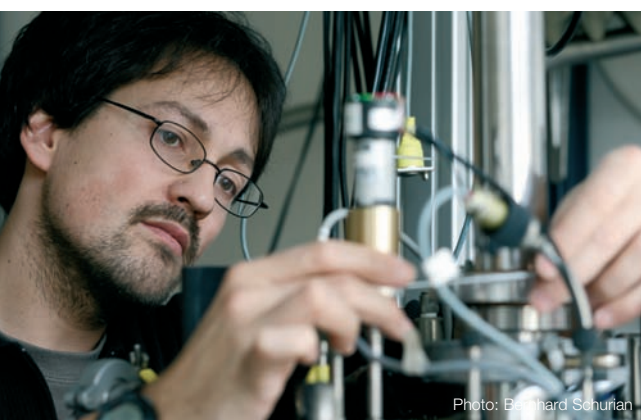


Photo: Bernhard Schurian

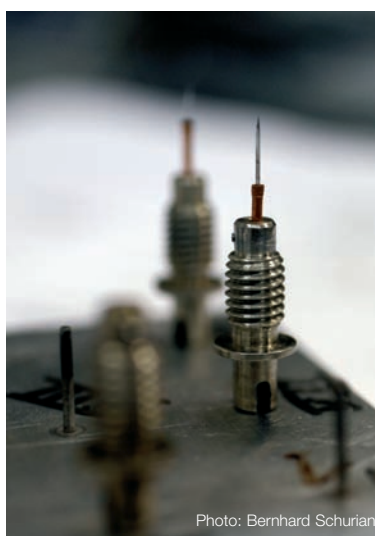


Photo: Bernhard Schurian



Photo: Peter Witt

the corresponding instruments are now available for external users. Since the 1st of May, 2005 after a half year commissioning phase, both the white beam instrument EDDI for energy dispersive diffraction and residual stress analysis and the monochromatic instrument MAGS for resonant magnetic scattering and high resolution diffraction offer excellent opportunities for synchrotron experiments in many cases complementary to those at neutron facilities. The number and wide spectrum of the received proposals in the first round confirmed the demand and the special concept of the chosen instrumentation. First experiments were already carried out successfully and provided evidence that also investigations with hard x-rays up to the 100 keV regime are possible. Herewith, through the HMI, Berlin is one of the few places worldwide where neutron and synchrotron radiation are in parallel available whereby the access is easy and well organised at BENSIC in the framework of a common portal.

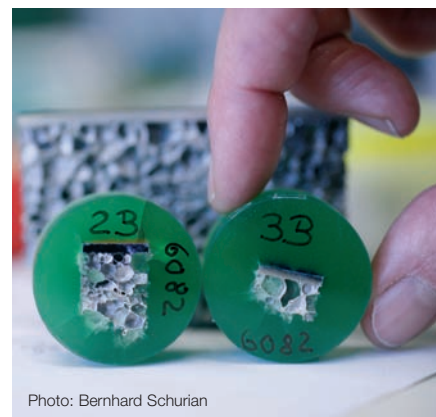
We are happy to announce that Dr. Bella Lake has joined the HMI. She will lead a so-called 'Helmholtz Young Investigators Group' and will become a Junior Professor at the Technical University Berlin (TU). The proposed projects address the understanding of high- $T_c$  superconductors, the investigation of exotic magnetism and non-equilibrium spin dynamics with its practical implications for functional devices. With her expertise we strengthen the area of magnetism and quantum phenomena at HMI and these research activities should play a significant role in fostering the cooperation with the TU Berlin.



HMI's scientific director Prof. Michael Steiner (left) and administrative director Dr. Ulrich Breuer

With this report we would like to commemorate and to impart a huge amount of successful activities and to thank the staff of the Hahn-Meitner-Institut, their collaboration partners and scientists from outside who have contributed to the results as a whole in 2005. Their motivation is most gratefully appreciated.

Thanks are also given to the funding authorities, the Federal Government, in particular to the Federal Ministry of Education and Research, the Senate of Berlin, the European Commission and all the other third party funding agencies for their continuing support.



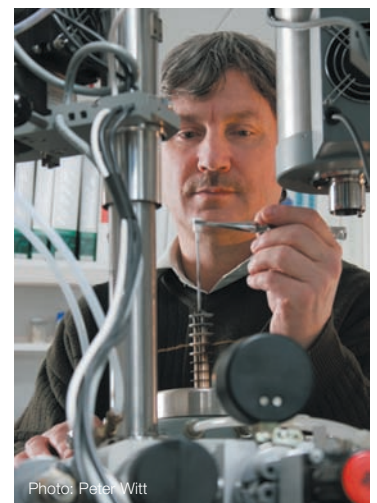
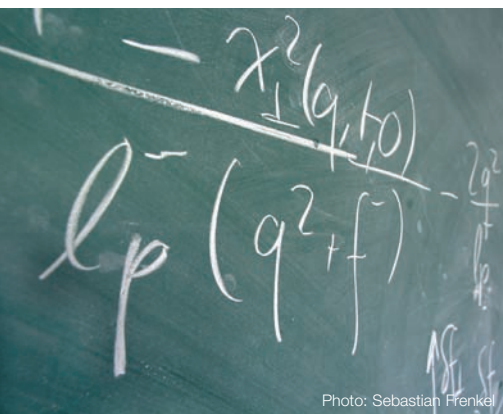
## HMI in brief

The Hahn-Meitner-Institut (HMI) in Berlin is one of Germany's leading centres for research on solar energy conversion, condensed matter and materials science. It has approximately 800 employees, including almost 300 scientists – most of them physicists and chemists. Most of the institute's annual budget of roughly 70 Million € is provided by the German Federal Government and the City of Berlin in a ratio of 9 to 1.

The Hahn-Meitner-Institut is member of the Helmholtz Association of National Research Centres, an organisation representing fifteen of Germany's largest scientific institutions. The common mission of the Helmholtz centres is to develop, set-up and operate large-scale facilities, to solve complex – often multidisciplinary – scientific and technological problems in long-term proactive research programmes and to develop high technologies for the future. The Helmholtz Association concentrates its work in six research fields: *Energy, Earth and Environment, Health, Structure of Matter, Transport and Space* and *Key Technologies*. For each of these fields, scientists develop several research programmes for 5-year periods. These programmes are then evaluated by a group of international experts. This evaluation forms the basis for the programme-oriented funding, which distributes the financial resources to the scientific programmes of the Helmholtz research fields rather than to the institutes.

Scientific work at the Hahn-Meitner-Institut is organised in two divisions reflecting the two main fields of activity: Solar Energy Research and Structural Research. The Solar Energy Research is part of the programme *Renewable Energies* within the research field *Energy*. Most of the activities of the Structural Research Division are part of the programme *Large-Scale Facilities for Research with Photons, Neutrons and Ions* in the research field *Structure of Matter*. The eye tumour therapy and the research on trace elements are conducted in the Helmholtz programmes *Cancer and Environmental Health* within the research field *Health*.

Solar energy research at the Hahn-Meitner-Institut is the largest effort in the field of sustainable energy within the Helmholtz Association and comprises approximately 25% of HMI's research and development efforts. As an interdisciplinary activity between solid state physics, material chemistry, optics and interfacial chemistry, it aims at creating scientific and technological preconditions for significantly increasing the contribution of sustainable energy to our energy supply over the next decades. This activity is taking advantage of an already well balanced research infrastructure and increasingly uses the unique measurement opportunities provided by the large scale facilities operated at the Hahn-Meitner-Institut.



At the centre of the solar energy research at HMI are materials and concepts for thin-film solar cells – activities covering the entire spectrum from basic research to the design of actual devices. The focus is on the currently most promising technologies, namely thin-film poly-crystalline silicon and compound semiconductors of the I-III-VI<sub>2</sub> and III-V type. Research projects aim at the development of efficient photo-voltaic solar cells which allow substantial reductions in the costs of solar power generation. The strategy is to develop existing thin-film technologies to a state of maturity and, in parallel, to explore new materials and concepts for solar cells of the future, e.g. nanocomposite crystalline materials.

Structural research at the Hahn-Meitner-Institut is focused on experimental investigations of structures and materials using neutrons and fast ions as probes. These two probes are provided by two in-house large-scale facilities sited on the institute's grounds in Berlin-Wannsee: The 10MW research reactor BER II with the Berlin Neutron Scattering Center BENSC and the accelerator complex of the Ion Beam Laboratory ISL. In addition to that, the Hahn-Meitner-Institut makes use of a third complementary probe – synchrotron radiation – by operating instruments at the 3<sup>rd</sup> generation electron storage ring BESSY, an independent research institution in Berlin-Adlershof.

All facilities are primarily operated for a national and international user community. About 70% of the beam time at the instruments is used by scientists from other research institutes, universities and industry from Germany and from abroad. It is HMI's policy to provide these users with full scale technical and scientific support, this way enabling them to make best possible use of the facilities. An outstanding highlight among the HMI activities are neutron scattering studies of samples in extreme sample environments such as very high magnetic fields and extremely low temperatures made possible by the institute's unique expertise on sample environment equipment. Fields in the focus of in-house structural research are magnetic phenomena, properties and design of engineering components and materials, soft matter and biological systems as well as theoretical physics.

At ISL, roughly a quarter of the beam time is used for the therapy of tumours in the human eye using 70MeV protons. The costs of the therapy are covered by the national health insurance companies.





During the Tutorial Session on Neutron Scattering

## News and Events 2005



## Dr. Ulrich Breuer becomes administrative director of the Hahn-Meitner-Institut



On July 1<sup>st</sup> 2005, Dr. Ulrich Breuer joined the Hahn-Meitner-Institut as the Institute's new administrative director.

A physicist by education, Ulrich Breuer began his transition from science into science administration whilst still working on his Ph.D. thesis at the Research Centre Jülich: He accepted the offer to become the assistant of the Chairman of the Board of Directors of the research Centre Joachim Treusch and started to work in this position in January 1991 – four months before his thesis defence. Although it was scientific work he was to administer in his new job and this way he remained true to science, Breuer remembers that he had to learn everything concerning the organizational and formal aspects of a scientific institute from scratch.

After four years in this position, Breuer changed his field of activity and replaced the retired head of the Public Relations department of the Research Centre devoting himself fulltime to presenting the science done at Jülich to a large public – an activity he had been working with even in his former position editing brochures and guiding groups of VIP visitors. In preparation for his new job, Breuer did an internship in the science department of the German quality daily *Frankfurter Allgemeine Zeitung* where he had the opportunity to learn the craft of science journalism by researching and writing several articles for the paper's science pages. Among the highlights of his time in the PR department were the celebrations of the 40 year anniversary of the Research Centre with an event that drew more than 40,000 visitors to the centre.

Although Breuer enjoyed working in PR, he felt that his mission was shaping things rather than only describing the work of

others. And he got his chance to influence developments when he became head of the Department *Scientific and Technical Planning* of the Research Centre Jülich in 2000. In this position, he was responsible for the overall long-term research and development planning at the research centre and held responsibilities for various international programmes. When the Helmholtz Association started the process towards developing the structure of the programme oriented funding, Breuer was on the main working groups and thus contributed to many aspects of the new Helmholtz structure.

Having spent 18 years at the Research Centre Jülich, Ulrich Breuer felt it was time for a change and a new challenge and so applied for the position at the Hahn-Meitner-Institut. He admits that being 44 years old he considered this to be the last opportunity for moving to a new place and starting anew – a big decision when taking into account that it would not only involve himself but also his wife and his three children.

What makes the new position at the Hahn-Meitner-Institut so attractive for him is the fact that – together with the scientific director – he is actually responsible for running the every day business of the institute and in this way can have a strong impact on the developments of the institute even beyond the administrative realm. Breuer sees that his main task is making sure that the Hahn-Meitner-Institut is well-positioned in the world-wide landscape of science. Part of this is developing a programme for the future development of the institute for the next 15–20 years and making the success of the institute visible in the scientific community, the public and among politicians. In his plans, Breuer puts a particular emphasis on activities connected to applications and names the founding of the company Sulfurcell as a particularly successful example.

But Breuer does not only feel responsible for the institute's development. Although he thinks that the organization of the institute is very good as nobody would let a badly organized institution run a reactor – he sees room for improvement in the administrative procedures, internal communication and some other fields. He wants to make sure that the administrative departments see themselves as service providers for the scientists and in the long run sees more financial independence for the two scientific divisions as an important goal.

However, it is not only the professional challenge, Breuer emphasizes, that makes moving to Berlin so attractive, it is also the chance to live in a city with a unique vibrant cultural life and he hopes to be able to benefit from it as much as possible. Having found a house for himself and his family on the outskirts of the town, he will be able to enjoy the city life and the surrounding landscape of Brandenburg where he plans to train for his next (short) triathlon.

## Bella Lake becomes head of young investigators group at the Hahn-Meitner-Institut

The English physicist Bella Lake has become head of the first young investigators group at the Hahn-Meitner-Institut and junior professor at the Technische Universität Berlin. Here, she is going to continue her successful work on investigating superconductivity and quantum magnetism by means of neutron scattering. In her new position, she can run her own research group and employ a PhD-student and a post-doc. The institution of young investigators groups has been introduced by the Helmholtz-Association as a way of enabling young researchers to work independently at an early stage in their career.

Bella Lake has been a frequent guest to the Hahn-Meitner-Institut in the past years, and she has performed numerous neutron scattering experiments using the institute's unique sample environment equipment. These experiments resulted in many remarkable results, some of them published in the journals *Nature* or *Nature Materials*. In the present issue of the *Hahn-Meitner-Institut Annual Report*, Bella Lake discusses the most recent results of her research on the role antiferromagnetism plays in making high temperature superconductivity stable against external magnetic fields (page 42).

Bella Lake was born and brought up in England. She studied physics at the University of Oxford and did her PhD there with a thesis on *Neutron scattering studies of alternating chain antiferromagnets*. After that, she worked at the University of Toronto (Canada), Risø National Laboratory (Roskilde, Denmark), Oak Ridge National Laboratory (Tennessee, U.S.A) and again at Oxford. During her time at Oxford, she held the prestigious Advanced Research Fellowship of the Engineering and Physical Sciences Research Council. Before coming to HMI she was assistant professor at Iowa State University in the USA.

Since September 22, 2005 Bella Lake has been working at the Hahn-Meitner-Institut, and she is not only happy about the excellent technical equipment but also praises the working conditions in general. "One has better opportunities to try out completely new experiments than at the larger neutron sources. Often, one does not have enough time there to make a novel set-up run. In that sense, one can do better science here." she says.



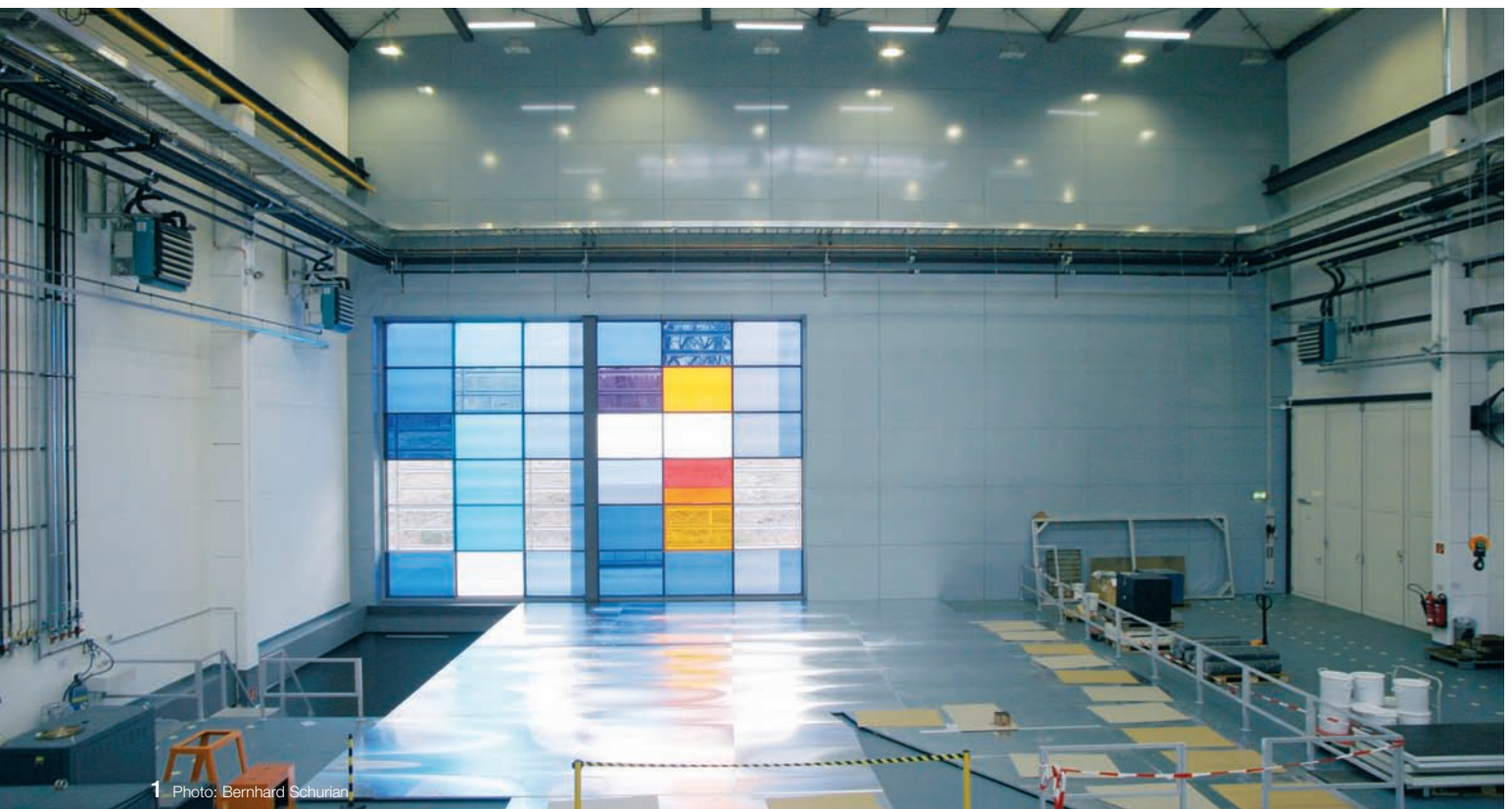
Photo: Bernhard Schurian

# News from the Instrumentation Project in Neutron Guide Hall II

By the end of 2004, important milestones for the integration of the new second neutron guide hall (NGHII) into the Berlin Neutron Scattering Center (BENSOC) were reached: The building structure was completed as an extension to Neutron Guide Hall I, where experiments have been performed since 1992. Particular challenges related to this project were the deep foundation in the neighborhood of existing buildings, the unusual condition to use only hardly magnetizable reinforcement steel for this type of constructions in an area of approximately 750 m<sup>2</sup> which is meant for heavy loads. Another problem was the connecting opening to NGH I, where valuable instrumentation sensitive to dust is installed in a radiation protection area. The replacement of the old neutron guide elements by a conceptionally new extraction guide at a tight schedule of approximately 6 weeks was a logistical challenge, in particular because manifold technical and radiological safety requirements had to be fulfilled. The new innovative extraction guides were implemented at a neutron source

for the first time ever. The exchange of the neutron guide was the general prerequisite to resume the highly demanded user operation at all instruments except for the three that were located on the old NL4 guide. Hence, the thermal beam ports and the experiments using cold neutrons on the remaining guides NL1–3 were operational again by January 2005.

In 2005, the construction and delivery of the components of the complex neutron guide system at continued operation of the neutron source made good progress. The most prominent achievement in the guide section was the completion of the common initial section which then splits into three individual guides. The necessary biological shielding, which has the function to guarantee for safe top quality working conditions, was installed subsequently. This set the stage for successful tests and a swift resumption of the user operation of the upgraded (increased flux) neutron reflectometer at the beginning of 2006.



1 Photo: Bernhard Schurian

By the end of 2005, the infrastructure components were completed to a large extent. The guest groups will cooperate with their local contacts in spacious cabins that host control units and computer equipment for the experiments. Neutron choppers which will be implemented into the neutron guides will define the velocity of the neutrons before they hit the sample under investigation. Infrastructure systems required to accommodate the three big instruments in NGHII, i.e. a Very Small Neutron Scattering Instrument (VSANS) for soft matter investigations, e.g. bio-systems, polymers, etc., a Large Angle Spin Echo Spectrometer (SPAN), for the investigation of slow dynamics in matter, and a versatile Extreme Environment Diffractometer (EXED) have been prepared and the instruments have partially been installed. It is planned to combine the EXED instrument with a 25–35 Tesla magnet, which will provide the highest magnetic field world wide available in neutron scattering techniques, strengthen the leading role of HMI in this area of research and provide exciting new information on magnetic structures.

- 1 The stained glass window of the Neutron Guide Hall II reflected in the metal platform. The sample position and the detectors for EXED will be located on this platform.
- 2 The neutron guides leading from the reactor to the instruments in Neutron Guide Hall II are being installed
- 3 General view of the Neutron Guide Hall II in early 2006. The Spin Echo Spectrometer SPAN is already in its new position. In the foreground: components to be used for building up the new instruments.
- 4 January 2005: New Year reception in the Neutron Guide Hall II
- 5 Open double disc chopper. The neutrons will be able to pass through the slits in the white rings.
- 6 The disc choppers will select the neutrons for the instrument EXED. Not yet in their final position.



2



Photo: Bernhard Schurian 3



4



5



6 Photo: Bernhard Schurian

## Meetings and Conferences

Several meetings, schools and conferences have been organised at or by the Hahn-Meitner-Institut in 2005. A table presents an overview; some events are described in more detail.

Event	organized together with	Location	Dates
26 <sup>th</sup> Tutorial Session on Neutron Scattering	–	Hahn-Meitner-Institut	February 21–25
RADAM 05 – Conference on Radiation Damage in Biomolecular Systems	Organized within the COST P9 Action	Potsdam	March 17–20
FVS-Workshop TCO III Transparent Conducting Oxides for Thin Film Solar Cells and other Applications	Solar Energy Research Association (FVS – Forschungsverbund Sonnenenergie)	Freyburg/Unstrut	April 10–12
Summer Student Programme	–	Hahn-Meitner-Institut	August/September
1 <sup>st</sup> International Summer Academy on Photovoltaics	Research Centre Jülich	Berlin	August 24–September 4
PIANO Summer School on Physics with Ions – from Analysis to Nanotechnology	GANIL (Caen, France)	Blainville-sur-Mer, France	September 19–26
BENSC Users' Meeting	–	Hahn-Meitner-Institut	September 22–23
4 <sup>th</sup> Workshop on Orbital Physics and Novel Phenomena in Transition Metal Oxides	University of Hamburg	Hamburg	October 5–6
PNAM Autumn School about Application of Neutrons and Synchrotron Radiation in Engineering Materials Science	GKSS, DESY, Technical Universities of Berlin, Claustahl, Dresden and Vienna	Hamburg	October 10–14
4 <sup>th</sup> Workshop on Metallo- and Metalloid Proteins (Herbsttagung)	GSF – National Research Center for Environment and Health	Hahn-Meitner-Institut	November 24–25



1-3 At the 2005 BENSC Users' Meeting  
4-6 At the 4<sup>th</sup> Workshop on Metallo- and Metalloid Proteins (Herbsttagung)

# First International Summer Academy on Photovoltaics

In summer 2005, the First International Summer Academy on Photovoltaics took place in Berlin. In the time from the 28<sup>th</sup> of August until the 4<sup>th</sup> of September, a scientific overview of the field as well as expert knowledge ranging from the fundamentals to the forefront of current research was provided. More than 60 PhD students and young scientists from 14 countries followed the invitation of the Hahn-Meitner-Institut (HMI) and the Research Centre Jülich (FZJ). The participants, selected from a large number of applicants, were predominantly PhD students working in the fields of physics, chemistry and material science. In addition to these participants from academic institutions, scientists from the photovoltaic industry attended the Academy as well.

The participants were first presented with an overview of Fundamentals of Semiconductors. This was followed by the topics Solar Energy Conversion and Characterisation of Materials and Solar Cells. In the presentations in the topic Preparation of Materials for Solar Cells, not only these physical fundamentals were covered, but also practical questions such as the upscaling of cells from laboratory-size to industrial-size production were discussed. In Computer Modelling and Simulation, the participants could experience the com-

plexity of a solar cell, for even in a simple model more than 100 materials parameters are necessary to define the electrical behaviour of a cell. Additionally, aspects of wider interest like System Analysis, Scenarios, Sustainability and Technology for Solar Cells and Modules were covered. One day of the academy was used to visit the laboratories of the HMI, providing first-hand insights into modern research technology.

The response from the participants exceeded all expectations. Especially the multitude of overview presentations was highly welcomed, for they offered a compact and specific introduction to the relevant subject. A comparable event in this field – so the unanimous opinion – had not been offered before.

The booming market in photovoltaics creates an increasing demand for qualified specialists in this field. In the Helmholtz Association, the HMI and the FZJ are researching the physical and technological aspects of photovoltaics. In both institutes together, more than 200 scientist work on this key technology. By organising the summer academy, the institutes reacted to an increasing demand for further education on photovoltaics.

# Discussing novel instrumentation

The 91<sup>st</sup> meeting of the *Studiengruppe für Elektronische Instrumentierung* (SEI) (Study group on electronic instrumentation) was held at the Hahn-Meitner-Institut in the time September 26–28, 2005. For 44 years, the focus of these meetings has been the exchange of experience in building large scientific measuring instruments between scientists and engineers from various institutes (e.g. Helmholtz Centres, the Federal Institute for Materials Research and Testing BAM, Germany's national metrology institute PTB and many others), Universities and electronic companies.

The main topics of this meeting were data-acquisition systems for neutron detectors using time stamp data with 100 ns resolution, front-end electronic for large position sensitive detectors, new concepts for stepping motor controller and high resolution frequency measurements which are necessary to standardize voltage measurements. One presentation showed an on-line measurement system at the Lehrter Hauptbahnhof – Berlin's new central railway station to monitor with high accuracy the different motions

of this large building. An in-situ beam loss monitor system in combination with a total ionization dose measurement system for electron accelerator (e.g. TTF2 at DESY) was presented.



# PIANO 05: French-German Summer School on Physics with Ions

Following the first German-French summer school TRACKS03 in Mühlhausen, Thüringen, in 2003, the second French-German summer school *PIANO 05 Physics with Ions – from Analysis to Nanotechnology* was held September 19–26, 2005 in the holiday resort Blainville-sur-Mer in Normandy. Like already two years earlier, the school was organized jointly by scientists from ISL at the Hahn-Meitner-Institut and the centre for interdisciplinary research CIRIL at the accelerator centre GANIL (Caen, France) additionally sponsored by the Université-Franco-Allemande UFA – Deutsch-Französische Hochschule DFH in Saarbrücken and several French institutions: the research association CNRS, the technical university ENSICAEN and the Université de Caen.

The school was attended by 71 participants including 24 lecturers, most of them from Germany and France, but other nationalities were also represented. The main goal of the school was, to present the fundamentals of ion-solid interaction and to cover the use of ions in materials analysis as well as problems in the production of micro- and nanostructures with fast heavy ions and their characterization with complementary methods. Among the complementary methods discussed were the small angle scattering techniques with neutrons and synchrotron radiation, x-ray absorption spectroscopy (like EXAFS), and x-ray-diffraction, thus illustrating the power of combining the three “probing radiations” of PNI (photons, neutrons, and ions). It was an important intention of the organizing scientists to bring together young scientists, from the graduate student to the university teacher or researcher at national laboratories.

Additional tutorials on computer simulations – most likely a novelty for such a school – were also part of the programme. In these tutorials, the participants had the chance to explore modern characterization techniques by using analytical programs and to benefit from explanations and guidance by the experts. In the discussion at the end of the school, these tutorials received high marks as a very good means for presenting the subjects and were highly recommended for future schools and workshops.

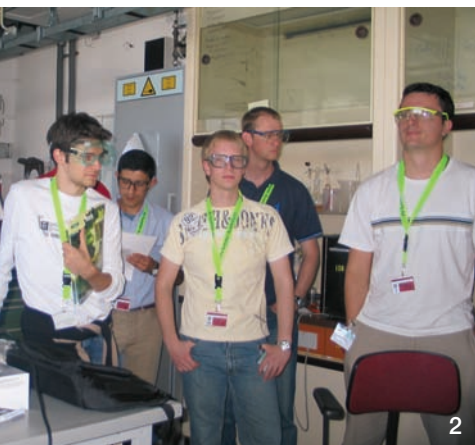
Besides the scientific programme, the participants had enough time to familiarise themselves with some special features of the area such as the culturing of oysters in extended off-shore fields being intermittently visible or covered by water because of the large difference in tides along the coast of Normandy and Brittany. The participants also took a short trip to Mt. Saint Michel and to St. Malo in Brittany.

In summarizing the summer school PIANO05, one can quote a commentary of one of the participants, Mme. Sophie Jequier, University of Bordeaux:

*As a lecturing researcher in physics at the University of Bordeaux, I appreciated the efforts and achievements in presenting the different aspects of the field. I particularly want to emphasize how well the workshops on numerical simulations, that constitute a new approach necessary these days, were received.*

At the end of this report one can only repeat the wish expressed by many of the participants to try to organize a German-French school under a well defined subject in two years again.

- 1–3 Summer Academy on Photovoltaics
- 4 PIANO 05 – Summer School on Physics with Ions



## Insights for the public: The Hahn-Meitner-Institut participated in the annual *Lange Nacht der Wissenschaften*

It has become a good tradition in Berlin that every year about one hundred research institutes invite people to the *Lange Nacht der Wissenschaften* – the largest and most important event for the general public interested in science in Berlin. The Hahn-Meitner-Institut also used this opportunity to give insights into its research activities and to rouse people's interest in physics.

In connection with the *Einstein Year 2005*, the Hahn-Meitner-Institut presented its solar energy research and introduced some aspects of Einstein's popular papers about the properties of light that formed today's basic principles of photovoltaics. About 3.000 people came to the locations in Wannsee and Adlershof and visited laboratories, talks and experiments.

In Wannsee, for example, visitors could observe how many steps are needed to fabricate solar cells with thin films of the semiconductor CIS at laboratory scale. Scientists informed also about the quality control and diagnosis of solar cells. They invited people into their laboratories and explained different procedures, for example scanning electron microscopy, infrared thermography and photoluminescence.

Many guests were attracted by a zeppelin model powered by ultra-thin, flexible solar cells which scientists from the Hahn-Meitner-Institut are developing for – amongst others – space-use. People interested in solar modules for their house roofs acquired information about materials and efficiencies of different types of solar modules offered by certain manufacturers.

The institute's scientists working at BESSY explained to visitors how they use synchrotron radiation to gain insights into the three-dimensional structures of technical components.

The *Lange Nacht der Wissenschaften 2005* was very successful – in Berlin and at the Hahn-Meitner-Institut. According to a questionnaire in Wannsee, 90 percent of the guests really enjoyed visiting the institute, felt well informed and were satisfied. The next *Lange Nacht der Wissenschaften* will take place on May 13, 2006. On this occasion, the Hahn-Meitner-Institut will present its structural research.



- 1 The building of the Department of Silicon Photovoltaics in Berlin-Adlershof illuminated for the *Lange Nacht der Wissenschaften*
- 2 Visitors to the Department of Silicon Photovoltaics making their own solar cells
- 3 An infrared camera showing the different temperatures in the head
- 4 The solar zeppelin – powered by a ring of strong lamps
- 5 The energy bike – measuring the power humans can produce
- 6 A PhD student happy to present her work on fuel cells



4



2



5



3



6

## The school lab is in town

Educating future scientists and creating interest in natural sciences in the general public are some of the main tasks of a large scientific institution like the Hahn-Meitner-Institut. An important part of this effort is the institute's school lab *Blick in die Materie* (Looking into Matter) – a place where pupils from primary and secondary school have the chance to experience the atmosphere of a scientific institute, to perform physics experiments on their own and to feel the thrill of real science. In the two years of its activity, the school lab attracted more than 50 school classes comprising more than 700 pupils from all over Germany. In addition to that, the school lab offers education programmes for teachers, and particularly interested pupils get the opportunity to work in the school lab for a longer period of time. Being located on the institute's premises, the school lab in its every day work contributes to the institute's visibility almost only among the visitors themselves, their friends and families.

- 1 The magnetic accelerator presented by the school lab of the Hahn-Meitner-Institut
- 2 Exploring eddy currents at the school lab presentation in central Berlin



In order to present their work to a broader public, the school labs of nine institutes within the Helmholtz-Association joined forces and opened for one week in June a science village right in the city centre of Berlin at the magnificent boulevard of *Unter den Linden*, between the main building of the Humboldt University and the Opera House. The school labs attracted more than 12,000 people from a large crowd of passers-by enjoying a walk in the wonderful sunny weather. The school lab of the Hahn-Meitner-Institut – present in the science village for three days – gave them the opportunity to do various simple but revealing experiments about magnetism – one of the foci of its activities.

Following the route from playing via experiments to understanding, the visitors of the Hahn-Meitner-Institut school lab learned how to build an electric motor from a screw, a wire and a small magnet or how to produce electricity using magnetic induction. A more sophisticated experiment showed the reorientation of magnetic domains in a magnetic material. However, the most impressive exhibit did not fit into the pavilion and had to be placed outside: a simple magnetic accelerator speeding up steel balls to a surprisingly high velocity.

The reactions of the younger visitors showed how much they were impressed by the fact that science can be taught via hands-on experiments instead of standard school lessons. "I liked it because it wasn't boring at all. Kids don't like boring stuff." was the comment a thirteen year old girl wrote in the guest book.

## PhD students meet at the Hahn-Meitner-Institut

In September 2005 a joint PhD students day was organised by the Hahn-Meitner-Institut and the Helmholtz Juniors – the Helmholtz Association's newly founded organisation for PhD students. Students from all Helmholtz research centres in Berlin and Brandenburg were invited to learn about possible career opportunities after the completion of their theses and to discuss their plans and ideas for the future. In addition, the initiative Helmholtz Juniors itself was presented.

Approximately 70 PhD students from the seven research centres located in the region attended the event. As an introduction, Professor Gereon Fink from the Research Centre Jülich (FZJ) gave a scientific talk about the functional anatomy of the human brain. Afterwards, the PhD students could learn about national and European funding opportunities as well as about the application procedures

for projects supported by the German Federal Ministry of Education and Research (BMBF). An alternative option to a scientific career was presented by the directors of the two start-up companies Sulfurcell and sglux. Dr. Nikolaus Meyer (Sulfurcell) and Dr. Tilman Weiss (sglux) discussed with the PhD students about their own experience and important points to consider when starting a business. In the following poster session, the PhD students presented their own scientific results to their colleagues stimulating an intensive interdisciplinary exchange. During a barbecue evening the PhD students had further opportunity to initiate and develop new contacts in a relaxed atmosphere.

The event was a great success and this format might, in the future, serve as a model for meetings at other Helmholtz research centres.

PhD students from different Helmholtz centres arriving to the meeting of the Helmholtz-Juniors



# New partner for neutron autoradiography

For more than 20 years, the Hahn-Meitner-Institut has been using neutron autoradiography for the investigation of old masters' paintings. With this method, layers of paint and pencil drawings hidden behind the surface become visible. The results of these investigations allow art historians to get access to important information about the techniques used by the painter – his typical hand –, changes made during the creation and sometimes even help decide whether a painting is an original or a forgery.

Jean-Baptiste Pater's painting *The Fair at Bezons* (owned by the Prussian Palaces and Gardens Foundation Berlin-Brandenburg) on its way into the irradiation box at the HMI



In an autoradiography experiment, the painting is irradiated with neutrons. Some atoms in the image absorb one of the incoming neutrons and thus become radioactive. When the painting is then put on an X-ray film or on imaging plates, the radiation emitted creates an image showing all the layers in the painting. Due to the different half lives of the different nuclei, one can even distinguish particular pigments in the hidden layers by comparing autoradiographs taken at different times.

Until now, almost all the paintings investigated at the Hahn-Meitner-Institut were owned by the *Gemäldegalerie Berlin* and were mostly works of Italian and Flemish painters of the 16<sup>th</sup> and 17<sup>th</sup> centuries. In late 2005, the Hahn-Meitner-Institut started a new cooperation with the Prussian Palaces and Gardens Foundation Berlin-Brandenburg administering the former Prussian royal residences in and around Berlin including hundreds of paintings purchased by the Prussian kings. As there is no doubt as to the painter in these cases, it is more the study of the painter's style and the chronology of his works that drives the interest in the investigations. As works of French painters of the 18<sup>th</sup> century make up an important part of the collections of the Palaces and Gardens Foundation, the scientists at the Hahn-Meitner-Institut now have the opportunity to extend their expertise to a new class of paintings. The first painting investigated in the framework of the cooperation was Jean-Baptiste Pater's *The Fair at Bezons* (approx. 1733) from the Sans Souci Palace in Potsdam. This painting is a smaller version of Pater's masterpiece now owned by the Metropolitan Museum of Art in New York.

# Theory and experiment – a really interdisciplinary cooperation within the Helmholtz Association

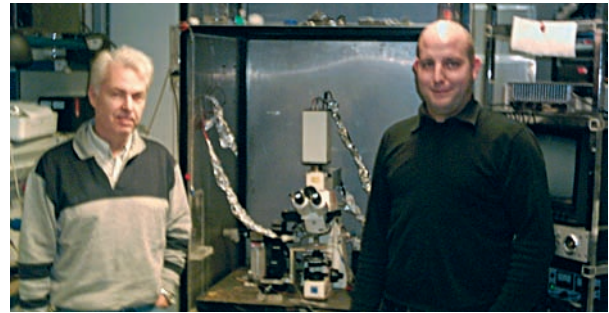
Usually, a theoretical physicist is not the kind of person one meets in a biological laboratory doing experiments with cell cultures. But in the case of a current project initiated by Martin Falcke within the department Theoretical Physics (SF5) of the Hahn-Meitner-Institut, it actually became necessary for Alexander Skupin, a new PhD student expected to work on theoretical studies of the Calcium dynamics in living cells, to perform the necessary experiments himself.

The goal of the project is to create and test a mathematical model describing the dynamics of Calcium ions in living cells. Calcium ions act as second messengers in the cells by for-

warding information arriving from outside within the cell. Among the typical features of calcium dynamics are oscillations of the calcium concentration in the cell. And it is the detailed behaviour of these oscillations (Do the times between subsequent concentration maxima vary and if so how do they vary?) that carries the information necessary to decide whether the mathematical model suggested by the theoretical physicists correctly describes the processes going on inside the cell. But, as it turned out, the oscillations had never before been investigated in the detail necessary to test these theoretical predictions and this is why Skupin had to become an experimentalist for a few months.

That Skupin managed to collect the necessary data is thanks to the hospitality of two biology labs that opened their doors to the theorist – both of them located at other Helmholtz research centres: H. Kettenmann's laboratory at the Max-Delbrück-Centrum in Berlin-Buch and M. Wartenberg's laboratory at the GKSS outstation in Teltow outside Berlin. In addition to that, results achieved by other researchers at C. Taylor's laboratory at the University of Cambridge and M. Bootman's laboratory at the Babraham Institute in Cambridge were used.

Now, Skupin is back at his desk and his computer and working on his theories. The first results of this project can be found on p. 62 of this report.



In the biology lab at the Max-Delbrück-Centrum: the lab's boss Prof. H. Kettenmann (left) and Alexander Skupin, the theoretical physicist doing biology experiments there

## Virtual institute to solve real problems

Non-destructive techniques employing neutrons and synchrotron radiation are becoming more and more important in the development of novel engineering materials. But do the materials scientists always know how to use the full potential of these techniques? And do the scientists running the experiments always know which are the most pressing questions the materials scientists need answers to and do they develop their equipment according to these needs?

In order to bring together expertise from both fields and to develop the techniques in joint projects, the three Helmholtz research centres: Hahn-Meitner-Institut, GKSS, and DESY as well as the Technical Universities of Berlin, Dresden, Clausthal and Vienna have founded the virtual institute *Photon and Neutron Research on Advanced Engineering Materials (PNAM)*. On January 1<sup>st</sup>, 2006, the Max-Planck Institut für Eisenforschung in Düsseldorf replaced the Technical University of Vienna as partner of the virtual institute.

[The participants of the PNAM Autumn school on Applications of Neutrons and Synchrotron Radiation in Engineering Materials Science](#)



A project run by the Hahn-Meitner-Institut and the Technical University of Dresden may serve an example for the approach of the virtual institute. Scientists at the Chair for Powder Metallurgy, Sintered Materials and Composites at the Technical University of Dresden investigate the processes going on in a metal powder during sintering, and they would like to be able to observe the sintering process in real time. The department *Materials (SF3)* of the Hahn-Meitner-Institut operates a facility for synchrotron tomography – a method providing three dimensional images of the interior of different objects with a resolution of down to a few micrometers. In a joint project, a sintering furnace will be installed on the tomography facility, and it will thus become possible to take tomography images during the running sintering process.

In addition to the scientific work, an important goal of the virtual institute is educating young scientists beginning to work in the fields of non-destructive testing and materials science: The cooperation partners have hired several PhD students to work on projects within the institute and in 2005, PNAM organised an autumn school on Applications of Neutrons and Synchrotron Radiation in Engineering Materials Science. The autumn school took place in a small conference centre right outside Hamburg. In five days, it provided a theoretical and practical introduction into the fields covered by the institute: three days of lectures were followed by two days at the GKSS research centre and at Hasylab – DESY's synchrotron radiation facility. Inspired by the success of the 2005 autumn school, the partners of the virtual institute PNAM plan to organise the next autumn school in Berlin in 2007.

The virtual institute is part of the Helmholtz Association's initiative to strengthen the cooperation between universities and Helmholtz-centres and is funded by the Association via the President's Initiative and Networking Fund.

# From laboratory to production – research meets market

### The company Sulfurcell

The technology company Sulfurcell intends to offer modules for the photovoltaic generation of energy at attractive prices and to help solar technology to become more economic. Being the first company world wide using Copper-Indium-Sulphide (CIS) as absorber material, Sulfurcell has begun setting up production for solar modules. The technology used for the industrial production at Sulfurcell was developed at the Hahn-Meitner-Institut (HMI) in Berlin. The innovative use of sulphur is characteristic of the technology and also influences the company name.

In 1991, HMI scientist Roland Scheer produced the first CIS solar cell with 10% efficiency. Following further promising results, in 1998 the European research project Sulfurcell was initiated, leading to the creation of the company Sulfurcell in 2001. The Senate of Berlin honoured these efforts by granting 7m Euro for research and development activities in 2003. At the end of that year, pilot production commenced. In 2005, production was finally launched. In 2006, Sulfurcell started a cooperation with the photovoltaics company IBC Solar to promote and distribute the modules. Located in the middle of Berlin's modern Science and Technology Park Berlin-Adlershof, Sulfurcell and its more than 20 employees are planning to distribute the first modules in the 2<sup>nd</sup> quarter of 2006.

### The production hall of Sulfurcell



Photo: Sulfurcell

### The Technology

Sulfurcell is processing ordinary window glass and transforms the glass into solar modules generating electric energy. At the heart of the solar module is the thin CIS-layer, which absorbs as much sunlight as Silicon wafers of conventional solar modules being a hundred times thicker. The use of sulphur reduces the number of processing steps by one third and the amount of energy needed for manufacturing by two thirds compared to a conventional solar module. Apart from the p-type absorber CIS – this is where the absorbed light is transformed into electric current – a module consists of a second, n-type semiconductor layer, a metallic back contact and a transparent, conducting front contact. Within a module, a number of solar cells are series-interconnected.

The most common solar PV modules are based on crystalline silicon as absorbing material. CIS, the material Sulfurcell uses as absorber, has significantly better absorption properties. Therefore, the thickness of a CIS solar cell can be reduced to about 1% of the thickness of a common solar cell based on crystalline silicon.

The various layers a solar module consists of are deposited one after another on a glass substrate. The glass substrate serves two purposes: as support for the very thin solar cells and as part of the later encapsulation. For the deposition of the various layers of a CIS based solar PV module, techniques such as sputtering are used which have been applied successfully for a long time in the area of large scale glass pane deposition for architectural applications. By using sputtering, one can deposit large areas at low energy consumption.

On the molybdenum back contact precursors consisting of copper and indium are deposited. In the presence of elemental sulphur vapour at a temperature of about 500°C the precursor reacts within a short time to form the absorber material CIS. The device is completed by the deposition of a front contact, and after the contacting, it is encapsulated to secure it from climatic influences. The resulting modules produce 45 to 55 Watt, depending on the model, and impress by their elegant design.

The logo for Sulfurcell, featuring a stylized green and blue graphic of three horizontal bars of varying lengths to the left of the word "SULFURCELL" in a bold, blue, sans-serif font.

## Information day for the industry

Many of the methods used for investigating matter at the large scale facilities of the Hahn-Meitner-Institut provide unique opportunities for solving technological problems in materials science and engineering. The institute should be thus considered an obvious cooperation partner for innovative industrial companies. However, a large scientific facility focusing on fundamental science is not the first place where a development engineer would look for solutions to his problems.

Thus, it is an important task for the institute to approach relevant companies, to inform them about the research opportunities offered and to emphasize that they when cooperating with the Hahn-Meitner-Institut they will find a reliable partner offering convenient conditions adjusted to each particular case. Due to extensive networking, some methods – in particular the investigation of residual stresses by means of neutron scattering – struggle with a high demand from various companies. Others are still virtually unknown among prospective industrial users. This is especially the case for methods that might be applied in many different fields of industry. In 2004, the Hahn-Meitner-Institut has founded the application centre NIXE (Neutrons, Ions and X-Rays for Engineering).

At the centre of 2005's marketing activities at the Hahn-Meitner-Institut was the *Industrietag* on June 1<sup>st</sup> – an information day for the industry – offering engineers and researchers an opportunity to visit the institute, get an overview of the offer and to discuss possible modes of cooperation with the scientists.

More than 60 representatives of companies and institutions supporting the transfer of knowledge accepted the invitation and spent an interesting day at the Hahn-Meitner-Institut. A large number of participants were mainly interested in the applications of the institute's imaging methods – in particular for the investigation of processes in fuel cells. Neutron tomography and radiography are the only methods that can show the flow of water in a running fuel cell.

In his opening address, Berlin's Permanent Secretary for Economics Volkmar Strauch, welcomed the participants and thanked the institute for its initiative to draw the attention of the German industrial community to Berlin's activities in the field of applied science.

As usual, the impact of the event went beyond the immediate circle of participants. Many recipients of the promotional material sent out to inform about the event got in touch with the Hahn-Meitner-Institut without being able to come as did the readers of a news-paper article announcing the event. Thus, the *Industrietag* turned out to be an efficient method of promoting the applications of materials research at the large scale facilities to the prospective user from the industry.

- 1 Poster session during the *Industrietag*. Discussing the use of neutron tomography for investigations on fuel cells
- 2 Berlin's Permanent Secretary for Economics Volkmar Strauch welcomes the participants of the *Industrietag*



# The new neutron tomography instrument

Using neutron tomography, one can investigate the macroscopic inner structure of large objects (with sizes of up to several hundreds of cubic centimeters) with a spatial resolution of down to 100 micrometers. The method provides three-dimensional images of the material distribution inside the object. It is particularly well suited for showing the distribution of light elements in or behind metals because the neutron beam can easily pass through several centimeters of metal, but it is strongly attenuated by small amounts of hydrogen, boron or lithium. This makes neutron tomography a unique tool for non-destructive testing with applications in industry, materials science and various other fields.

In a tomography experiment, one takes several hundred two-dimensional radiography images – similar to medical x-rays – from different directions. Using sophisticated reconstruction software, one can create a data set con-

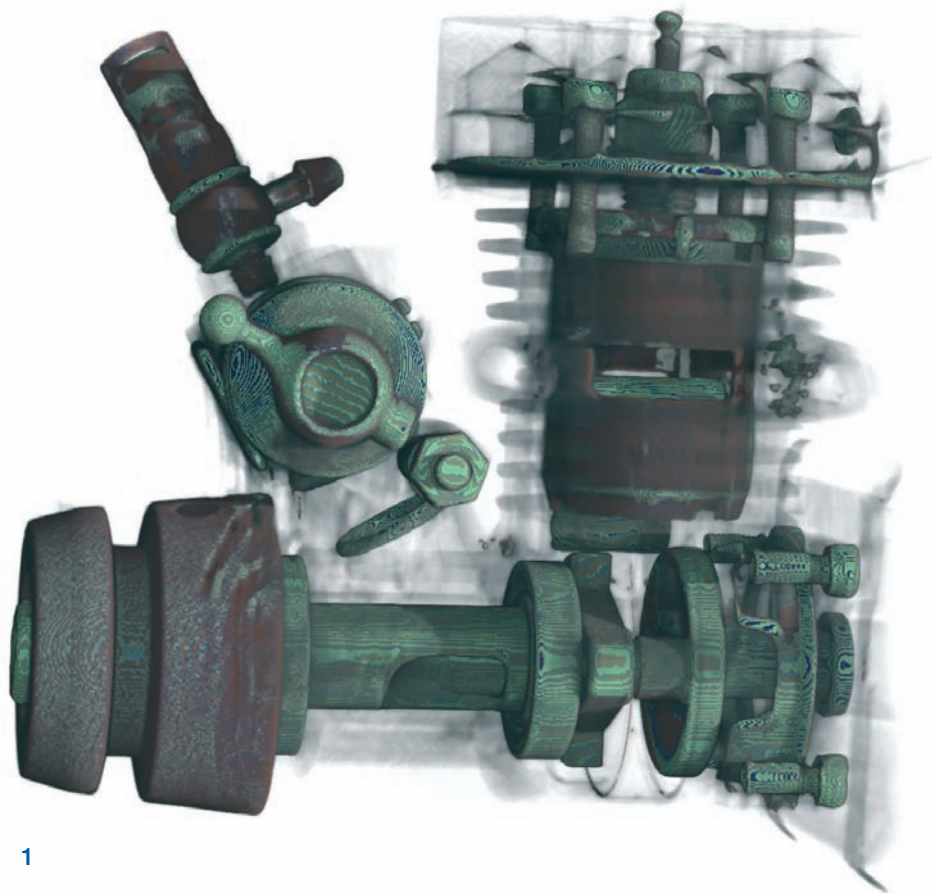
taining the complete information about the three-dimensional material distribution in the sample. Based on this data set, one can produce various images of the sample's inner structures. In the case of fast processes, it is often impossible to take many pictures of the object in exactly the same state and therefore only two-dimensional radiography images are achievable. It is, however, possible to take the radiography images with very short time intervals between them and thus to follow the developments in the investigated object in real time.

The main application tasks for neutron radiography and tomography are investigations connected with in-situ visualization of water management in fuel cells and quality tests of Diesel particulate filters, adhesive joints and lubricate films. Interesting applications in archeology and medicine were reported recently.

**1** Image of a small combustion engine taken at the new neutron tomography facility of the Hahn-Meitner-Institut. Inner components of the engine – usually hidden behind the aluminium casing – are clearly visible.

**2** The new neutron tomography facility CONRAD of the Hahn-Meitner-Institut

**3** Neutron radiography images showing the water uptake in a tomato seedling. From some point in time, the plant was watered with heavy water that is clearly visible in black in the image.



1

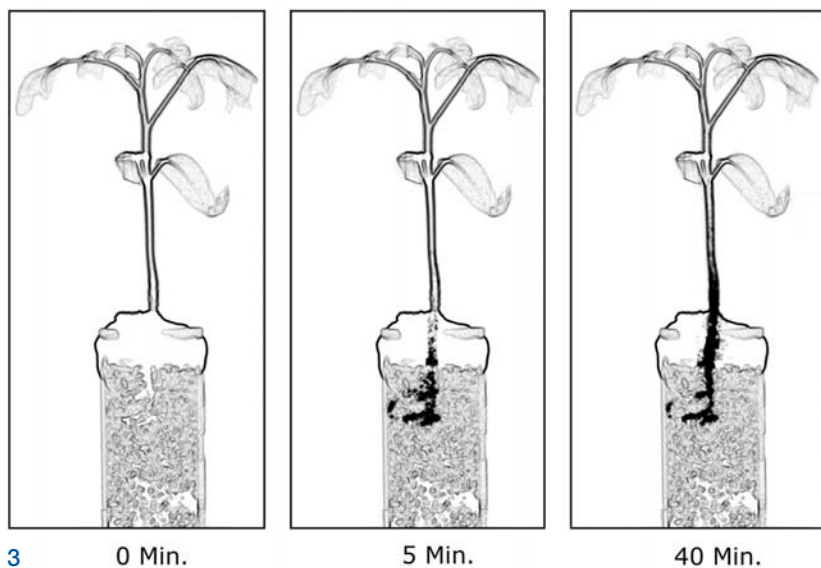
The high potential of neutron tomography was the motivation for setting up a new neutron tomography facility at the Hahn-Meitner-Institut. The facility has been designed to meet the needs of high flux applications such as real time imaging and high-speed tomography as well as high-resolution applications and phase-contrast tomography and to provide high flexibility for different kinds of radiographic and tomographic measurements.

The new tomography instrument CONRAD is a multifunctional facility for radiography and tomography with cold neutrons. It is located at the end of a curved neutron guide facing the cold neutron source of the research reactor BER II. The geometry provides a cold neutron beam with wavelengths between 2 Å and 12 Å.

Two measuring positions are available for radiography and tomography investigations. The first one is placed at the end of the guide. It is optimized for in-situ experiments, in which a high neutron flux is required. The available flux at this position is approx.  $10^9 \text{ cm}^{-2} \text{ s}^{-1}$ . The second measuring position uses a pin-hole geometry, which allows better beam collimation ( $L/D$  up to 1000) and higher image resolution in the range of  $100 \mu\text{m}$  in the CCD based detector system ( $10 \times 10 \text{ cm}^2$ ). The use of cold neutrons for radiography purposes increases the image contrast and improves the sensitivity for example in detecting small amounts of materials containing water and hydrogen in metal matrices. In addition to that, the cold neutron beam can easily be modified by diffraction and neutron optical techniques. This enables one to perform radiography and tomography experiments with more sophisticated measuring techniques such as phase-contrast imaging, imaging with polarized neutrons, energy-selective radiography and microtomography.



Photo: Bernhard Schurian 2



3 0 Min.

5 Min.

40 Min.

# First experiments using the new Small Angle X-ray Scattering Instrument at BESSY

A new instrument for Small Angle X-ray Scattering (SAXS) developed, constructed and assembled by the Hahn-Meitner-Institut has been taken into operation by HMI at the synchrotron source BESSY. This instrument is designed for the non-destructive characterization of structures in the nanometre range. In addition to normal SAXS, the instrument will be used for Anomalous and Grazing Incidence SAXS (ASAXS and GISAXS).

ASAXS allows the user to identify the elemental composition of the nanosized structures investigated. The method is based on the element dependent variation of the scattering amplitude near the X-ray absorption edges. GISAXS yields structural information on lateral and vertical nanostructures close to the surface using incidence angles close to total reflection ( $<1^\circ$ ).

The detector of the instrument is mounted at the end of an evacuated tube with a diameter 285 mm. This tube is built as an edge welded bellow system that allows for continuous variable sample-detector distances between 750 mm and 3750 mm. The edge welded bellow system consists of two parts: The longer one runs on support tracks and can be removed. The whole system is mounted on an optical bench that can be tilted up to  $3^\circ$  for GISAXS experiments.

The samples for the experiments will be mounted on the Huber diffractometer used by the instrument for magnetic scattering MAGS. Several different sample environments – not connected to the bellow system – will be available for the experiments. Currently, an in air sample changer and a high temperature furnace are available.

In the course of the year 2005, the SAXS instrument was installed at the monochromatic beam of the 7T Wiggler operated by the Hahn-Meitner-Institut at the synchrotron source BESSY. The commissioning measurements for the SAXS instrument were done in 2005. A first successful ASAXS test experiment was performed on gold nanoclusters in an oxide glass showed that it is possible to extract the weak anomalous scattering effect.

The SAXS beamline is run in time sharing with MAGS. It has been available for user service since March 2006.

**1** The SAXS instrument in its measuring position at a beamline operated by the Hahn-Meitner-Institut at BESSY. Left hand side: detector chamber, right hand side: diffractometer used together with the instrument for magnetic scattering MAGS.

**2** The detector chamber of the new Small Angle X-ray Scattering instrument in the HMI workshop before being brought to BESSY



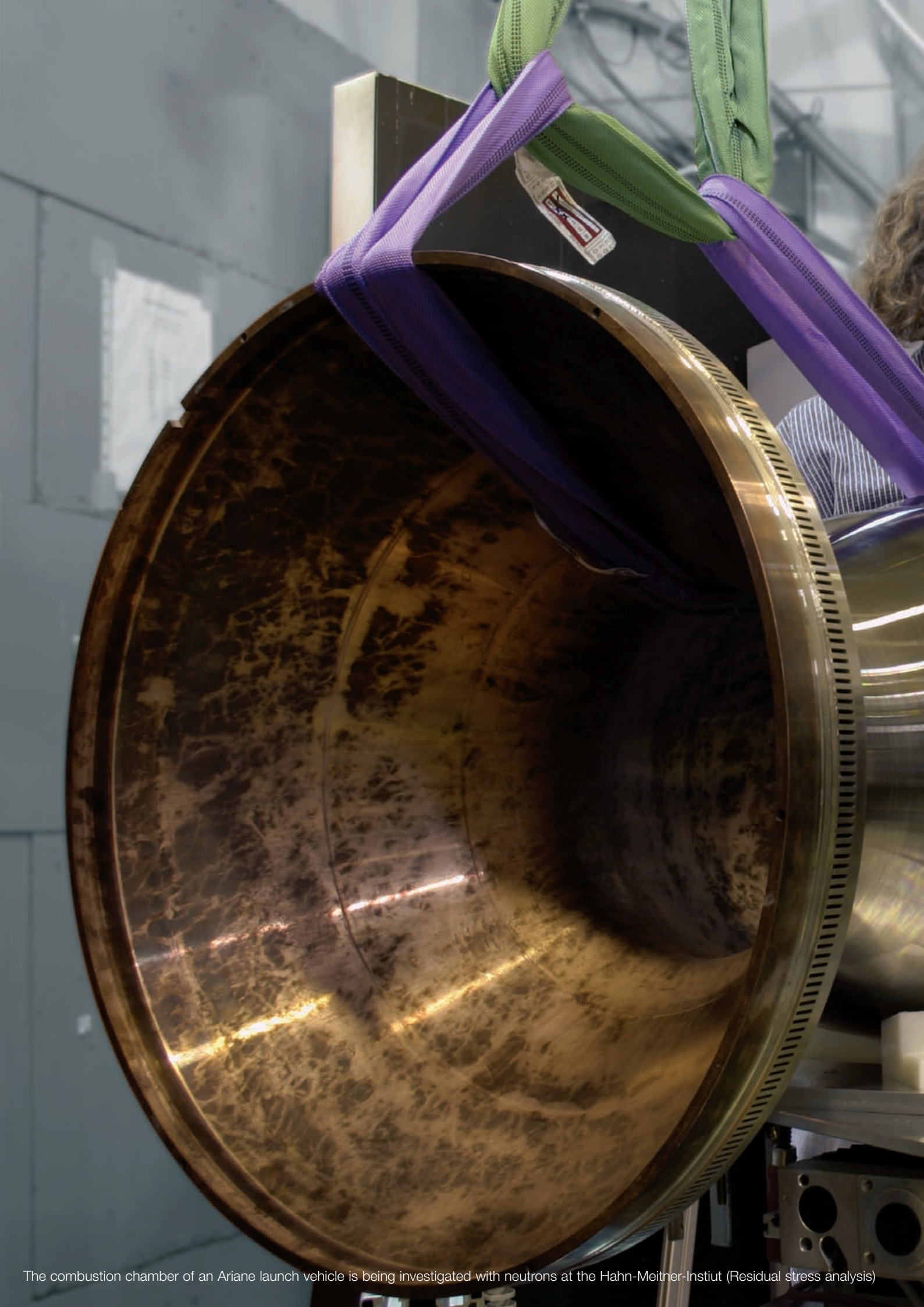
## The new 7T high field end station – a unique instrument for magnetic studies of ultrathin films and nanostructures

Experimental studies of magnetic properties of ultrathin films and nanostructures are demanding concerning photon source and sample environment because these systems consist of small quantities of material. In order to get a measurement signal of sufficient intensity they have to be excited with extraordinarily high photon flux. Measurements with elemental resolution and strong magnetic effects are possible with radiation sources which are monochromatic, tunable in energy and polarized. In the soft x-ray range these demands as to the photon source are fulfilled by state-of-the-art beamlines like our UE46-PGM at the electron storage ring BESSY.

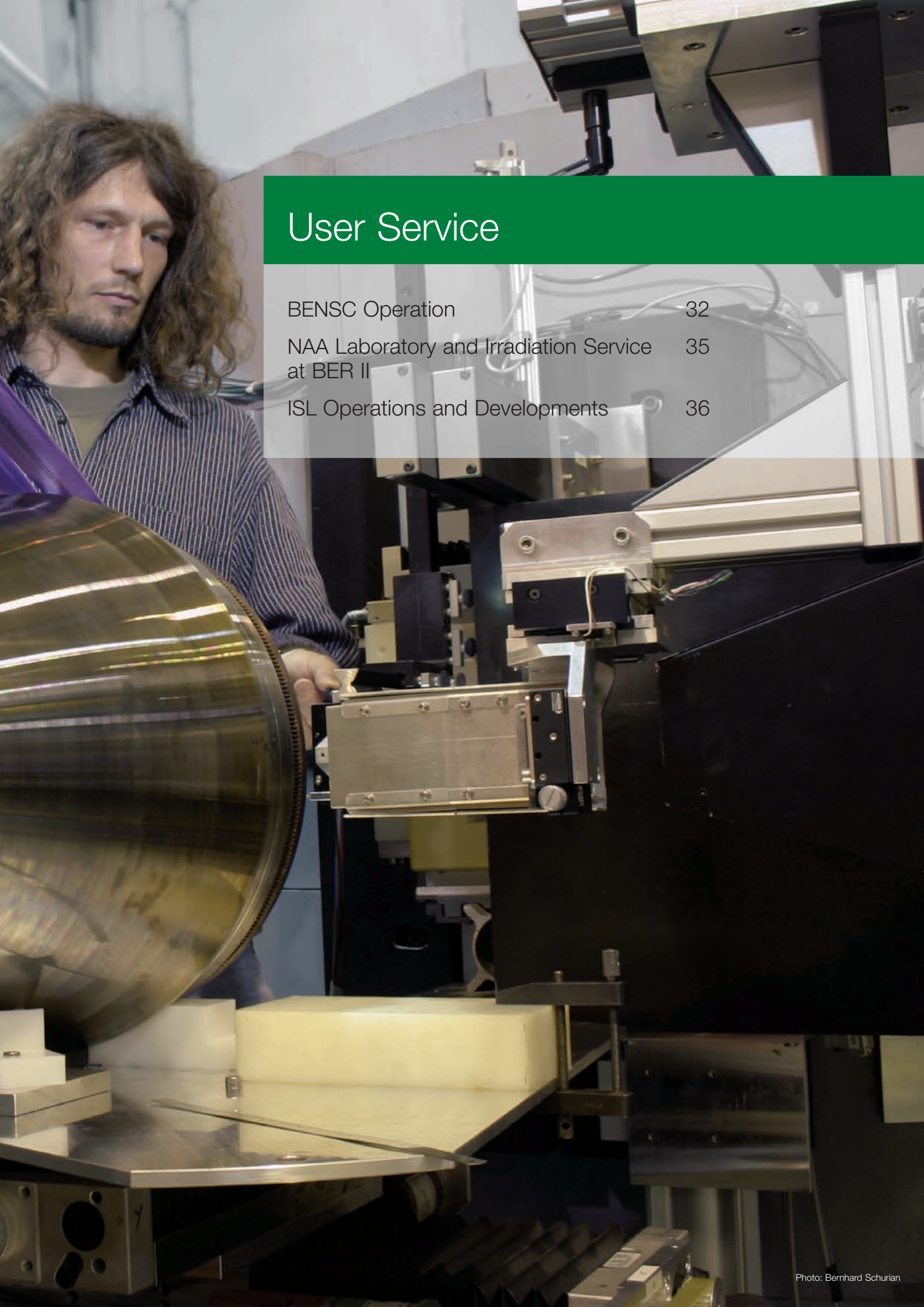


In addition, ultrathin films and nanostructures are reduced in dimension which leads to great demands on the sample environment, namely external magnetic field and temperature under ultra high vacuum conditions. In order to also fulfil these criteria we have constructed our new high-field end station which combines magnetic fields up to 7 T with sample temperatures down to 2.6 K. It has been designed for the two methods X-Ray Magnetic Circular Dichroism (XMCD) using the total electron yield to monitor the absorption and X-Ray Resonant Magnetic Reflectometry (XRMR). The absorption option has been tested and successfully applied during a beamtime immediately after the installation of the high-field end station in the experimental hall of BESSY. Measurements at a sample temperature of 3.4 K and a magnetic field of 6.5 T were routinely performed. The reflectometry option is going to be tested and used during beamtimes in the second semester of 2006.

The new ultra high vacuum high magnetic field reflectometer at the UE46-PGM beamline operated by the Hahn-Meitner-Institut at BESSY



The combustion chamber of an Ariane launch vehicle is being investigated with neutrons at the Hahn-Meitner-Institut (Residual stress analysis)



## User Service

BENSC Operation	32
NAA Laboratory and Irradiation Service at BER II	35
ISL Operations and Developments	36

# BENSC Operation

Director: Prof. Ferenc Mezei

It is the mission of the Hahn-Meitner-Institut as a research center of the Helmholtz Association to *operate large-scale facilities for providing best state-of-the-art research opportunities for the national and international user community*. The Berlin Neutron Scattering Center (BENSC) was established at the HMI to accomplish this task for the neutron research community and more recently also for users of synchrotron radiation with a particular focus on promoting the complementary use of both probes: neutrons and photons.

BENSC is characterised by two important strengths: extreme sample environment providing the world's highest magnetic fields and lowest temperatures in neutron scattering and development of new instrumentation concepts and techniques both for continuous and pulsed neutron sources. As a result, experimental capabilities at several BENSC instruments are unique or competitive with the best at high-flux sources. Other BENSC instruments provide solid performance for a nearly complete spectrum of neutron scattering studies, for purposes of both high quality research and education of students and new neutron users. Between 3 and 7 diploma as well as between 12 and 16 PhD theses are based on experiments performed at BENSC each year. Once a year, a tutorial is held for students from European countries allowing hands-on experiments at various BENSC instruments. The user programme has been highly rated and is strongly supported by the EU since 1993.

## Profile of BENSC

BENSC is characterized by an extraordinarily wide ranging instrumentation, which is remarkable for a medium flux neutron facility. With the exception of a backscattering machine, a complete spectrum of instrument types allows experiments to be performed in practically all areas of neutron science, from basic to applied research. Several advanced BENSC instruments provide neutron intensities and resolutions competitive with the best available worldwide. Most instruments have the option of using polarized neutrons. Examples for especially advanced and partly unique instruments are

- the polarized neutron option SANSPOL
- the multidetector option of the time-of-flight spectrometer NEAT
- the wide-angle spin-echo spectrometer SPAN with a time-of-flight option
- the flat-cone diffractometer

and in particular the sample environment.

BENSC has a long-standing, world-wide recognised tradition in developing and providing sample environment for extreme conditions. Experiments can be performed over a large range of temperatures and magnetic fields. Two cryomagnets designed by Oxford Instruments in cooperation with HMI scientists allow users to routinely carry out neutron scattering experiments at fields up to 15 T in combination with temperatures down to 30 mK. For temperatures down to 1.5 K, the magnetic field can be increased up to 17.5 T, the highest static magnetic field world-wide available for neutron scattering experiments. BENSC strives for further pushing the present field limit towards significantly higher values in cooperation with the National High-Field Laboratory of the USA in Tallahassee. A design study for a new magnet has been undertaken aiming at a field of 25 T with the option of a further upgrade to 35 T.

The BENSC neutron scattering instruments are described in detail on the BENSC webpage: [http://www.hmi.de/bensc/instrumentation/instrumentation\\_en.html](http://www.hmi.de/bensc/instrumentation/instrumentation_en.html).

A new colour-printed instrument brochure replacing the present brochure (HMI-B 577) published in March 2001 will be available on request end of 2006. A detailed technical handbook on the BENSC sample environment is also available on the web: [http://www.hmi.de/bensc/sample-env/index\\_en.html](http://www.hmi.de/bensc/sample-env/index_en.html)

## The New Neutron Guide Hall II

Completing the instrumentation in the new Neutron Guide Hall II is presently the most important upgrade project of BENSC. The construction of the building itself was finished end of 2004. Beginning of 2005, the multi-spectral beam extraction system replacing the old neutron guide 4 had been installed and reactor operation could start again. Further during the year 2005, the first part of the guide system for the new hall was mounted and connected to the extraction system. This novel extraction system feeds cold as well as thermal neutrons into the guide for the new time-of-flight diffractometer EXED. Two other guides serve for the new high resolution SANS-instrument (VSANS) which is presently constructed and for the spin-echo instrument SPAN which was shifted from the old neutron guide hall to the new one. The *Extreme Environment Diffractometer* EXED was especially designed for investigations using the planned 25 T magnet (later upgraded to 35 T) which shall ensure

the leading position of BENSCH in neutron scattering experiments at high magnetic fields.

**BENSCH User Policy**

BENSCH is open to the national and international scientific community. About 70% of the beam time is available to external users, 30% to in-house researchers. A minor part of the beam time for external users (up to 20% of the total beam time of an instrument) can be given to long term collaborating groups from German universities and other research institutions, the rest (at least 50% of the total beam time) is given to short term projects via a peer-review selection process. The long term collaborations serve mainly two purposes: they (i) allow university groups a reliable planning of thesis works and (ii) enlarge the pool of scientific expertise available at BENSCH. Proprietary research by commercial companies is also possible at request, mainly at special instruments, but will be charged.

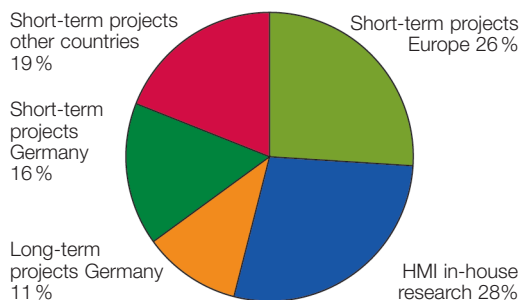


**Fig. 1:** Distribution of BENSCH instrument time in 2005

**BENSCH User Service**

BENSCH provides extensive logistic, technical and scientific support for all external users at the scheduled instruments. Beam time allocation and assistance in all logistic matters are organised by the BENSCH user office.

**Beam time allocation**

The beam time allocation is based on a proposal system with two proposal rounds per year. Proposals for short-term projects submitted by external users are peer-reviewed by an international Scientific Selection Panel, which is meeting and discussing the proposals at the HMI. Following the decisions of the Scientific Panel, proposers of accepted short-term projects are invited to perform the proposed experiment at BENSCH. In general, all rejections are accompanied by comments with the objective to help for a potential resubmission or give further suggestions, e.g. references of better suited instruments at other sources.

**Logistic support**

BENSCH is prepared to assist external users with travel and subsistence expenses, whereby users from

German Universities get preferential treatment. Users from EU member states and associated states are eligible for grants provided by the European Commission for access to BENSCH. EU users can get full travel refund for up to two participants per experiment. The BENSCH guest office is assisting the users in all these logistic matters including housing. BENSCH runs a 30 bedroom hostel on site.

**Technical and scientific support**

All external users carrying out experimental work at BENSCH have HMI instrument scientists as local contacts who assist in preparing and performing the experiments thus ensuring the efficient use of the beam time. In addition, a pool of BENSCH technicians is available for technical assistance during the preparation and running of the experiments. For experiments under extreme sample environment conditions special staff is taking care of the sample environment such as the high-field cryomagnets.

**BENSCH User Statistics 2005**

For 2005, more than 160 short-term projects of external users have been accepted by the Scientific Selection Panel (see Table 1) with over 1060 days of beam time allocated. Although three normally scheduled instruments of the neutron guide hall were still out of operation due to the ongoing upgrade project Neutron Guide Hall II, the figures are almost identical to those of 2003, the last "normal" year with a complete instrument suite and full reactor operation.

Countries of origin	accepted projects	allocated days
Germany	54	282
EU + Associated	81	454,5
Russian Federation	7	191
Australia, Indonesia, India, Japan, Republic of Korea, Mongolia, USA, South Africa	20	141
Sum:	162	1068,5

**Table 1:** Allocation of BENSCH beam time for short term projects in 2005

**BENSCH user service at BESSY**

To promote the complementary use of neutrons and synchrotron radiation, the HMI has initiated an upgrade project for the synchrotron source BESSY including the development and installation of two new insertion devices: the undulator UE46 providing soft X-rays with worldwide highest brightness and flux density and the 7T wiggler 7T-MPW shifting the photon energies to the hard X-ray regime. HMI-BENSCH has built and operates 3 beamlines with four instruments S1–S4 at these devices and a further instrument, the X-ray tomography station S5, at a non-HMI beamline. Access to these instruments is organised via the BESSY proposal system, <http://www.bessy.de/boat/www/> while the user service is performed by HMI-BENSCH personnel.

The instrument S1 at the undulator beamline has been in routine user operation since 2003. In 2005,

a second experimental station was commissioned in addition to the spectroscopy chamber: a reflectometer with a magnet providing a field of 7T at the sample position (see p.29). This high-field reflectometer opens up exciting new possibilities, in particular for investigating thin magnetic films and nanostructures.

Two beamlines are installed at the 7T wiggler: a monochromatic beamline providing photons with energies between 4keV and 40keV for the instruments S2 and S3 and a white beamline providing photons of energies up to 150keV for the materials science instrument S4. The instrument S2 is specialised on resonant magnetic scattering and high resolution diffractometry, the instrument S3 on anomalous small-angle scattering (ASAXS) and grazing incidence scattering (GISAXS) (see p.28). S2 and S3 are operated alternatively at the monochromatic beamline. The instrument S4 at the white beamline is dedicated to materials science and engineering investigations, in particular to stress analysis using energy dispersive methods. All three wiggler instruments have been commissioned in 2005. S2 and S3 are in full user operation since April 2005, S4 since beginning of 2006. The X-ray tomography instrument S5 operated by HMI-BENSC at the 7T wavelength-shifter beamline of the Bundesanstalt für Materialprüfung (BAMline) at BESSY is in full user operation since 2004.

A detailed description of these five instruments is given in the new instrument brochure of BENSC which will be available end of 2006 and on the BENSC web pages.

	Main instrument characteristics	External groups	External beamtime	Inhouse groups	Inhouse beamtime
S1 at UE46	Spectroscopy/reflectometry	16	24 weeks	6	14 weeks
S2 at 7T-MPW	Res. magn. scatt./high-resol. diffract.	5	7 weeks	3	11 weeks
S3 at 7T-MPW	ASAXS/GISAXS (commissioning)	–	–	1	4 weeks
S4 at 7T-MPW	Materials Science stress analysis	6	10 weeks	5	6 weeks
S5 at BAMline	Tomography	20	24 days	5	6 days

**Table 2:** Short user statistics for HMI-BENSC instruments at BESSY in 2005

### Support for European Access to BENSC from the European Commission

Right from the beginning of the BENSC user programme in 1993, the access of European research groups to BENSC was generously supported by the European Commission under framework programmes FP3, FP4, FP5 and FP6 of the European Commission – with funds for the BENSC access programme increasing from contract to contract.

The successful European Access programme to BENSC is presently continued under the 6th EU Framework Programme (FP6), however, with a slightly modified contractual situation: BENSC is now a partner in the Integrated Infrastructure Initiative for Neutron Scattering and Muon Spectroscopy (NMI3). NMI3 brings together 23 partners from 14 countries, including 11 research infrastructures, together with other interested organisations. The most important branch of NMI3 includes 12 different Access Activities offering European users approximately 5000 beam days of access to 150 instruments at different facilities with support for travel and subsistence. Under NMI3, BENSC will provide a minimum access of 1040 instrument days, distributed over four years.

In 2005, the second year under NMI3, over 60 projects of European user groups have been completed. BENSC delivered 360 instrument days. A total of 119 users from 56 groups from 16 countries were involved. Since the start of NMI3, BENSC has thus provided already more than 800 days for the European user community.

### BENSC User Meeting 2005

The BENSC User Meeting held in September 2005 attracted more than 100 participants. One half of them came from national and foreign research institutions. 15 invited talks and 46 posters gave ample opportunity for lively discussions and scientific exchange on the latest results from experiments performed at BENSC.

### Scientific Results of Experiments performed at BENSC

Each short-term project carried out at BENSC must be followed by an *Experimental Report* within due time (not more than half a year delay). These are short descriptions of the experiments performed and the data obtained. It is clear that the results given in the reports can often only be preliminary. The reports are collected and published annually as *BENSC Experimental Reports*. They are distributed to all users of BENSC and give a complete overview on the scientific activities at BENSC. Starting with the year 2000 the *BENSC Experimental Reports* are also available on the BENSC web pages (<http://www.hmi.de/bensc/user-info/reports.htm>). Most important for the reputation of BENSC, however, are the regular publications of its users, a remarkably high fraction of them being published in high ranking journals.

Three examples of highlight results from external user groups are included in the Scientific Highlights Section of this Report.

# NAA Laboratory and Irradiation Service at BER II

D. Alber, G. Bukalis, B. Stanik, A. Zimmer  
 ■ HMI, SF6

The laboratory for neutron activation analysis (NAAL) at HMI's research reactor BER II provides irradiation services for universities, scientific institutions and industry. Typical fields of applications are:

- Trace elements analysis by means of neutron activation analysis (NAA) for example in biology, medicine, geology and archeology. Certification of reference materials.
- Irradiation experiments, such as isotope production for medical applications, sources for Mößbauer spectroscopy and production of tracers for scientific and industrial applications.

The operation and further development of the irradiation devices at BER II and of the NAA measuring systems are a central task of the department SF6.



**Fig. 1:** Granules of pure Silicon enclosed in ampoules made of highly pure silica

### Irradiation devices

Three irradiation devices are available for different applications.

- DBVK: irradiation device in the reactor core
- DBVR: rotatable irradiation device in the Beryllium reflector of the reactor core
- TBR: dry irradiation device outside the Beryllium reflector

DBVK and DBVR are used for long term irradiation experiments. Up to nine aluminum containers can be irradiated simultaneously. Short time irradiation experiments are carried out by means of TBR. A fast rabbit system (SRT) is closed for the time being.

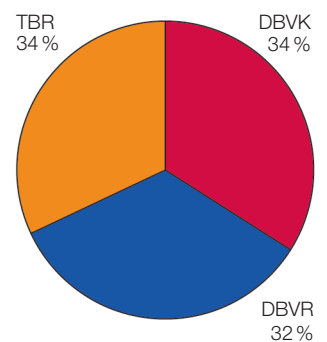
Device	$\Phi_{\text{thermal}}$ [1/cm <sup>2</sup> s]	$\Phi_{\text{fast}}$ [1/cm <sup>2</sup> s]	Container
DBVK	$1,5 \times 10^{+14}$	$4,3 \times 10^{+13}$	6
DBVR	$7,5 \times 10^{+12}$	$1,9 \times 10^{+10}$	9
TBR	$3,4 \times 10^{+12}$	$2,2 \times 10^{+10}$	1

### Irradiation Experiments 2005

Since June 2004, irradiation of destructible material, particularly biological material in the DBVK has been possible. Consequently, the contribution of this device rose from 9% in 2003 to about 35% in 2004 and 2005.

A total of about 3700 samples were irradiated in 2003. Two thirds of the 333 irradiation experiments were performed with the DBVK or DBVR. With these devices it is possible to irradiate up to 24 samples simultaneously in one aluminum container. About 48% of the irradiation experiments and the analysis of samples were done for external users.

Utilization of the different Irradiation devices



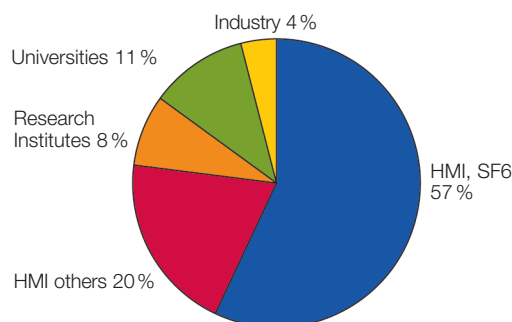
### Internal users

Most of the internal users are from the Dept. SF6, but irradiation and analyses were also performed for users from other departments (SF2, SF4, SE5, reactor department).

### External users

Irradiation experiments and NAA were performed for users from German universities (Berlin, Gießen, Mainz, Heidelberg, Leipzig, Munich, Kiel, Nuremberg) and from research institutes such as the Federal Institute for Materials Research and Testing BAM (Berlin), the Leibniz Institute for Zoo and Wildlife Research IZW (Berlin), the National Research Center for Environment and Health GSF (Neuherberg), DESY (Hamburg) and the Dresden branch of the Fraunhofer Institute for non-destructive testing.

Origin of Samples irradiated in 2005



# ISL Operations and Developments

Scientists: H. Homeyer, A. Denker, W. Pelzer, C. Rethfeldt, J. Röhrich

Operators: J. Bundesmann, R. Grünke, G. Heidenreich, H. Lucht, E. Seidel, H. Stapel

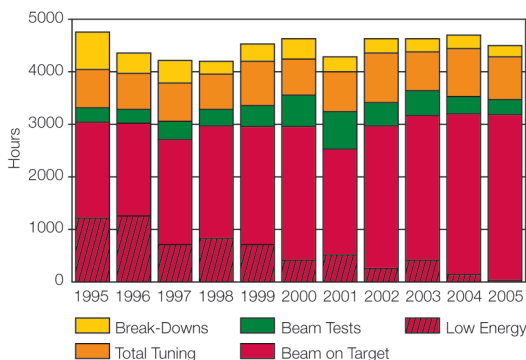


**Fig. 1:** ISL Operations since 1995: ISL's operation has been very stable over the past ten years. In 2005, the same beam time on target as 2004 could be produced with lower total scheduled operation time.

The Ion-Beam Laboratory ISL offers ion-beams from various accelerators and accelerator combinations with energies ranging from some tens of eV to several hundred MeV dedicated to the application of ion-beam techniques. Internal and outside users study the basics of the interaction of ions with solids. They modify and analyse materials with ion beams and they perform radiotherapy of eye tumours with fast protons in a joint venture with university clinics. Users have at their disposal 15 different irradiation areas equipped with specific instrumentation.

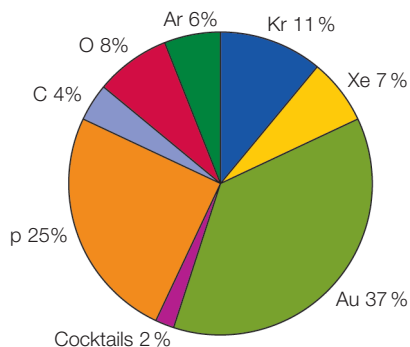


**Fig. 2:** Ions produced at ISL in 2005: Au-beams with a share of 37% are the most frequently used beams at ISL. Main applications are ion beam analysis (ERDA) and ion beam induced materials modifications.

ISL operations went smoothly in 2005 (see Fig. 1) except for one major breakdown. Over a shut-down weekend, a water leak arose at the RF-coupling loop of the RFQ leading to a complete flooding of the injector. It took some days for a complete repair, cleaning and drying.

Within the scheduled operation time of 4500 hours, 3200 hours of beam time on target were produced. The loss of scheduled beam time due to break-downs was again lower than 5%. The high reliability of 95% is essential for a successful user programme, in particular for the therapy of ocular melanomas with high energy protons. As in the years before, Au-ions and protons were again the most attractive beams used in 2005. Au-beams are used as projectiles for materials analyses and ion beam induced materials modifications. Apart from therapy, there is a large demand for high energy proton beams, either for high-energy PIXE, radiation hardness testing or device testing for a large proton therapy machine.

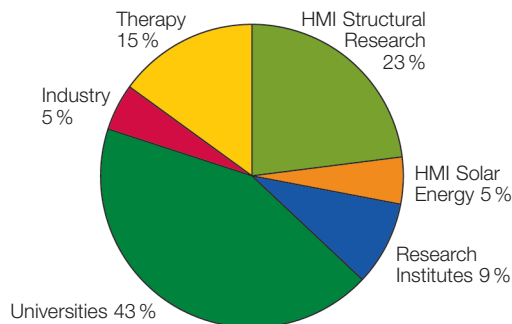


**Fig. 3:** Home institution of ISL-users: HMI-activities (SF4 and solar energy) use less than 30% of the beam time. University based researchers are still the largest subgroup at ISL.

In total, 39 different projects (49 in 2004) involving more than 100 scientists received beam time in 2005. In total, more than 80 projects were active at ISL. More than 40% of the users came from universities, their main topic of research being materials modifications. Research groups of the HMI use less than 30% of the beam time. This reflects ISL's importance as an outside user facility (see Figs. 3 and 5)

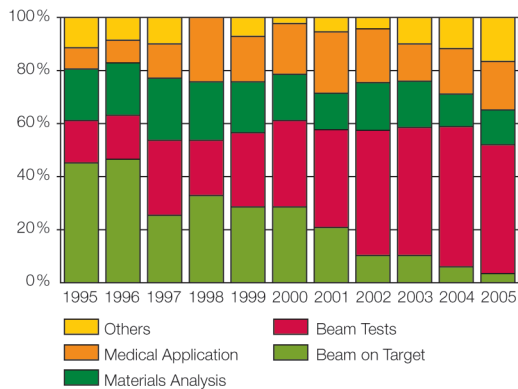


**Fig. 4:** Use of ISL ion beams: Materials modifications have become the largest part of research and development at ISL. The corresponding user groups come essentially from universities documenting ISL's importance for the FSI (*Forschung mit nuklearen Sonden und Ionenstrahlen* – Research with nuclear probes and ion beams.) community.

Materials analyses with an average of 15 % of the beam time have been performed exclusively with fast ions. The ERDA method uses the heaviest ions to determine the stoichiometry of thin layers for the solar cells development programme of the HMI. High-energy PIXE utilizes fast protons preferentially for the analysis of objets d'art or archaeological samples. Eye tumour therapy was performed at 10 therapy blocks (5 days/block) for more than 140 patients. The total medical share of 15 % includes beam time for research work. It turns out that, since 2002, the relative share of beam time for the different ion beam applications at ISL is relatively stable (see Fig. 4). The rise of "others" reflects guest activities in nuclear physics with the excellent ISL beams and the Q3D magnetic spectrometer. As shown in Fig. 5, the amount of beam time used by external users varies slightly around 70 %.

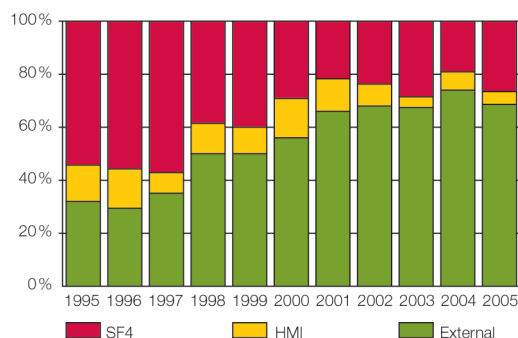


**Fig. 5:** User Facility ISL: development into a user facility. External users including proton therapy used 75 % of the beam-time in 2004.

Most of the development was dedicated to keeping the reliability of the facility in general. These activities included the replacement of CAMAC power supplies for the control system, power supplies for some quadrupole and dipole magnets and ion getter pumps. The upgrade of the control system was continued. Both ion sources are now being VISTA controlled.

The most important innovation was the end of the commissioning phase of the new ion source platform. The new platform has been in full operation since the beginning of 2006. Tuning new beams has become easier since the next beam can be started while the previous experiment is still running.



**Fig. 6:** New ion source platform: A rather unconventional layout of the new platform was necessary to fit it into the existing building

For the final 12 months of ISL's operations users applied for 368 shifts in addition to 96 shifts left over from the last meeting. At its last annual meeting before the shut-down of ISL by the end of 2006, the programme advisory committee carefully checked 48 proposals. On the basis of the proposals' scientific merit, their status and obligations 44 proposals, 20 new ones and 24 addenda to running experiments were accepted, partially with severe reductions of the applied beam-time.



398



# Scientific highlights Structural Research 2005

BENSC User Service	40
NAA User Service	46
SF1 Methods and Instruments	48
SF2 Magnetism	52
SF3 Materials	56
SF4 Structure and Dynamics	60
SF5 Theoretical Physics	62
SF6 Molecular Trace Element Research in the Life Sciences	64

# X-rays help find out how parts of historic organs were made

A. Manescu<sup>1</sup>, A. Giuliani<sup>1</sup>, F. Fiori<sup>1</sup>, B. Baretzky<sup>2</sup>

■ 1 Università Politecnica delle Marche, Dipartimento SASC, Ancona, Italy ■ 2 Max-Planck-Institut für Metallforschung, Stuttgart, Germany



**Fig. 1:** Organ in the Holy Ghost (Dominican Church) in Vilnius (Lithuania) built by Adam Gottlob Casparini (1715–1788) and completed in 1776. Brass tongues from similar organs were investigated in the experiments described in the present article.

## Introduction

The organ, one of the most sophisticated musical instruments, is an important symbol of European culture. Nowadays, one of the main problems organ builders have to confront is the difficulty in obtaining the warm and beautiful sound of historic organs by using modern materials and technologies. Achieving true Baroque sound requires overcoming significant materials science challenges, as it is known that the alloy composition and properties of the pipes strongly influence the organ sound [1]. An organ contains flue and reed pipes made of lead-tin alloys. There are no moving parts within a flue pipe. Reed pipes, however, contain an additional vibrating part, the copper-based alloy tongue that crucially influences its sound (see Fig. 3). A reed pipe produces a sound when wind entering the bottom of the pipe causes the small brass tongue to vibrate against the shallot. The sound produced this way is amplified then by the resonator.

We focused our research on determining the residual stresses – inner stresses present in the metallic material – of these brass tongues. From the literature [2] we found out the main processes the tongues were submitted to: hammering, cutting into a neat shape, annealing,

filing to achieve a neat thickness and inducing of the needed curvature at the end of the manufacturing cycle.

Hammering induces compressive residual stresses in the surface layers of the tongue. Annealing relaxes such stresses. In order to bring the tongue to the optimal thickness it is filed. It is important that the tongue is filed equally across its whole width so it is not distorted when vibrating [3]. Mechanical surface processing like grinding or filing are well known to have a deep impact on materials inducing further residual stresses. In order to be able to vibrate, the tongue must have a curvature at its free end, the other end being fixed by the wedge in the block. This curvature induces opposite residual stresses, tensile in the concave side and compressive in the other side of the tongue. However, the curvature induced stresses should be low due to the low level of the curvature.

In conclusion, the stress profiles in the brass tongues are the result of stress overlapping due to different manufacturing processes. As very few information from Baroque organ builders is available, the information obtained from the residual stress analysis is important because it gives modern organ builders a confirmation regarding the processes the tongues were submitted to and it helps them in their work of trying to reproduce the warm and beautiful sound of old organs. For determining the residual stresses at different depths in the organ tongues we chose to perform an energy dispersive diffraction experiment using white beam synchrotron radiation, i.e. synchrotron radiation containing a wide range of wave lengths. As residual stresses lead to distortions in the crystal structures of the crystallites making up the material, they can be detected using diffractive methods. Using a white beam, we not only recorded simultaneously a multitude of reflections in a single energy spectrum, but we also obtained additional depth information because the reflections differ in their energy, which is directly related to the material absorption.

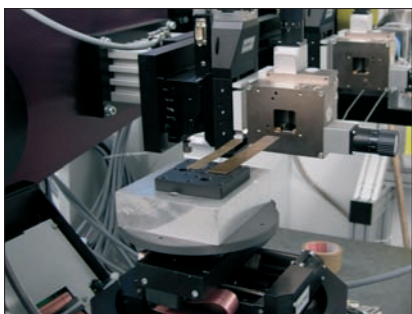


**Fig. 2:** The brass tongues from a baroque organ during the investigation at the EDDI beamline operated by the Hahn-Meitner-Institut at the synchrotron radiation source BESSY

### The Experiments

We received historic tongues from the following organs:

- Henk van Eeken, Netherlands, XVIII century
- Rimantas Gucas, Lithuania, XVIII century, Organbuilder: Jansen
- Mats Arvidsson, Överselö Church (Sweden), 1754, Johan Gren & Peter Stråhle
- Henk van Eeken, Magnuskerk Anloo (Netherlands), 1719, Organbuilder: Johannes Radeker and Rudolf Garrels
- Rimantas Gucas, Lithuania, 1780, Organbuilder: Miknevičius

The experiments were performed at the Berlin synchrotron source BESSY on the EDDI-beamline operated by the Hahn-Meitner-Institut. We used white radiation in an energy range from 10 to about 100 keV provided by a 7T multipole wiggler. The average dimensions of the samples were: 120mm × 15mm × 0.7mm. We analysed each organ tongue in three areas (see Fig. 4).

### Results

We observed the presence of compressive stresses in all the analysed samples, close to the surface of the tongues, due to the process of hammering. These stresses vary from sample to sample, depending on the force applied during hammering and depending on possible annealing treatments, between sequential hammering cycles, that partially relax such compressive stresses. We can consider the orthogonal stress as being the stress induced by hammering-annealing processes. In all samples, the orthogonal stresses remain constant in the different analysed points on the front side and also in the point on the back side of the tongues. The next result is that from a qualitative point of view and close to the sample surface, after the filing treatments, all the samples exhibit, in the direction parallel to the process a relaxation of the compressive stress induced by hammering. Also, a clear difference in some tongues can be observed between the values of the residual stresses in the filing direction in the fixed, middle and vibrating points. The tongues were more filed in the middle and vibrating part than in the fixed part. In four of the five analysed tongues, we observed less compressive stresses in the parallel direction in respect with the orthogonal direction for both sides of the tongues, which means that the filing was performed both on the front and on the back side of the tongues.

In conclusion, the energy dispersive diffraction experiment performed on historic brass tongues allowed us to identify the main manufacturing processes the tongues were submitted to, giving this way precious information to the organ builders in their work of reproducing the beautiful sound of Baroque organs.

### Acknowledgements

The authors would like to thank Dr. Christoph Genzel and his team at the outstation of the Hahn-Meitner-Institut at BESSY for their theoretical and experimental support, Prof. F. Rustichelli for consultation on tongue processing effects on residual stresses. They are further indebted to the Hahn-Meitner-Institut and BESSY for beamtime allocation. This research project has been supported by the European Commission under the 6<sup>th</sup> Framework Programme through the Key Action: Strengthening the European Research Area, Research Infrastructures. Contract n°: RIII3-CT-2003-505925 (NMI3). Finally the authors wish to express their thanks to the TRUESOUND European Project (CT.FP6-2002-SME-1 005876) partners, for the availability of the organ brass tongues and their precious consultation.

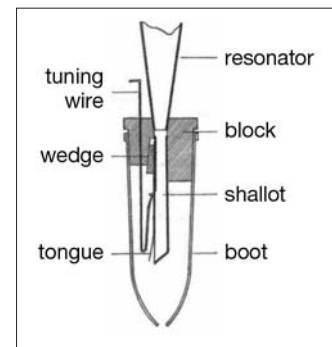


**Fig. 3:** Scheme of a reed pipe

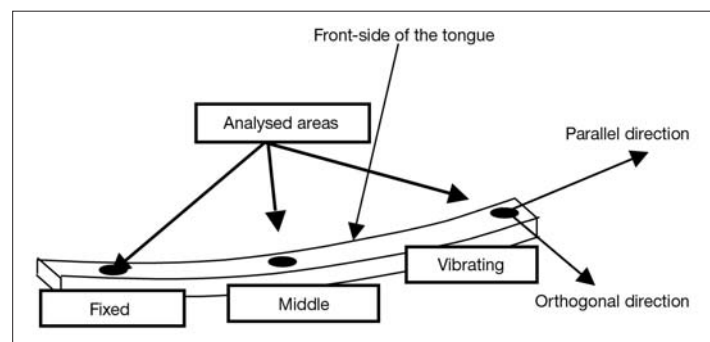


**Fig. 4:** Measurement points and directions in the investigation of organ tongues by x-ray diffraction

- [1] M. Kob, *Acta Acustica* **86** 642–648 (2000); W. Kluge, *Acta Organologica* **15** 181–212 (1981)
- [2] R. Gug, *Historic and experimental studies on brass used for reed tongues*, FOMRHI-Quarterly, **41**, Oxford (1998)
- [3] Geoffrey Crabb, *Concertina Reed Production – The Crabb Method*, [http://www.concertina.net/gc\\_make\\_reeds.html](http://www.concertina.net/gc_make_reeds.html), 2003

### Corresponding author:

A. Manescu  
a.manescu@alisf1.univpm.it

# Magnetic field-induced antiferromagnetism in a cuprate high-temperature superconductor

B. Lake<sup>1,2</sup>, K. Lefmann<sup>3</sup>, N.B. Christensen<sup>3</sup>, G. Aeppli<sup>4</sup>, D.F. McMorrow<sup>3,4</sup>, H.M. Ronnow<sup>5</sup>, P. Vorderwisch<sup>1</sup>, P. Smeibidl<sup>1</sup>, N. Mangkorntong<sup>6</sup>, T. Sasagawa<sup>6</sup>, M. Nohara<sup>6</sup>, H. Takagi<sup>7</sup>

■ 1 HMI ■ 2 Ames Laboratory and Department of Physics and Astronomy, Iowa State University, Ames, USA

■ 3 Materials Research Department, Risø National Laboratory, Roskilde, Denmark ■ 4 London Centre for Nanotechnology and Department of Physics and Astronomy, University College London, London, UK

■ 5 Laboratory for Neutron Scattering, Paul-Scherrer-Institut & ETH-Zurich, Switzerland ■ 6 Department of Advanced Materials Science, University of Tokyo and CREST-JST, Kashiwa, Japan ■ 7 RIKEN (The Institute of Physical and Chemical Research), Wako, Japan

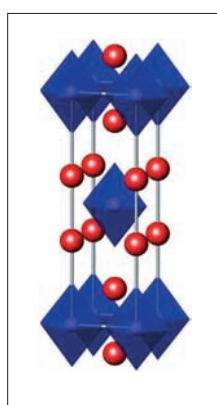


**Fig. 1:** Structure of a  $\text{La}_{2-x}\text{Sr}_x\text{CuO}_4$  (LSCO) crystal. The red balls stand for the lanthanum or strontium atoms. The oxygen atoms are located at the vertices of the blue octahedra, the copper atoms at their centres. Superconductivity occurs in the horizontal planes defined by the copper and oxygen atoms.

High temperature superconductors have been an active area of research for the past 20 years. The materials consist of nearly square  $\text{CuO}_2$  lattices alternating with  $\text{LaO}$  charge reservoir layers (Fig. 1). Replacing Lanthanum (La) with Strontium (Sr) – hole-doping – gives rise to superconductivity for certain concentrations of Sr. They are described as strongly correlated electron systems where exotic behaviour arises from competition on a quantum mechanical level involving collective electronic states such as antiferromagnetism, charge stripe order, non-fermi liquid behaviour as well as superconductivity. The mechanism for the superconducting process is not yet understood and is an active research field. In an applied magnetic field high temperature (high- $T_c$ ) superconductors behave like type-II superconductors: magnetic flux is able to penetrate the system via the formation of vortices, which are normal state metallic cylinders each carrying one flux quantum. The vortices form a lattice of resistive material embedded in the non-resistive superconductor. The vortex density increases with increasing field, and when the upper critical field  $H_{c2}$  is reached, superconductivity is destroyed altogether.

In the high- $T_c$ s the superconducting coherence length is anisotropic and small, in fact it is less

than the separation of the copper oxide planes. This means that three-dimensional superconductivity is only achieved via Josephson coupling between the planes. The superconducting coherence length is also a measure of the vortex size and the vortices are best regarded as two-dimensional disks or ‘pancakes’. Couplings regulating the stacking of the pancakes are therefore important for the establishment of phase coherent superconductivity in applied magnetic fields.

Here we discuss the effects of applied magnetic field on the high temperature, cuprate superconductor  $\text{La}_{2-x}\text{Sr}_x\text{CuO}_4$  (LSCO) with  $x=0.10$  and a superconducting transition temperature of  $T_c=29\text{K}$ . Previous measurements on LSCO indicate weak, long-period magnetic order in zero-field derived from defects which differ from sample to sample, and stronger field-induced order with all of the hallmarks of an intrinsic effect [1], including sample-independence and a sharp onset temperature indistinguishable from  $T_c$ . In all previous experiments the field was vertical and perpendicular to the  $\text{CuO}_2$  planes. This precluded an examination of the important inter-planar magnetic correlations. In these current measurements the field is now horizontal, allowing the field to be applied along the  $c$  direction and at the same time giving access to the out-of-plane magnetic correlations. What makes this experiment much more difficult than previous measurements is the restricted access of the neutron beam to the sample in the more complex magnet and the imperfect match between the signal shape (in reciprocal space) and the instrument resolution function.

The antiferromagnetic order was measured by neutron diffraction using the V2/FLEX triple axis spectrometer and the HM1 horizontal field magnet (Fig. 2). The details of the experiment are discussed in detail in the original publication [1]. In this report, we concentrate on the interpretation of the results.

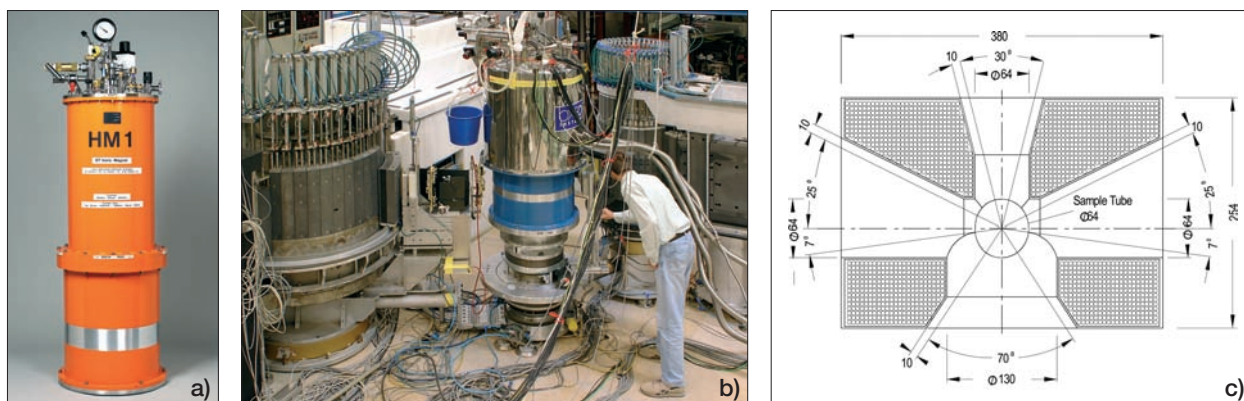


**Fig. 2:** a) The horizontal field magnet HM1 b) The Triple-Axis-Spectrometer V2/FLEX with a different cryomagnet mounted than the one used in the experiment c) Cross-section of the horizontal-field magnet (HM1). The magnet has four windows through which neutrons can pass, separated by four blind spots (hatched regions) which are opaque to neutrons. The LSCO crystal lies at the centre of the magnet.

Fig. 3a and 3b show a potential model of the zero-field order, the black dots represent the  $\text{Cu}^{2+}$  ions and the red arrows attached to them represent both the size and relative ordering direction of their spin moments. We envisage that there are magnetic regions within the crystal possibly nucleated by defects. These magnetic patches have large spatial extent within the  $\text{CuO}_2$  planes. They however have only small spatial extent perpendicular to the  $\text{CuO}_2$  planes giving rise to weak modulations in that direction. When a magnetic field is applied to LSCO, vortices are formed which thread through the superconductor parallel to the field. For a field applied parallel to **c** the vortices would be able to link the pre-existing antiferromagnetic regions along this direction providing a mechanism by which the magnetic correlations between the  $\text{CuO}_2$  layers are enhanced (Fig. 3b). The increased magnetic correlation length in the out-of-plane direction would be observed as an enhancement of the magnetic signal at the reciprocal lattice points as found experimentally.

These results are interesting for a number of reasons, firstly they imply that the field-induced magnetism is an intrinsic property of this material, secondly they show that a magnetic field can be used to tune the degree of interlayer coupling while at the same time varying the onset temperature for phase coherent superconductivity. Thirdly our results link the field-induced magnetism directly to the formation of vortices revealing the close interplay between magnetism and superconductivity in the high- $T_c$ s.

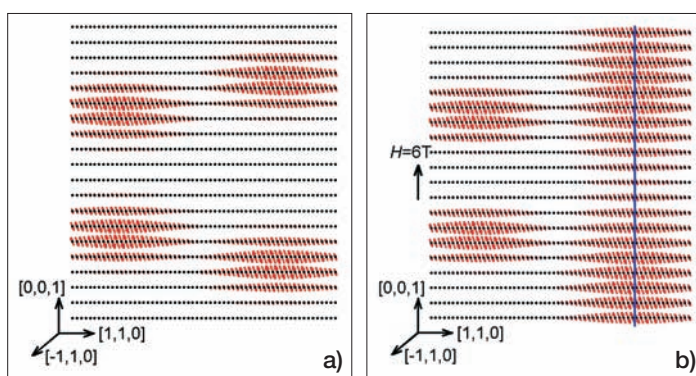


**Fig. 3:** Interpretation of the neutron scattering data. In zero field, **a**), defects nucleate magnetically ordered regions. The defects are located on the  $\text{LaO}_2$  planes and give rise to ordering in the neighbouring  $\text{CuO}_2$  planes; in the diagram, only the magnetic  $\text{Cu}^{2+}$  ions are shown, these are represented by the black dots while the size and direction of their ordered moments are represented by the red arrows. The magnetic regions are limited to a few  $\text{CuO}_2$  planes, but have large spatial extent within the planes (reduced here for visualization) and they are characterised by an inversion in the magnetic ordering at the bond-centred defect site. When a magnetic field is applied along the **c**-axis, vortices thread through the material parallel to the field. If a vortex (blue line) passes through a magnetically ordered region it increases the number of planes over which ordering extends as shown in **b**).

- [1] B. Lake, et al. *Nature Materials* **4**, 658–662 (2005)
- [2] B. Lake, et al. *Nature* **415**, 299–302 (2002)
- [3] T. Suzuki, et al. *Phys. Rev. B* **57**, R3229–R3232 (1998)
- [4] Xu, G. Y., et al. *Science* **289**, 419–422 (2000)

**Corresponding author:**

B. Lake  
bella.lake@hmi.de

# Neutron diffraction studies of $R_2Fe_{17}$ ( $R=Y, Lu$ ) intermetallics under pressure

J. Kamarád<sup>1</sup>, O. Prokhnenko<sup>1,2</sup>, K. Prokeš<sup>2</sup>, Z. Arnold<sup>1</sup>

■ 1 Institute of Physics AS CR, Prague, Czech Republic ■ 2 HMI, SF2

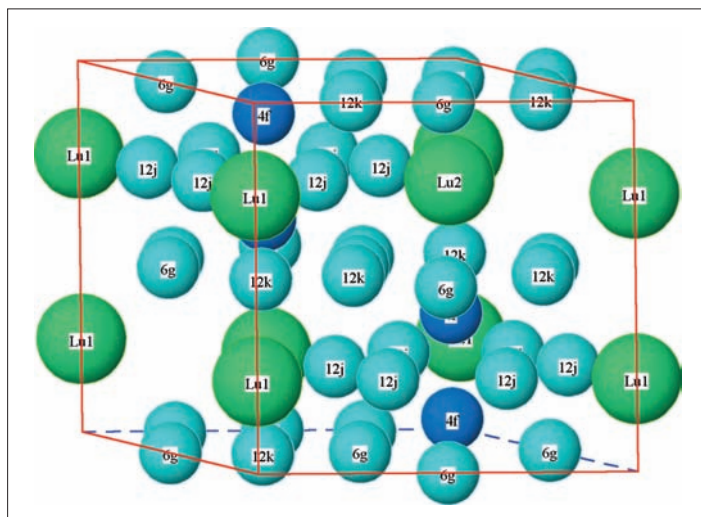


**Fig. 1:** Schematic representation of the layered crystal structure of  $Lu_2Fe_{17}$ . One hexagonal unit cell contains four lutetium (Lu) atoms in two inequivalent positions and thirty-four Fe atoms in four different crystallographic positions that are indicated by the so called Wyckoff symbol.

There are two main conditions for the occurrence of magnetic ordering: the existence of individual magnetic moments and the strength of an exchange interaction between the moments. Both factors depend mainly on the type, distances and geometry of the arrangement of atoms involved and can be influenced by temperature (thermal movement tries to destroy the geometrical arrangement of the moments, magnetic order exists only below a critical temperature), pressure (pressure compresses the atoms closer to each other destabilizing the individual moments) and magnetic fields (moments try to minimize their energy with respect to the field by rotating to an energetically more favourable orientation – this may change the type of order).

There are many types of magnetic ordering. The two basic types are

1. ferromagnetism: below the so called Curie temperature  $T_C$ , all moments point in the same direction leading to a non-zero magnetization
2. antiferromagnetism, in which below the Néel temperature  $T_N$ , for every magnetic moment pointing into one direction, there is another mo-

ment with exactly the opposite direction. This arrangement leads to zero net magnetization. From the point of view of the direction of moments, one can distinguish between collinear magnetic structures, where all the moments point along a single direction and non-collinear, in which more directions exist.

In this contribution, one particular type of magnetic order will be discussed – helimagnetic order, in which competing exchange interactions exist. As a result, the moments are arranged ferromagnetically within the planes. The direction, however, changes by a certain angle as one moves to the subsequent plane due to antiferromagnetic interaction between the planes. So, the individual planes in helimagnetic structures are ferromagnetic, but the sample as a whole exhibits zero magnetization.

Neutron diffraction plays a crucial role in the identification of magnetic structures because the neutron's magnetic moment can interact with periodically arranged magnetic moments resulting in interference phenomena that carry useful information regarding the coupling, direction and size of magnetic moments. As neutrons only weakly interact with most elements, one can use rather complicated sample environments – required to “prepare” suitable conditions for the existence of a particular magnetic phase – in the diffraction experiments.

Recent results have again drawn attention to non-collinear magnetism in iron and its alloys. Both, theoretical and experimental studies of these structures have been intensified and great progress has been reached in a description of the spin dynamics in systems where magnetism is caused by electrons that are almost free to move (the case of Fe). Recent studies of volume-change effects in the  $R_2Fe_{17}$  compounds under magnetic field with non-magnetic R-atoms (Y, Lu) have brought indispensable information [1]: Magnetization measurements showed that the ferromagnetic ordering in  $Y_2Fe_{17}$  is drastically modified under high pressure. The results indicated the presence of a pressure-induced non-collinear magnetic structure. This fact became subject of a controversy in the last decade because theoretical calculations did not indicate the instability of the ferromagnetic phase in this compound [2].

In contrast to those in  $\text{Y}_2\text{Fe}_{17}$ , the Fe-moments in  $\text{Lu}_2\text{Fe}_{17}$  order helimagnetically below the Néel temperature  $T_N = 275\text{ K}$  due to a competition of the ferromagnetic and the antiferromagnetic exchange interactions between the Fe-ions on different crystallographic sites [3]. With decreasing temperature and simultaneously increasing volume, the ferromagnetic exchange interactions dominate and helimagnetism transforms towards the ferromagnetic ground state below  $\Theta_T = 140\text{ K}$  with moments still confined within basal planes. At temperatures between  $T_N$  and  $\Theta_T$ , the Fe-moments remain collinear within the basal planes, but their direction changes from plane to plane on moving along the  $c$ -axis. The ferromagnetic ground state of  $\text{Lu}_2\text{Fe}_{17}$  can be also totally suppressed by a mediate hydrostatic pressure.

Despite technical complexity and resulting experimental limitations, we have decided to verify the changes of the magnetic structures as a function of pressure and magnetic field on a microscopic scale. We have performed several neutron diffraction experiments on small single crystals under pressure produced by a small clamped-type CuBe pressure cell that fits into several cryomagnets available at HMI. The single crystals of  $\text{Y}_2\text{Fe}_{17}$  and  $\text{Lu}_2\text{Fe}_{17}$  were fixed inside the pressure cell and placed in a vertical superconducting magnet with the  $a$ -axis being parallel to the magnetic field of up to 6.5 T. A mixture of mineral oils was used as a hydrostatic pressure-transmitting medium up to pressure 1.1 GPa in the cell. The details of the experimental results can be found in the original publication [4]. Here, we discuss the conclusions concerning the observed magnetic structures.

Measurements performed at the pressure 0.8 GPa revealed a helimagnetic structure in  $\text{Y}_2\text{Fe}_{17}$  in a narrow temperature range between 235 K and 255 K. In the temperature range 230 K down to 2 K under pressure of 0.8 GPa the gradual development of the ferromagnetic component can be observed. At a pressure of 1.05 GPa, a magnetic structure was found even at 2 K. However, the scans at temperatures from 2 K up to 270 K showed that the magnetic structure disappears in an intermediate temperature range between 115 K and 150 K. It is for the first time that this kind of discontinuity has been observed in the temperature behaviour. The pressure induced magnetic phase at higher temperature differs most probably from the one at low temperature. It follows from the experiments that the ferromagnetic arrangement of Fe-moments in  $\text{Y}_2\text{Fe}_{17}$  transforms into the incommensurate helimagnetic structure with increasing pressure, i.e. with decreasing volume. At 5 K and 1.05 GPa, the angle between Fe-moments in the adjacent basal planes amounts to  $19.35^\circ$ .

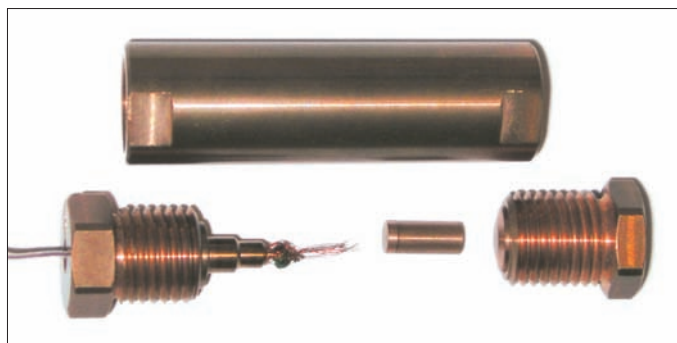


**Fig. 2:** CuBe clamped cell used in the pressure experiments. Below the main body of the cell from the left to the right: the fixing screw with the manganin pressure sensor and electrical leads, piston and the opposite fixing screw.

Neutron diffraction measurements on the  $\text{Lu}_2\text{Fe}_{17}$  single crystal confirmed the existence of three magnetic phases in  $\text{Lu}_2\text{Fe}_{17}$  already at ambient pressure. At the temperature  $\Theta_T = 140\text{ K}$ , a transition from the ferromagnetic ground state into the incommensurate helimagnetic structure occurs. An application of magnetic field along the  $a$ -axis of  $\text{Lu}_2\text{Fe}_{17}$  at 200 K results in the transition from the helimagnetic to the ferromagnetic phase. All these features show different character of the helimagnetic-ferromagnetic transitions induced by the temperature and/or forced by the magnetic field at ambient pressure. The detailed mechanism of the field induced transformation (e.g. through a distorted elliptical spiral) has to be solved unambiguously by further investigation.

#### Acknowledgments

The financial support of the projects 202/04/P014 GACR and AV0Z10100521 is acknowledged. This research project has been also supported by the European Commission under the 6<sup>th</sup> Framework Program through the Key Action: Strengthening the European Research Area, Research Infrastructures. Contract n<sup>o</sup>: RII3-CT-2003-505925 (NMI3)

- [1] Z. Arnold, J. Kamarád, P.A. Algarabel, B. Garcia-Landa, M.R. Ibarra, IEEE Trans. Mag. **30**, 619 (1994)
- [2] R.F. Sabirianov, S.S. Jaswal, Phys. Rev. B **57**, 7767 (1998)
- [3] D. Givord, R. Lemaire, IEEE Trans. Magn. **MAG-10**, 109 (1974)
- [4] O. Prokhnenko, J. Kamarád, K. Prokeš, Z. Arnold, A.V. Andreev, Phys. Rev. Lett. **94**, 107201 (2005)

#### Corresponding author:

K. Prokeš  
prokes@hmi.de

# Use of arsenic isotopes for molecular imaging and endoradiotherapy

M. Jahn, M. Jennewein, M. Piel, F. Rösch

■ Institute of Nuclear Chemistry, Johannes Gutenberg-University, Mainz, Germany

Positron emission tomography (PET) is a non-invasive diagnostic imaging technique for measuring the metabolic activity of cells in the human body. It is particularly useful clinically in patients with certain diseases affecting the brain, heart and in patients with certain types of cancer. PET is unique because it produces images of the body's basic biochemistry and functions. Chemical compounds are labeled with radioactive atoms that decay by emitting positrons. The positron combines with an electron in the medium and is annihilated into two 511 keV photons that are emitted in coincidence at 180°. This radiation is detected outside the body, and it is possible to localize and quantify the measured activity in vivo. The standard positron emitters  $^{11}\text{C}$  ( $T_{1/2}=20\text{ min}$ ) and  $^{18}\text{F}$  ( $T_{1/2}=109\text{ min}$ ) allow only the observation of relatively fast biological processes. In contrast the element arsenic provides a range of radioactive isotopes with potential interest in radiopharmaceutical chemistry and PET. In particular, the long half-lives of  $^{72}\text{As}$  ( $T_{1/2}=26\text{ h}$ , 88%  $\beta^+$ ) and  $^{74}\text{As}$  ( $T_{1/2}=17.8\text{ d}$ , 29%  $\beta^+$ ) allow the investigation of slow physiological or metabolic processes, like the enrichment and distribution of antibodies in tumor tissue or cell trafficking.  $^{77}\text{As}$  ( $T_{1/2}=38.8\text{ h}$ , 100%  $\beta^+$ ) is used for the development of new labeling strategies with arsenic because it is easily accessible

at nuclear reactors. It also might be used in tumor-targeting radiotherapeutics because of its low  $\gamma$ -dose rate and its moderate average  $\beta^-$ -range (1.2 mm) in tissue. It was thus the aim of this project, to investigate (i) the production route of high batch activities of  $^{77}\text{As}$ , (ii) its effective chemical separation and (iii) the use of  $^{77}\text{As}$  to study radiopharmaceutical synthesis strategies with radioarsenic.

## Production of isotopes

All arsenic isotopes can be produced by irradiating  $\text{GeO}_2$ -Targets.  $^{77}\text{As}$  is the most important radionuclide for the development of new arsenic radiopharmaceuticals because its production is very cheap compared to the cyclotron produced positron emitters  $^{72}\text{As}$  and  $^{74}\text{As}$ . These are only used when the labeling chemistry of a radiopharmaceutical has been optimized with  $^{77}\text{As}$ .  $^{77}\text{As}$  is produced via  $^{76}\text{Ge}(n, \gamma)^{77}\text{Ge} \rightarrow \beta^- (T_{1/2}=11.3\text{ h}) \rightarrow ^{77}\text{As}$  at the TRIGA reactor of the Institute of Nuclear Chemistry of the University of Mainz ( $\phi=4.0 \times 10^{12}\text{ n/cm}^2\text{ s}$ ). All irradiations were performed using 100 mg of  $^{76}\text{GeO}_2$ . Due to the low neutron capture cross section of  $^{76}\text{Ge}$  ( $\sigma=0.15\text{ barn}$ ) and its low natural abundance (7.44%), 6 h of irradiation yields about 2 MBq of  $^{77}\text{As}$  12 h after reactor shut down. This is enough for chemical experiments while for ERT much higher activities of about 4 GBq are needed. Thus  $^{76}\text{GeO}_2$  targets were irradiated for 96 h at the reactor BER II of the Hahn-Meitner-Institut to yield about 1.5 GBq of  $^{77}\text{As}$  (calculated). Due to logistic problems the maximum activity isolated from the target in Mainz was about 200 MBq, so some logistics need to be optimized. For future applications the use of highly enriched  $^{76}\text{GeO}_2$  targets is aimed. This would increase the maximum achievable  $^{77}\text{As}$  activity by a factor up to 13 and simultaneously decrease the formation of byproducts like  $^{71}\text{Ge}$  and  $^{75}\text{Ge}$  significantly. At high flux reactors the production of enough  $^{77}\text{As}$  for ERT is possible.

The positron emitting arsenic isotopes  $^{74}\text{As}$  and  $^{72}\text{As}$  are produced at cyclotrons. Indirectly,  $^{72}\text{As}$  can be also produced as a daughter radionuclide of the relatively long-lived  $^{72}\text{Se}$  ( $T_{1/2}=8.5\text{ d}$ ). This  $^{72}\text{Se}/^{72}\text{As}$  radionuclide generator [1,2] has the advantage of avoiding cyclotron in house production of  $^{72}\text{As}$ .

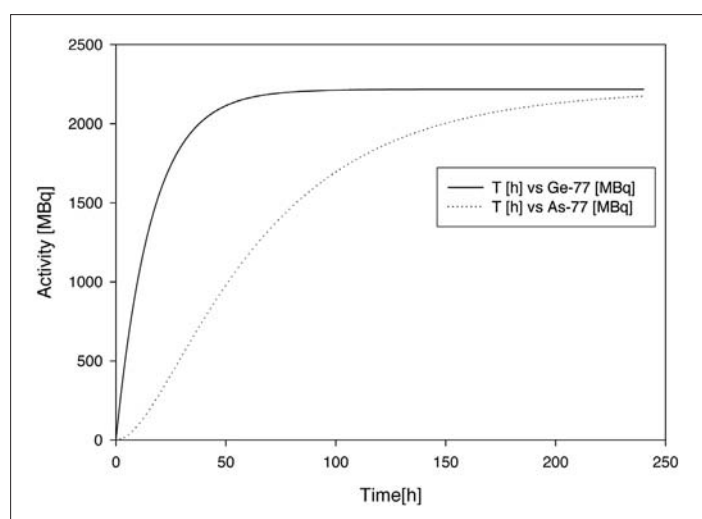
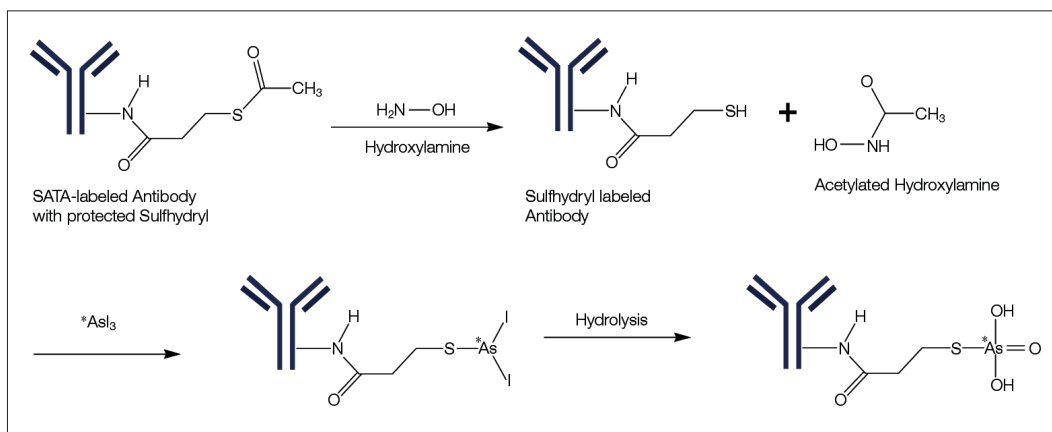


Fig. 1: Calculated kinetics of the activation of 230 mg  $^{nat}\text{GeO}_2$  at BER II



**Fig. 2:** Reaction scheme for labeling of SATA-modified antibodies with radioactive arsenic isotopes

### Separation of arsenic from the target

Irradiated germanium oxide targets were dissolved in 5 ml HF at room temperature for 1 h whereby GeF<sub>6</sub><sup>2-</sup> is formed [3]. Potassium iodide was added for the quantitative formation of [<sup>77</sup>As]AsI<sub>3</sub>. The mixture was transferred to an ENV-solid phase extraction cartridge and [<sup>77</sup>As]AsI<sub>3</sub> was fixed to the solid phase, while macroscopic GeF<sub>6</sub><sup>2-</sup> was eluted quantitatively with the mobile phase. The elution of the [<sup>77</sup>As]AsI<sub>3</sub> was performed with 500–1000 µl of various organic solvents and directly used as labeling synthon.

### Radiolabelling of antibodies

As a proof-of-principle study for the application of arsenic labeled compounds in biological systems, the high affinity of arsenic to sulfur was utilized to conjugate arsenic to HS-protein structure elements. SATA (N-Succinimidyl-S-acetylthioacetate) was applied [4] to increase the number of free

sulfhydryls in the protein (Fig. 2). Deprotection of the sulfhydryl groups with hydroxylamine was performed directly before the labeling. For subsequent radioarsenic labelling of the proteins, a [<sup>77</sup>As]AsI<sub>3</sub> containing ethanolic solution was added to the solution of the SATA modified proteins and the [<sup>77</sup>As]AsI<sub>3</sub> was coupled to one SH under elimination of iodide. First biodistribution studies, autoradiography and PET of SATA-derivatised antibodies were performed (Fig. 3).

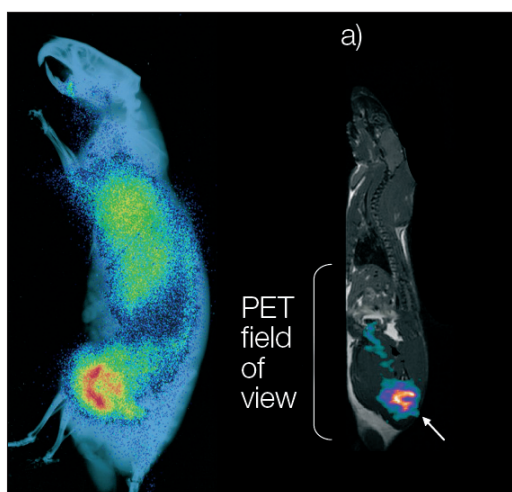


**Fig. 3:** Autoradiography of [<sup>77</sup>As]SATA-ch3G4 and [<sup>74</sup>As]SATA-ch3G4 small animal PET

- [1] Jennewein, M., et al., *A no-carrier-added <sup>72</sup>Se/<sup>72</sup>As radionuclide generator based on solid phase extraction*. *Radiochimica Acta*, **93** (9–10), 579–583 (2005)
- [2] Jennewein, M., et al., *A no-carrier-added <sup>72</sup>Se/<sup>72</sup>As radionuclide generator based on distillation*. *Radiochimica Acta*, **92**, 245–249 (2004)
- [3] Jennewein, M., et al., *A new method for radiochemical separation of arsenic from irradiated germanium oxide*. *Appl Radiat Isot*, **63** (3), 343–51 (2005)
- [4] Duncan, R.J., et al., *A new reagent which may be used to introduce sulfhydryl groups into proteins, and its use in the preparation of conjugates for immunoassay*. *Anal Biochem*, **132** (1), 68–73 (1983)

### Corresponding author:

M. Jahn  
jahnma@uni-mainz.de

# Where are the limits of non-exponential relaxation?

C. Pappas<sup>1</sup>, A. Hillier<sup>2</sup>, P. Manuel<sup>2</sup>, R. Cywinski<sup>3</sup>, I.A. Campbell<sup>4</sup>, P. Bentley<sup>1</sup>, F. Mezei<sup>1</sup>

■ 1 HMI, SF1 ■ 2 ISIS, Didcot, UK ■ 3 Physics and Astronomy Department, University of Leeds, UK

■ 4 Université de Montpellier 2, France

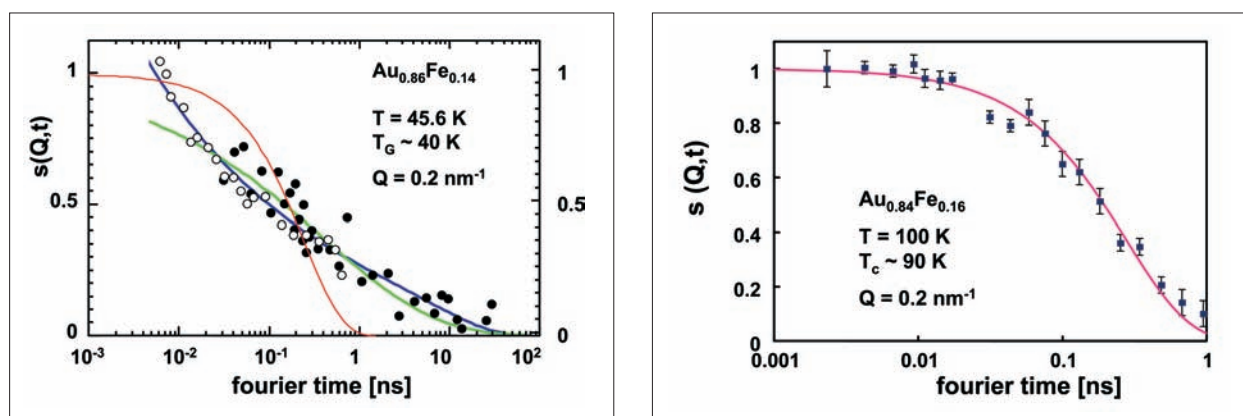


**Fig. 1:** NSE signal of the spin glass  $\text{Au}_{0.86}\text{Fe}_{0.14}$  and the disordered ferromagnet  $\text{Au}_{0.84}\text{Fe}_{0.16}$ . Both spectra were collected at  $Q=0.2\text{ nm}^{-1}$  and at 10% above the corresponding ordering temperatures slightly above  $T_C$ . The continuous red lines are the best fit of the data to a simple exponential decay. The eminently non-exponential decay of the spin glass  $\text{Au}_{0.86}\text{Fe}_{0.14}$  is best fitted by the so-called Ogielski function  $t^{-\beta}\exp[-(t/\tau(T))^\beta]$  (blue line).

Non-exponential relaxation is a general phenomenon found in systems as diverse as glasses, spin glasses, heavy fermions, polymers, biological systems, financial markets, earthquakes etc. Even though these very different and complex disordered systems show strong similarities, the existence of universal relaxation functions and mechanisms is still an open question. The situation is even more complex, when disorder is too weak to completely overcome and destroy the long-ranged spatial periodical order. In systems like disordered ferro- and antiferromagnets, neutron scattering reveals a purely exponential spin relaxation in contradiction with long standing theoretical arguments first introduced by Griffiths [1], which predict anomalous effects and non-exponential relaxation [2,3]. This puzzling and enduring discrepancy between theory and experiment incites to go beyond the existing experimental results and investigate relaxation of disordered ferromagnets at different length and time scales by combining zero field muon spin relaxation ( $\mu\text{SR}$ ), a local probe, with the mesoscopic time and length scales of Neutron Spin Echo (NSE) spectroscopy.

The solid solution  $\text{Au}_{1-x}\text{Fe}_x$  is an archetype disordered ferromagnet, where the magnetic moments, carried by the  $\text{Fe}^{3+}$  ions, are randomly

distributed over the non-magnetic Au fcc lattice. The oscillatory RKKY magnetic interactions lead to positive (ferromagnetic) nearest-neighbour interactions, negative (antiferromagnetic) next nearest neighbour interactions and so on. The system is a disordered ferromagnet at high Fe concentrations and becomes a spin glass at  $x < x_C$ , with  $x_C \sim 0.155$ , a concentration between the nearest neighbour and next nearest neighbour site percolation thresholds for the fcc lattice. In spite of the dilution, the strong magnetic moments of  $\text{Fe}^{3+}$  ( $S=5/2$ ) and their ferromagnetic correlations make this system ideal for neutron and muon spectroscopy. The samples covered the whole spectrum from the spin glass phase with  $\text{Au}_{0.86}\text{Fe}_{0.14}$  ( $x=0.14$ ) to the disordered ferromagnetic phase with  $\text{Au}_{0.84}\text{Fe}_{0.16}$ ,  $\text{Au}_{0.82}\text{Fe}_{0.18}$  and  $\text{Au}_{0.80}\text{Fe}_{0.20}$  ( $x=0.16, 0.18$  and  $0.20$  respectively).

At the limit of very strong disorder, in the spin glass phase for  $x=0.14$ , both NSE and  $\mu\text{SR}$  reveal a strongly non-exponential relaxation and there is excellent agreement between the two techniques, which unambiguously proves the homogeneous character of the spin glass relaxation [4]. The agreement between  $\mu\text{SR}$  and NSE in the spin glass phase is in contrast with the disagreement between the two techniques in the

disordered ferromagnetic phase. A slight increase of 2% in the Fe concentration leads to an abrupt change of the relaxation seen by neutrons as illustrated by Fig. 1. At  $x=0.14$ , the spin glass intermediate correlation function is strongly non-exponential (Fig. 1a) whereas at  $x=0.16$  the relaxation of the disordered ferromagnet is purely exponential (Fig. 1b). Both spectra were measured with NSE slightly above (10%) the corresponding ordering temperatures  $T_G$  and  $T_C$ .

The increase of the Fe concentration, however, has no dramatic effect on the  $\mu$ SR spectra, which remain non-exponential even well above the disordered ferromagnetic phase. As shown on Fig. 2 the  $\mu$ SR spectra are best fitted by the stretched exponential form  $\exp[-(t/\tau)^\beta]$  even for the ferromagnetic sample. Furthermore, as seen in Fig. 3, the deviations from the simple exponential decay quantified by the parameter  $\beta$  are basically the same at high temperatures for both the spin glass ( $x=0.14$ ) and the disordered ferromagnet ( $x=0.16$ ). In the view of the NSE results, this is a surprising finding, which for the first time unambiguously confirms Griffiths' theoretical predictions.

The puzzling discrepancy between NSE and  $\mu$ SR is obviously at the origin of the failure of all attempts to identify the Griffiths phase in disordered magnets with neutron scattering and macroscopic magnetization measurements up to now. In the case of disordered ferromagnets, the ferromagnetic critical phenomena and seen on NSE and magnetisation completely mask all other contributions even though the infinite ferromagnetic cluster close to the percolation threshold is extremely ramified and involves only a fraction of the magnetic moments. Muons on the other hand, average with the same probability over the local magnetic fields and see the integral of the susceptibility over the whole Brillouin zone [5]. Therefore muons are also sensitive to the relaxation of the magnetic moments besides the ferromagnetic backbone and in this case can detect the effects related to the disorder in a different way than neutrons. Furthermore, muons can follow the relaxation well above the ferromagnetic phase, at temperatures, where neutrons fail because of intensity reasons.

The comparison between muons and neutrons shows the complementarity of the two probes and is also an illustration of the complexity of disordered systems, where the combination of several techniques covering a wide phase space is obviously necessary to pin down the relevant information. The observation of the Griffiths phase by muons and of the disordered ferromagnetic

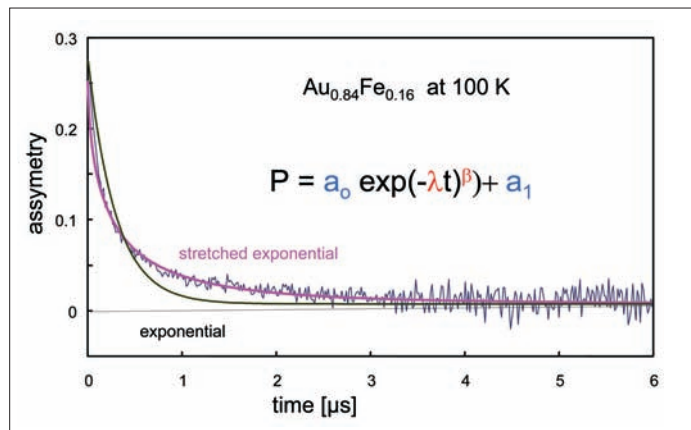


**Fig. 2:** Zero field  $\mu$ SR spectrum of  $\text{Au}_{0.84}\text{Fe}_{0.16}$  at 100 K, exactly the same temperature as the NSE spectrum of Fig. 1b. The data do not follow a simple exponential and are best described by a stretched decay (see text).

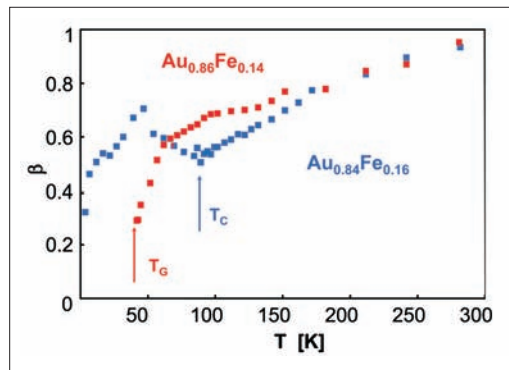


**Fig. 3:** Temperature dependence of the stretched exponential exponent  $\beta$  for the spin glass  $\text{Au}_{0.86}\text{Fe}_{0.14}$  (red squares) and the disordered ferromagnet  $\text{Au}_{0.84}\text{Fe}_{0.16}$  (blue squares).

transition with neutrons provides a deeper link between theory and experiment and gives a natural explanation of the marked influence of strong disorder on the ferromagnetic and antiferromagnetic second order phase transitions [6].

- [1] R. B. Griffiths, Phys. Rev. Lett. **23**, 17 (1969)
- [2] M. Randeria, J. P. Sethna and R. G. Palmer, Phys. Rev. Lett. **54**, 1321 (1985)
- [3] R. G. Lloyd, P. W. Mitchell, J. Phys. C **1**, 5013 (1989)
- [4] C. Pappas, F. Mezei, G. Ehlers, P. Manuel, I. A. Campbell, Phys. Rev. B **68**, 054431 (2003)
- [5] S. W. Lovesey, E. B. Karlsson, K. N. Trohidou, J. Phys.: Condens. Matter **4**, 2043 (1992)
- [6] C. Pappas, M. Alba, A. Brulet, F. Mezei, J Appl. Phys. **79**, 6158 (1996)

#### Corresponding author:

C. Pappas  
pappas@hmi.de

# Time scale of nuclear fission: fast or slow?

C.-M. Herbach, D. Hilscher, U. Jahnke, V. Tishchenko

■ HMI, SF1 in collaboration with FZ Jülich, GANIL (Caen, France) and University of Rochester (USA)

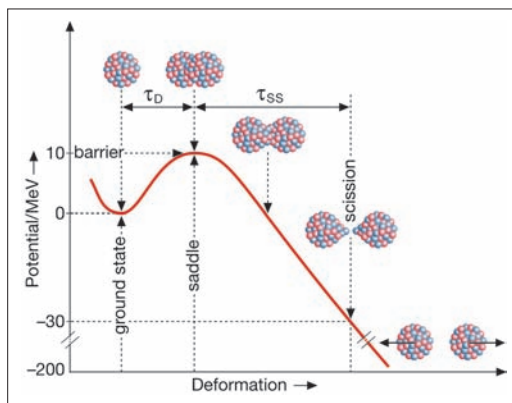


**Fig. 1:** Sketch of the potential energy as a function of deformation with the transient time  $\tau_D$  and the saddle-to-scission time  $\tau_{SS}$  indicated

Nuclear fission<sup>1</sup> denotes the binary splitting of a heavy nucleus into two fragments of roughly equal size. Obviously, this process implies an enormous distortion of the shape of the heavy nucleus: It has to deform axially to cigar-like shape which is further on constricted to dumbbell shape. Somewhere along this course of deformation the system reaches the saddle point in the potential energy (Fig. 1) or the fission barrier, where the short-range attractive nuclear forces become compensated by the Coulomb repulsion of the protons inside the nucleus, and from then on the pre-fragments separate under the Coulomb repulsion until the neck between them ruptures at the scission point.



**Fig. 2:** The NESSI detector at the COSY accelerator

It is this large-scale collective motion and its close connection to the still poorly known properties of nuclear matter such as dissipation or viscosity which makes fission so fascinating to this day: Does nuclear matter behave like a thin fluid such as water or viscous like honey or, alternatively, is the fission process fast or slow?

This problem is nearly as old as all our knowledge about fission. The importance of dissipation/viscosity for fission was recognized [1] right from the very beginning of fission research and it was argued that a purely static description of fission, i. e. considering nothing but phase space, might not be adequate.

Part of this problem was already solved some 15 years ago in favor of a large viscosity by the well known neutron clock experiments [2]. They have shown that the highly-excited compound nucleus releases most of its energy by evaporation of neutrons prior to scission, or that the total fission process is much slower than evaporation. The neutron clock experiments determine, however, the viscosity rather close to the end of the fission reaction, i. e. at low temperature and large deformation and do not allow for conclusions on a variation of the viscosity with these parameters.

The fission probability  $P_f(E^*)$  as a function of excitation energy  $E^*$ , the primary objective of our investigation, instead, provides insight into dissipation or viscosity at small deformation and high excitation. This is because fission is decided upon at the saddle point and thus at small deformation and high excitation. The saddle point is, so to say, the point of no return: Any further elongation drives the system irreversibly towards scission.

Once more here, before the collective flow reaches the saddle, the nucleus is subject to evaporation. However, now at high temperature the particle emission times are much shorter than near scission. A dynamic hindrance of fission or a long transient delay  $\tau_D$  for fission would thus strongly favor neutron and proton emission and thus reduce the systems fissility. Conversely, low viscosity at the saddle or a minimum transient delay  $\tau_D$  tends to keep fission competitive with particle evaporation even at high excitation. The fission probability, hence, reflects the magnitude of nuclear viscosity/dissipation at high  $E^*$  and low deformation.

<sup>1</sup> More than six decades of extensive research in fission have elapsed since its discovery in 1938 by Hahn and Straßmann. But due to the extreme complexity of this many-particle process there is still no comprehensive dynamical model for it available – which did, however, not hamper the well known applications of fission.

Our experiments [3] were performed within the NESSI-collaboration (HMI, FZJ, GANIL, Univ. Warsaw and Univ. Rochester) aiming at the systematic investigation of GeV-proton spallation reactions for the European Spallation Source (ESS) project.

We have used the 2.5 GeV proton beam from the COSY accelerator at FZJ in order to excite 3 target nuclei, Au, Bi, and U with largely different fission barriers of 21, 12, and 5 MeV, respectively. The fission probability  $P_f(E^*)$ , i.e. the portion of all reactions which lead to fission, was measured up to  $E^*=1000$  MeV with our unique NESSI-detector [4] (Fig. 2) which registers virtually all emissions, neutral and charged, from the de-excitation process.

Figure 3 exhibits the experimental  $P_f(E^*)$  and compares it to a simple statistical model simulation which does not account for the expected dynamic hindrance of fission. It is obvious that these calculations reproduce the characteristically different trends in  $P_f(E^*)$  for Au, Bi, and U at lower  $E^*$  as well as the almost equal  $P_f$  at the highest  $E^*$  nearly quantitatively, and, most importantly, they do so *without adding any additional transient time*. Fig. 3 also shows (red dashed histogram) a calculation for p+Au where an additional delay time of  $\tau_D=2 \times 10^{-21}$  s has been introduced, which was found indispensable in a recent investigation at GSI [5]. This calculation clearly contradicts our measurement at low as well as at high  $E^*$ .

It is furthermore noteworthy that the experimental  $P_f(E^*)$  for Au and U is very similar to what has been observed with antiproton reactions at LEAR/CERN [6] and thus does not depend on the particular mode of excitation.

In the same experiment we also determined the saddle-to-scission time,  $\tau_{SS}$ , and as a matter of fact this was the first experiment in which both essential fission times,  $\tau_D$  and  $\tau_{SS}$ , were deduced simultaneously. Fig. 4 shows as an example of this investigation the energy spectra of  $\alpha$ -particles which are emitted at  $E^*=600$  to 900 MeV either in the flight direction of the fission fragments or rather in the direction of the motion of the compound nucleus before scission. Their closer analysis shows that only about 20% of the  $\alpha$ -emission originates from the separated fragments, while 80% is emitted prior to scission. The fragments are, hence, relatively cold at scission and the evaporation cascade is much faster than the fission process – in complete agreement with previous observations [2].

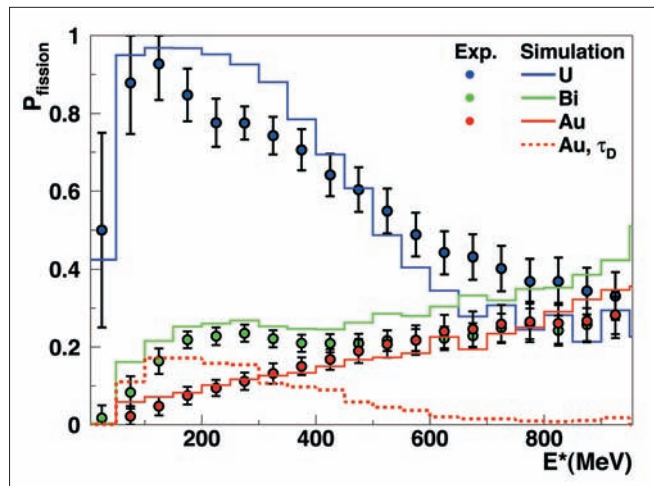


**Fig. 3:** Comparison of experimental and simulated fission probability as a function of  $E^*$

In summary, we have shown that fission is decided upon on a *very fast time scale* with no dynamic hindrance and, by contrast, that the total fission process is slow compared to evaporation. Thus, nuclear dissipation or viscosity either seems to vary with temperature or with deformation.

- [1] H.A. Kramers, Physica VII, no. 4, 284 (1940)
- [2] D. Hilscher et al., Phys. Rev. Lett. **62**, 1099 (1989)
- [3] V. Tishchenko, C.-M. Herbach, D. Hilscher, U. Jahnke, J. Galin, F. Goldenbaum, A. Letourneau, W.-U. Schröder, Phys. Rev. Lett. **95**, 162701 (2005)
- [4] U. Jahnke et al., Nucl. Instrum. Methods A **508**, 295 (2003) and C.-M. Herbach et al., ibid. A **508**, 315 (2003)
- [5] B. Jurado et al., Phys. Rev. Lett. **93**, 0725501 (2004)
- [6] U. Jahnke et al., Phys. Rev. Lett. **83**, 4959 (1999)

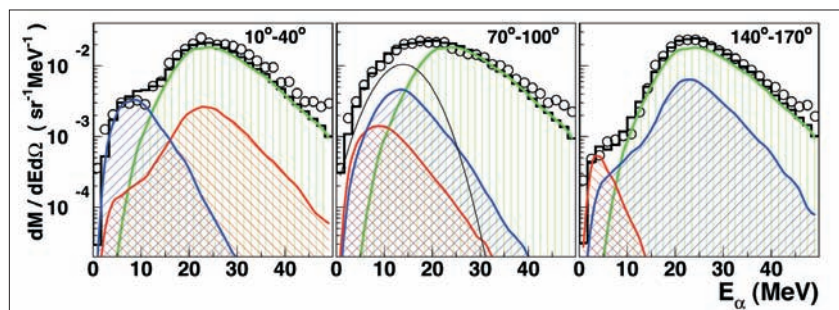


**Fig. 4:** Energy spectra of alpha-particles emitted in the flight direction of the light (left), the heavy (right) fission fragment or the heavy nucleus before fission (middle). The green histograms exhibit the strong emission before scission. Emission from the light and heavy fragments is shown in red and blue, respectively.

**Corresponding author:**

U. Jahnke  
jahnke@hmi.de

# Probing magnetic complexity in cobalt nanoparticles

P. Imperia<sup>1</sup>, D. Schmitz<sup>1</sup>, H. J. Maletta<sup>1</sup>, J. Bansmann<sup>2</sup>, P. Andreazza<sup>3</sup>

■ 1 HMI, SF2 ■ 2 Institut für Physik, Universität Rostock, Germany ■ 3 Centre de Recherche sur la Matière Divisée, France

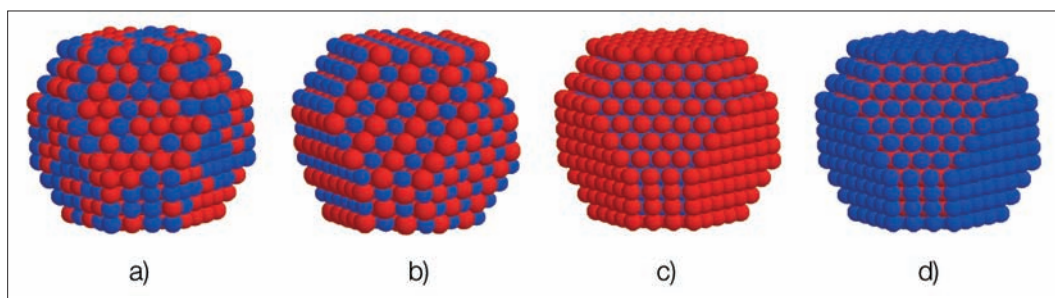


**Fig. 1:** Snapshots of the 807-atoms (around 2.5 nm size) platinum/cobalt Wulff polyhedral nanoparticles (blue spheres stand for Co atoms and red spheres for Pt): chemically disordered (a), ordered L10 (b), Pt surface segregated (c) and Co surface segregated model (d)

Magnetism in nanosized metallic particles with diameters in the range from 2 nm to 100 nm might hold the key to the future of magnetic memory devices. These tiny particles, composed of between a few hundred and a few tens of thousands of atoms, truly bridge the scales between the more familiar single atomic and solid state worlds. They show new physical properties different from those present in both: the isolated atom and the bulk. In fact, it is the significant proportion of atoms lying at the surface of the clusters and their interaction with the core that lies at the heart of the distinctive emergence of novel magnetic behaviour at cluster size. The orbital and spin magnetic moments ( $\mu_l$  and  $\mu_s$ ) carried by the atoms in the cluster differ not only from the bulk material, but do so in a way that holds the promise of leading to technological applications. Electron d-bands at the surface in iron or cobalt nanoparticles narrow significantly and produce those higher orbital moments and enhanced magnetic moments that are important technologically. Understanding these small clusters and their processing thus provides fascinating scientific challenges of wide potential impact.

The ability to produce batches of nanoparticles with a high degree of uniformity in size (monodispersity) and properties is essential for their application and elucidation. Chemical synthesis provides one of the most promising routes for the industrial synthesis of the particles, and the production of cobalt and iron nanoparticles [1] has

become simple and inexpensive. However, cleaning the surfactants involved in synthesis off the nanoparticles is far from trivial and oxidised surfaces readily develop [2]. Using *in situ* sample preparation techniques – portable clusters sources [3] attached to the ultra high vacuum (UHV) chambers on our beamlines – allows us to deposit monodisperse batches of pristine nanoparticles on a host of different substrates for study. The metallic clusters are produced by erosion from a hollow cathode of highly pure material. So far, particles of sizes ranging from 1 to 15 nm as well as bimetallic nanoparticles prepared by vapour deposition have been studied. It has been found that unusually well defined crystallographic structures in cobalt and cobalt/platinum core/shell nanoparticles are stabilised on specially prepared silicon substrates making them of particular interest [4], and the core/shell systems with a platinum core, ferromagnetic cobalt shell and an antiferromagnetic shell of cobalt-oxide wrapped around it, display a very high ratio of orbital to spin moment. To probe the intricate interplay of magnetism in these tiny particles requires a technique of great versatility and sensitivity. Synchrotron X-rays provide photon beams of the intensity needed for these tiny samples and X-ray magnetic dichroism (XMCD) can pick out the magnetic state in each of the constituent elements in a selective way.

In XMCD, photoabsorption spectra are recorded around the L edges of Co, Fe or Ni. Then, the magnetic orbital and spin moments can be calculated independently by integrating the difference and the sum of the spectra recorded by shining the samples with circular polarized light of opposite direction according to the sum rules [5]. Absorption spectroscopy is a surface sensitive and material selective technique, and the magnetic properties of each of the constituent atomic species can be deduced separately. However, in order to measure magnetic dichroism one has to use magnetised samples. Our ability to investigate such nano-range particles has been significantly enhanced by the commissioning (in 2005) of a new high-field chamber at the beam line UE46 PGM operated by the Hahn-Meitner-Institut which is specially designed for the application of fields up to 7 T at temperatures as low as 2.6 K. Combined with the high density of photons delivered by an APPLE II type undulator at the 3<sup>rd</sup> generation synchrotron radiation source BESSY and state of the art instrumentation (including a choice between a focused beam of  $16 \times 64 \mu\text{m}^2$  or a parallel beam of  $1 \times 1 \text{mm}^2$ ), the set-up allows experiments to be performed on small atomic clusters with a low surface coverage at which the clusters are non interacting.

To gauge the impact of processing on the final magnetic properties, nanoparticles obtained with different kinds of preparation techniques have now been investigated. Chemically synthesized cobalt nanoparticles were studied in a range of post preparation surface treatments to assess the residual surfactant (oleic acid) load and cobalt oxide (CoO) surface layering. In-situ Ar<sup>+</sup> ion sputtering [2] effectively removes the surfactants but leaves the oxide layer. Using H<sup>+</sup> ions as well, however, cleaned off the oxide layer [2]. The processing also impacts significantly on the magnetic properties with Ar<sup>+</sup> sputtering strongly enhancing the orbital versus the spin moment which is a somewhat unexpected consequence of surface damage to the nanoparticles: Ar<sup>+</sup> bombardment disrupts the surface integrity and reduces crystal field quenching of orbital moments. This change in orbital moment can be measured as a function of processing time and conditions and the properties optimised. Treatment by H<sup>+</sup> ions alone [2], in contrast, cleans off the CoO layer and causes little surface damage leaving magnetic properties much more similar to those observed in bulk material.

Investigations of cobalt clusters in their pristine state on different substrates [3] show that the choice of the substrate provides control of the magnetic properties, as well. While cobalt clusters grown on ferromagnetic substrates show no enhan-

ced orbital moments, clusters grown on a non-magnetic surface like gold or silicon oxide (SiO<sub>2</sub>) have strongly enhanced values of the important orbital to spin moment ratio. A further enhancement has been observed upon exposing the samples to a small amount of oxygen. Nanoparticles with a diameter of 9 nm oxidised with 500 L\* of oxygen, show a strong increase in the ratio from  $\mu_I/\mu_S=0.08$  (clean cobalt clusters) to  $\mu_I/\mu_S=0.16$  after oxygen exposure. Simultaneously, the spin moment decreases from  $\mu_S=1.5 \mu\text{B}$  to  $\mu_S=0.7 \mu\text{B}$ . Indeed, the findings on the oxidised nanoparticles point to a novel spin reorientation transition driven by the structural characteristic of the interface between the ferromagnetic and the non-magnetic substrate.



**Fig. 2:** The new ultra high vacuum high magnetic field reflectometer at UE46 PGM, BESSY

The results found show how the engineering of the samples leads to different magnetic properties of the nanoparticles. Further studies and more detailed analysis based on improved data sets will allow a better understanding of the complex interplay between structure, composition, size and the magnetic properties in the "nano world".

#### Acknowledgements

The technical assistance of S. Rudorff as well as the continuous support and encouragement of E. Holub-Krappe, H. Rossner and A. Tennant are kindly acknowledged.

\*L is the symbol of the unit langmuir. 1L corresponds to the exposure of a surface to a gas at  $10^{-6}$  torr for 1 second.

- [1] C. B. Murray et al., IBM J. Res. & Dev. **45**, 47 (2001)
- [2] P. Imperia et al., Phys. Rev. B **72**, 014448 (2005)
- [3] J. Bansmann et al., Appl. Phys. A **82**, 73 (2005)
- [4] P. Andreatza et al., submitted to Nucl. Instr. and Meth. B (2005)
- [5] B. T. Thole et al., Phys Rev. Lett. **68**, 1943 (1992); P. Carra et al., Phys Rev. Lett. **70**, 694 (1993)

#### Corresponding author:

P. Imperia  
imperia@hmi.de

# Climbing spin spirals: towards new magneto-electric materials

D. N. Argyriou

■ HMI, SF2

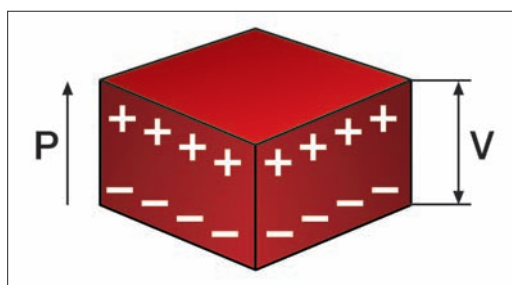


**Fig. 1:** In a ferroelectric material, electrical dipoles are created due to the movement of positively charged ions relative to negatively charged anions. If the dipoles point all in the same direction, the crystal is said to be polarized. The result is an electrical potential difference in a single crystal of a ferroelectric as shown above.

Ferroelectrics are one of the triumphs of modern materials science as they form the basis of a number of valuable instruments. From ultrasound machines that make images of the internal organs in our bodies to actuators and sensors one finds in cars and airplanes; all depend on ferroelectric materials. The unique property of ferroelectrics is that a block made of such material can form an electric potential across one of its dimensions (see Fig. 1). Applying an electric field to it can cause changes to this dimension even at very high frequencies. This allows the construction of ultrasound probes for example used in health care.

The control of the ferroelectric polarization ( $\mathbf{P}$ ) with an external magnetic field ( $\mathbf{H}$ ) in a material opens an enormous opportunity for new types of magneto-electric devices. The realization of such devices is based on multiferroic materials in which magnetism and ferroelectricity are combined and are strongly coupled. The number of multiferroic materials available is limited; however, recent advances have suggested that materials where magnetism is frustrated may offer an enhanced control of ferroelectricity with magnetic field. One of these new multiferroics –  $\text{TbMnO}_3$  – exhibits a novel flop of its electric polarization from one direction to another when a magnetic field is applied. In these multiferroics, ferroelectricity arises as a secondary effect from the coupling of the lattice to a complex magnetic structure.

At the HMI, we used single crystals of  $\text{TbMnO}_3$  and materials like it that we grow in our labs and apply high magnetic fields along all the dimensions that define their unique atomic arrangement. We found that the essential physics that describes this flop in the polarization arises from changes in the magnetic structure of the material.

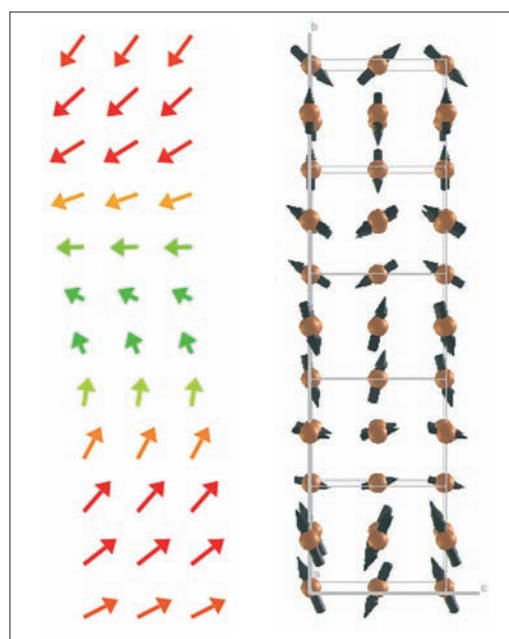


**Fig. 2:** Two examples of magnetic spin spirals. On the left, we illustrate the spin directions of a hypothetical spin spiral arrangement in a single layer of a magnet. Here, the direction of the magnetic moments spiral from pointing to the right at the bottom of the page to the left at the top. Similarly we show an illustration of the magnetic arrangement of  $\text{TbMnO}_3$ . Here the magnetic moments are tied to the manganese (Mn) atoms. In terms of symmetry, magnetic spin spirals can break inversion symmetry, a property that allows displacement of positively charge ions against negatively charged anions that make ferroelectricity possible in a crystal lattice.

### Unravelling a spin spiral

The multiferroic properties of these materials arise from a complex arrangement of the magnetic moments of the manganese (Mn) ions. In simple terms, this complex arrangement can be described as a spiral as shown in Fig. 2. Theory tells us that magnetic materials such as these manganites become ferroelectric because magnetic moments in the manganese atoms organize themselves in such a spin spiral [1]. Theoretically, it works out that the symmetry of a spiral can break what is known as inversion symmetry and make ferroelectricity possible. To change the direction of the polarization with a magnetic field – and make a working device – theory tells us that we need to kick the spiral on its side. At the HMI, we have been investigating to see what happens when we apply high magnetic fields on these spin spirals to see if they indeed flop to their side. These measurements allow us to not only understand this mechanism better but also test the theory to see if it is correct. Our work on  $\text{TbMnO}_3$  and  $\text{DyMnO}_3$  showed a much more complicated behaviour than was anticipated. Firstly, when we apply a magnetic field in two ways we find a series of transitions from one magnetic arrangement to another which has a different periodicity [2] (by this we mean the characteristic length in which the spin arrangement repeats itself). This means that the spin flops in one or multiple steps (see Fig. 3). Secondly, we find that the magnetic moments on the terbium (Tb) and dysprosium (Dy) atoms also play a critical role both in the formation of the ferroelectric phase but also in helping it to flop the spiral with magnetic field [3].

Are the theorists right? Well, this is not clear. Our measurements find that once the spin spiral flops the magnetic structure may be a lot simpler than first thought. Indeed so simple that we have produced a straight forward model that explains the direction of the polarization without the need to use a complicated theory. However, these materials are relatively young and complicated and hold many surprises still.

[1] N. Aliouane, et al. *Physical Review B* **73**, 020102 (2006)

[2] M. Mostovoy, *Phys. Rev. Lett.* **96**, 067601 (2006)

[3] R. Feyerherm *Physical Review B* **73**, 180401(R) (2006)

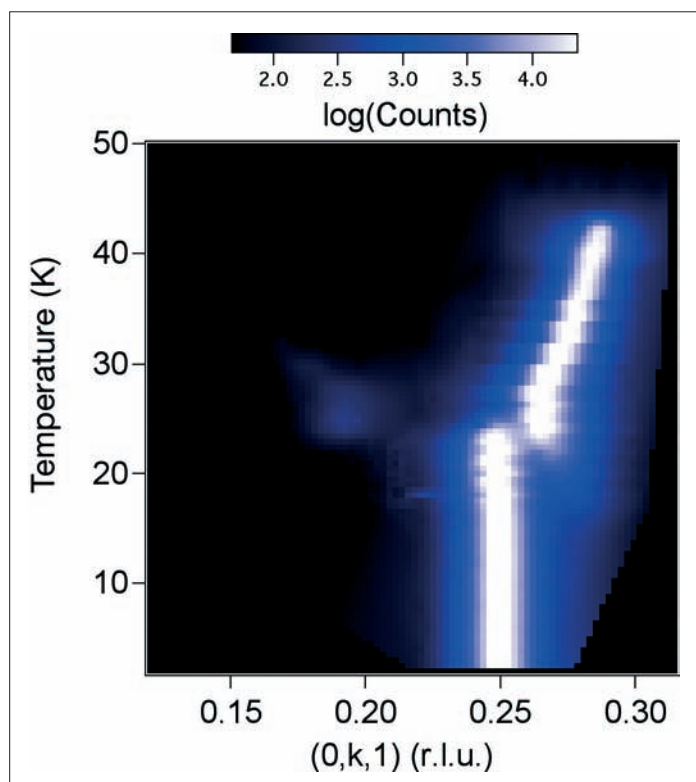


**Fig. 3:** Here, we show diffraction data measured from a single crystal of  $\text{TbMnO}_3$  in a magnetic field of 10 T applied parallel to the *a*-crystallographic axis. The colour image shows how a magnetic diffraction peak varies in position with temperature in the magnetic field. At high temperature, the periodicity is not a rational fraction and indicates that the length that this spiral needs to repeat itself is long  $\sim 7\times$  the chemical unit cell. However, when the repeat changes discontinuously the spiral “shrinks” to a commensurate value of  $4\times$  unit cell ( $k=1/4$ ).

# Characterization of Precipitates in Inconel 706 Superalloys by Three-Dimensional Atom Probe and Transmission Electron Microscopy

N. Wanderka, V. Kindrachuk

■ 1 HMI, SF3



**Fig. 1:** Blades and discs of a gas turbine

Three-dimensional atom-probe (3DAP) is an analytical microscope able to map out the three-dimensional distribution of chemical species on an atomic scale [1,2]. 3DAP makes it possible to measure quantitatively the chemical composition of small regions that can be selected arbitrarily in the reconstructed volume. In the present work, a three-dimensional atom probe was used to carry out a high resolution microchemical analysis of superalloys.

Due to its combination of high mechanical strength with good fabricability and machinability, the superalloy Inconel 706 (composition 40.68Ni-37.63Fe-17.52Cr-1.87Nb-1.85Ti-0.44Al (at.)) is under consideration for ultra high temperature steam turbine applications (Fig. 1) with prospective steam temperatures up to 973 K. The alloy properties directly depend on the precipitation hardening process, which is based on precipitation of two kinds of  $A_3B$ -type compounds with different crystal structures. One kind of precipitate with the composition  $(Ni_3[Ti,Nb,Al])$  is referred to as  $\gamma'$  phase, the other one with the composition  $(Ni_3[Nb,Ti])$  as  $\gamma''$  phase. Small  $\gamma'$  and  $\gamma''$  precipitates about 15–20 nm in size as shown in Fig. 2 are embedded in a matrix consisting mostly of nickel and iron. However, these small  $\gamma'$  and  $\gamma''$  precipitates in this alloy are metastable and transform into large laths of  $\eta$  phase  $(Ni_3[TiNb])$  upon exposure to temperatures  $> 923$  K. This process – usually called overageing – is accompanied by an unacceptable loss of creep and tensile strength.

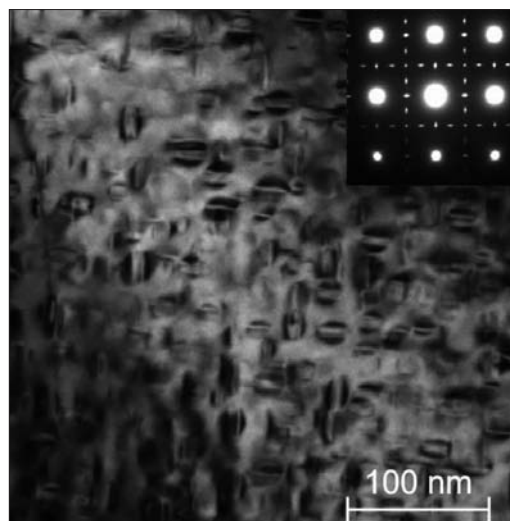


**Fig. 2:** Bright field TEM image of microstructure of Re-modified In-conel 706 alloy. Fine hardened  $\gamma'$ ,  $\gamma''$  and  $\gamma'/\gamma''$  precipitates embedded in the  $\gamma$  matrix can be observed. A [001] zone axis diffraction pattern is represented in the inset.

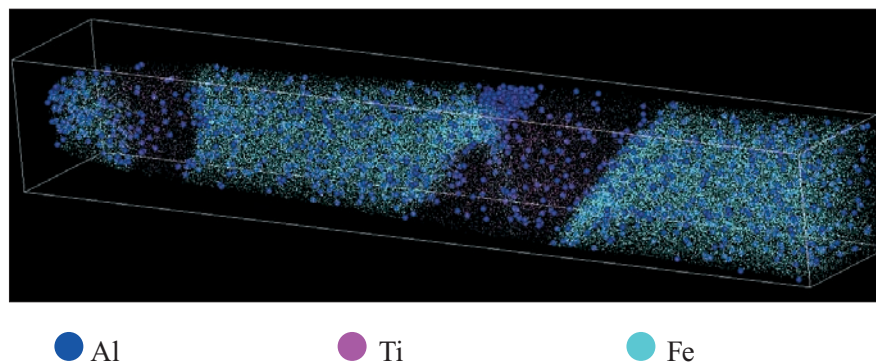


**Fig. 3:** Three-dimensional reconstruction of Re-modified Inconel 706 superalloy after ageing at 750°C for 750h. The spatial arrangement of Al (dark blue), Ti (purple) and Fe (light blue) atoms in a volume of  $14 \times 14 \times 235 \text{ nm}^3$  is shown, representing three  $\gamma'$  precipitates embedded into the matrix.

In order to overcome this impasse, two different stabilization concepts were tested. On the one hand, it was attempted to create a diffusion barrier in the matrix surrounding the  $\gamma'/\gamma''$  precipitates by adding Rhenium to the composition of Inconel 706. Rhenium is known to effectively retard  $\gamma'$  coarsening in cast single crystal Ni-base superalloys, as the interface segregation of the Rhenium strongly influences the stability of the precipitates. On the other hand, the  $[\text{Ti}+\text{Al}]/[\text{Nb}]$  ratio of Inconel 706 was specifically refined in order to minimize the thermodynamical tendency to transformation of  $\gamma'/\gamma''$  into the h phase. This modification was associated with a redesign of the Inconel 706 chemistry, resulting in a new alloy named DT706.

The microstructure of Inconel 706, Re-modified Inconel 706, and DT706 were investigated by means of electron microscopy (TEM) and 3 dimensional atom probe (3DAP) in the as-heat treated condition as well as after long-term exposure at 1023 K (Fig. 3). Results show that Rhenium was homogeneously dissolved in the matrix, but its partitioning ratio is too low to provide an effective obstacle to  $\gamma'/\gamma''$  coarsening. In contrast, the microstructural degradation in DT706 (Fig. 4) was retarded as compared to Inconel 706, although the formation of h phase was not completely suppressed.

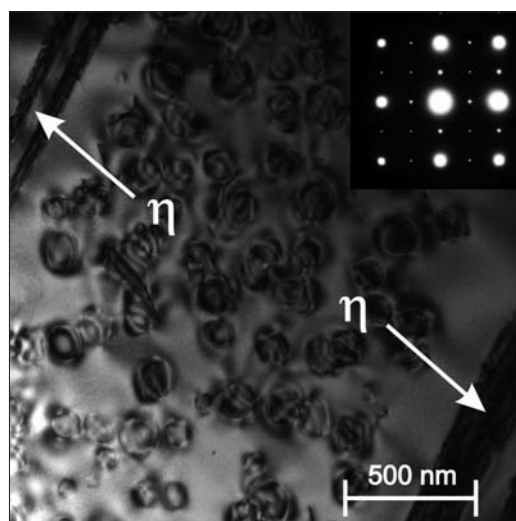


**Fig. 4:** Bright field TEM image microstructure of DT706 superalloy after ageing at 1023 K for 5000h. Small  $\gamma'$  cubes can be seen; additionally  $\eta$  phase is formed. A [001] zone axis diffraction pattern is given in the inset.

- [1] A. Cerezo, T. Godfray and G. Smith, Rev. Sci. Instrum. **59**, 862 (1988)
- [2] D. Blavette, A. Bostel, J. Sarrau, B. Deconihout and A. Menand, Nature **363**, 432 (1993)

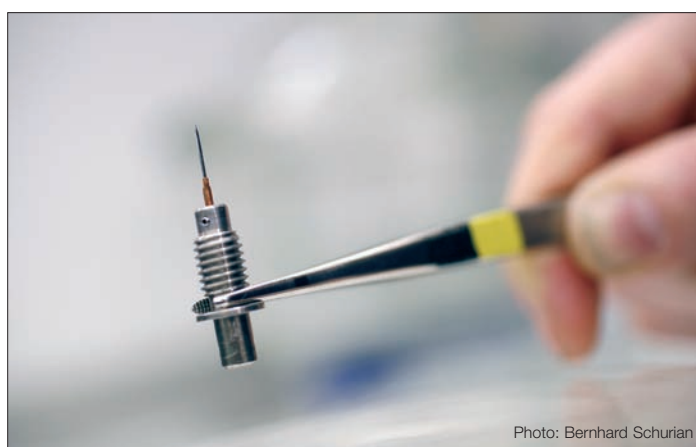


**Fig. 5:** A sample for the 3-dimensional atom probe (3DAP)

# Stroboscopic neutron scattering investigations of dynamics in nanosized magnetic systems

A. Wiedenmann<sup>1</sup>, U. Keiderling<sup>1</sup>, J. Haug<sup>1</sup>, R.P. May<sup>2</sup>, Ch. Dewhurst<sup>2</sup>

■ 1 HMI, SF3 ■ 2 ILL Grenoble

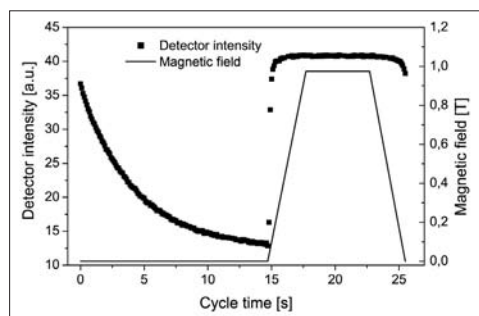


**Fig. 1:** Magnetic field and total detector intensity during the SANS experiment on Cobalt-Ferrofluid particles

Small angle neutron scattering (SANS) is an efficient method for investigating systems of nanosized particles that allows one to gain information about the size and form distribution as well as the ordering of the particles. Real-time investigations of time dependent processes in nanosized inhomogeneities by means of SANS, however, are usually limited to processes that are so slow that during data acquisition the system remains in a quasi-steady state.

For oscillating processes, stroboscopic SANS measurements are possible in short time slices when data collection can be synchronized with the periodic process. Here, we report on the set-up of a new time-resolved stroboscopic technique that allows relaxation processes to be studied at time constants of several 100ms, which are too fast for conventional SANS but by far too slow to be measured by quasi-elastic or spin-echo neutron scattering techniques. These methods are usually used for investigating time dependent processes with neutrons, but are appropriate for times below  $<10^{-8}$ s only.

An important field for studies of dynamic processes in nanosized particles are ferrofluids – magnetic liquids composed of magnetic particles a few nanometres large dispersed in a carrier liquid. The magnetic particles are coated by a surfactant stabilizing the liquid and preventing the particles from agglomerating. They can be investigated particularly well with polarized neutrons using a technique called SANSPOL developed at the Hahn-Meitner-Institut.

SANSPOL investigations of concentrated ferrofluids with cobalt cores (Co-Ferrofluids) have shown that an external magnetic field induces

inter-particle interactions giving rise to pseudo-crystalline ordering of the magnetic particles [1]. Here, domains of local hexagonal arrangements coexist with fragments of spontaneously formed chains of particles with moments aligned along the external magnetic field. By using time resolved SANS in a stroboscopic mode we intended to follow the onset and decay of the local ordering when the field is switched on and off in order establish the kinetics of these processes [2, 3].

The investigations have been performed on SANS instruments at the Hahn-Meitner-Institut (V4) and at the Institut Laue-Langevin (ILL) in Grenoble, France (D22).

In the experiment, a concentrated Co-Ferrofluid sample was placed in a homogeneous horizontal magnetic field  $H$  applied perpendicular to the incoming neutrons. The scattering intensities  $I(+)$  and  $I(-)$  for polarized neutrons with incident neutron spin polarizations parallel and antiparallel, respectively, to the magnetic field were measured. At ILL, the magnetic field could be switched off from 0.5 T to the remanence of 0.005 T within less than 100ms. SANS measurements were performed in time-slices of 500ms during a total time of 15s after switching off the magnetic field. For raising and stabilisation of the field at 0.5 T a waiting time of 5s was intercalated. Sufficient counting statistics were obtained after 400–600 cycles. At the HMI, a new readout system for the 2D detector is capable of producing data containing full position and time information for each single neutron. Extending a software package developed at HMI, these data allow for fully flexible control over the spatial and time resolution of the results *after* the experiments.

For the present case of superparamagnetic single domain particles the sum signal  $(I(+)+I(-))/2$  contains contributions from magnetic disorder of individual particle moments and from inter-particle correlations. In the SANSPOL difference intensity  $I(-)-I(+)$  all disorder scattering is cancelled leaving the nuclear-magnetic interference term which results solely from magnetic particles and which contains an anisotropic structure factor describing the inter-particle correlations.

In Fig. 1 the cycling of the magnetic field in the HMI experiment is plotted (solid line) together with the total detector intensity for the difference  $I(-)-I(+)$ . Each point has been calculated from one time frame with a width of 100 ms, after accumulation of approx. 700 cycles. The figure clearly shows the perfect statistics yielded by the presented stroboscopic technique. As soon as the field is applied, ordering sets in immediately and is nearly completed long before the field reaches the maximum. The ordering occurs so quickly that the limiting factor for the measured ordering kinetics appears to be the slope of the field up-ramp, rather than the native dynamics of the sample structure. Therefore, we do not discuss the ordering, but we emphasize that the presented technique easily allows the improvement of the time resolution *after* the experiment whenever, in a case like this, the first data processing results suggest that this may be useful. The scattering patterns measured at  $H=0.5\text{ T}$  and  $H=0$ , respectively, turned out to be identical when measured in the stroboscopic cycling or in the static mode which demonstrated that the ordering-disordering process was really reversible. In Fig. 2 the 2D iso-intensity patterns of the sum  $(I(+)+I(-))/2$  (left column) and the difference intensities  $I(-)-I(+)$  (right column) are shown. After averaging the patterns of Fig. 2 at the angle  $\alpha=30^\circ$  with respect to the horizontal direction of the magnetic field over a width of  $\Delta\alpha=20^\circ$  the scattering intensities are plotted in Fig. 3 as a function of the momentum transfer  $Q$ . Fig. 2 and Fig. 3 reveal clearly the decay of the peaks indicating the local hexagonal order. In the final relaxation state, the intensities show a  $Q^{-1}$  dependence at low  $Q$  which is a characteristic feature of short fragments of dipolar chains. This shows that the hexagonal order gradually transforms into chain segments. Since the decay of the peak intensities was observed in the sum as well as in the difference patterns, we conclude that nuclear inter-particle correlations disappear simultaneously with the magnetic correlations. Further analysis shows that the structures decay exponentially with time with a characteristic relaxation time in the order of seconds. A detailed discussion of the basic relaxation mechanism in colloids is presented elsewhere [2, 3].

In summary the new stroboscopic SANSPOLE technique allowed the nature of magnetic ordering of nanosized objects to be visualised during magnetic relaxation processes on a time scale of few hundred ms. In concentrated  $\text{Co}$ -Ferrofluids field induced magnetic and nuclear correlations were found to decay exponentially within a characteristic time of few seconds when the magnetic field is switched off. The local hexagonal particle arrangements with aligned magnetic moments transform gradually to uncorrelated segments of dipolar chains.

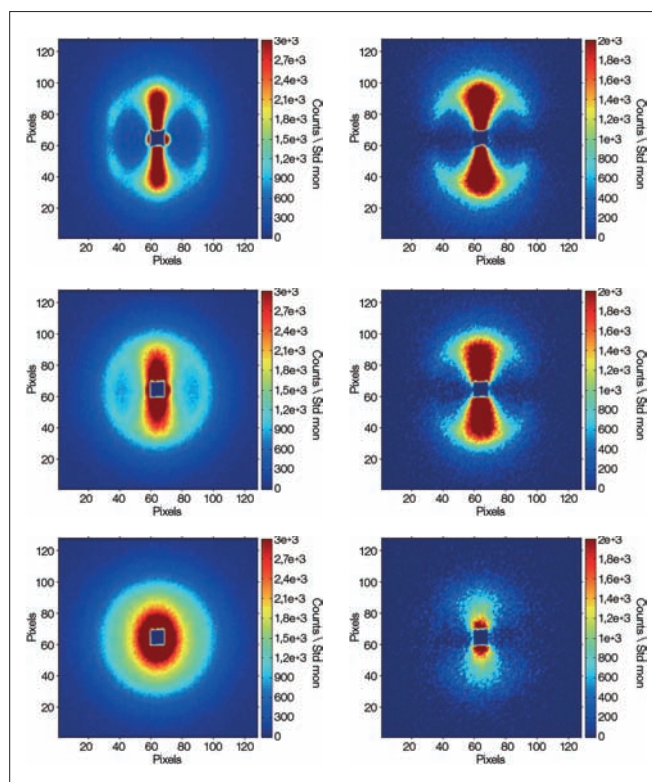


**Fig. 2:** 2D-SANSPOLE Sum  $(I(+)+I(-))/2$  (left) and Differences  $I(+)-I(-)$  (right) at  $t=0\text{ s}$ ,  $2\text{ s}$  and  $15\text{ s}$  after switching off the horizontal magnetic field of  $0.5\text{ T}$ . See text for details.

The project was supported by DFG Project Wi 1151/2 as part of the Priority program SPP 1104 (2000–2006).

- [1] A. Wiedenmann, A. Hoell, M. Kammel, P. Boeseck Phys Rev. E **68**, 031203, 1–10 (2003)
- [2] A. Wiedenmann, U. Keiderling, R. P. May, C. Dewhurst, accepted in Physica B (2006)
- [3] U. Keiderling, A. Wiedenmann, J. Haug, accepted in Physica B (2006)

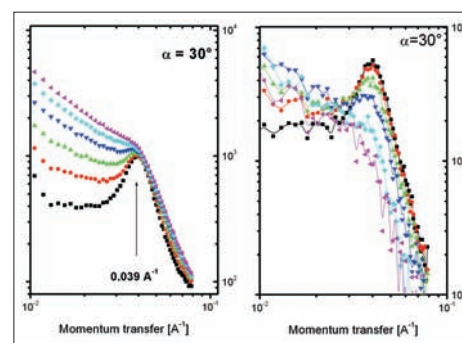


**Fig. 3:** SANSPOLE intensity Sum  $(I(+)+I(-))/2$  (left) and differences  $I(+)-I(-)$  (right) in the sectors  $\alpha=30^\circ$  averaged over  $\Delta\alpha=20^\circ$  at  $t=0.5\text{ s}$ ,  $1\text{ s}$ ,  $1.5\text{ s}$ ,  $2.5\text{ s}$ ,  $5\text{ s}$  and  $15\text{ s}$  after switching off the magnetic field of  $H=0.5\text{ T}$

**Corresponding author:**  
A. Wiedenmann  
wiedenmann@hmi.de

# Characterization of ion-beam induced nano-sized silver clusters in glass with synchrotron radiation

H.-E. Mahnke<sup>1</sup>, B. Schattat<sup>1</sup>, P. Schubert-Bischoff<sup>2</sup>, N. Novakovic<sup>1,3</sup>, I. Zizak<sup>1</sup>

■ 1 HMI, SF4 ■ 2 HMI, SF3 ■ 3 Research Institute VINCA, Belgrade, Serbia and Montenegro

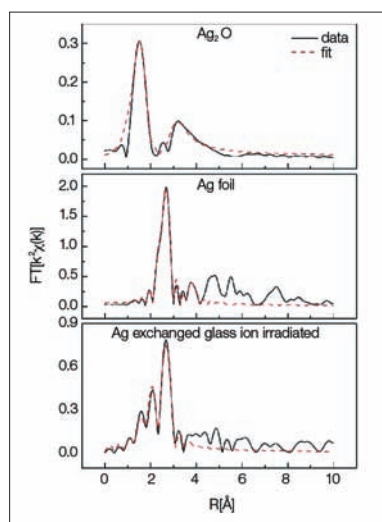


**Fig. 1:** Fourier transformed EXAFS signal ( $k^2$ -weighted): The irradiated glass sample (bottom) shows the ion beam induced formation of metallic silver. The EXAFS signature for metallic silver (middle) and for  $\text{Ag}_2\text{O}$  (top) are given for comparison.

Glasses containing metal clusters have attracted attention both in cluster research and in possible applications of such clusters for magnetic or opto-electronic purposes. Nanometer-sized clusters of noble metals in glasses exhibit strong absorption of visible light which, in addition, may be highly polarization dependent depending on size and shape with special alignment of the clusters [1,2]. Various preparation methods are pursued to obtain control of the mechanisms to form such clusters. A promising approach is the irradiation of glasses containing the wanted metal as a metal oxide with heavy-ion beams at energies of several MeV per atomic mass unit (i.e. per nucleon mass) [3,4,5]. At such velocities, the energy

deposited along the ion path leads to the formation of tracks in the material. In the following, we show how synchrotron radiation techniques help to characterize materials modifications induced by ion beams.

We have studied the formation of clusters of metallic silver in soda lime glass induced by heavy ion irradiation with X-ray absorption spectroscopy (XAS), complemented with transmission electron microscopy (TEM) and with small angle X-ray scattering (SAXS). Silver was introduced by ion exchange into 0.1 mm thick glass platelets (see [4]). While annealing under a reducing argon atmosphere with a few per cent of  $\text{H}_2$  already leads to the formation of metal clusters, such clusters are not very uniform in size and are randomly distributed over the silver-containing glass volume. We have irradiated these silver-containing

glass platelets kept at the temperature of liquid nitrogen with gold ions with energies of 600 MeV with fluences around  $10^{12}$  ions/cm<sup>2</sup> at the Ion Beam Laboratory (ISL) of the Hahn-Meitner-Institut. The ion flux was kept below  $10^{10}$  ions/cm<sup>2</sup>s.

Following the ion irradiation, the samples were investigated with X-ray absorption spectroscopy (EXAFS) at the Ag K-edge (25.514 keV) either with or without further annealing at the same temperature as for the ion-exchange preparation under a reducing atmosphere (5%  $\text{H}_2$ -Ar mixture) for 30 min (see Ref. [4]). EXAFS is a technique that allows deducing information on chemical bonds from details of the absorption spectra near the absorption edges. The EXAFS experiment was performed at the X1 beamline at the Hamburg Synchrotron Radiation Laboratory HASYLAB with the samples kept close to nitrogen temperature. The absorption was measured in fluorescence mode using a 7-element Ge detector. For comparison, the absorption was measured for samples of metallic silver and a sample of  $\text{Ag}_2\text{O}$  powder, mixed with graphite and polyethylene and pressed into a pill, too. The EXAFS spectra were analysed using the standard FEFF procedures [6,7,8] by which the coordination numbers and distances for at least the first and second coordination shells could be derived.

In Fig. 1, the ion-induced transformation from silver oxide into metallic silver is illustrated by the comparison of the different EXAFS signals. The extracted bond lengths correspond to the respective values known for the pure chemical systems. The bond length of Ag to O in the glass is slightly larger than in pure  $\text{Ag}_2\text{O}$ . This difference may reflect the substitution of Na by Ag as an impurity (details are presented in [9]).

As illustrated by the EXAFS spectrum, the transformation is not complete. Approximately 30% of the silver is surrounded by silver, while the major part of silver atoms is ambient by oxygen. With no post-irradiation heat treatment the metal fraction is at the detection limit. Obviously, the metal

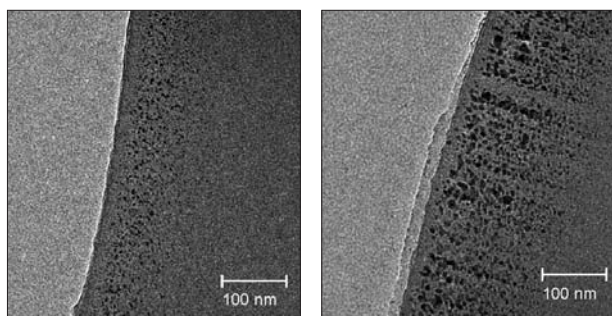


**Fig. 2:** Transmission electron microscope (TEM) picture of irradiated (right) and non-irradiated (left) glass samples: in the irradiated sample, after irradiation with gold ions and subsequent annealing. Clusters of metallic silver arranged in chains along the direction of the ion beam are visible. The TEM was operated at 120 kV.

fraction strongly depends on the treatment following the ion irradiation.

Complementary information on the distribution within the glass platelets, the shape and the sizes, was obtained from transmission electron microscopy (TEM) on thin slices of some 10 nm cut out of the samples parallel to the ion impact

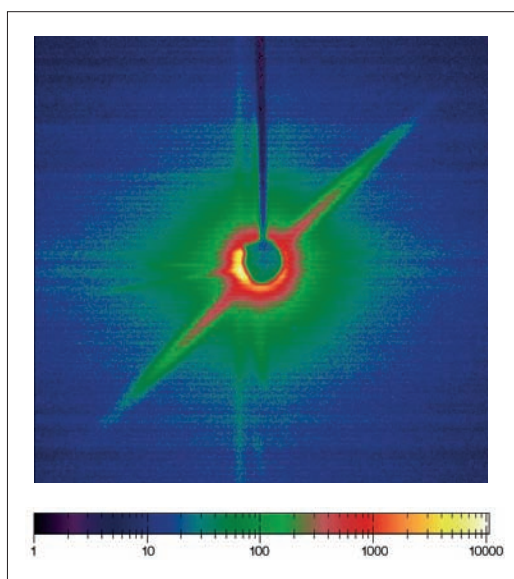


**Fig. 3:** SAXS image of the irradiated sample: In SAXS (Small Angle X-Ray Scattering) a cylindrical structure is represented by a disc, its length corresponds to the height of the disc and its diameter to the diameter of the disc. The dimensions in  $q$  space represented in the diagram correspond to a diameter of the “columns”, the arrangement of silver droplets along chains in the ion direction, of around 7 nm.

and deposited onto a fine grid. The comparison presented in Fig. 2 illustrates the significant influence of the ion irradiation: (i) the metal clusters have grown and their size distribution has become more uniform, but the most remarkable feature is that (ii) the clusters are arranged in chains parallel to the direction of the ion beam. Since some of the chains consist of clusters very similar in diameter and almost in contact, one is tempted to speculate that a totally columnar structure may be obtained by

controlling the influencing parameters such as the ion fluence and the annealing parameters. A more quantitative description of the arrangement seen in the TEM pictures can be achieved by SAXS measurements performed at the newly commissioned 7 T multipole wiggler beamline of the Hahn-Meitner-Institut at the Berlin Synchrotron Radiation Source BESSY. An illustration of the first experiment is given in Fig. 3. The ion fluence in this case was  $10^{11} \text{ cm}^{-2}$ , the sample was heat treated after the ion irradiation in the same way as the sample in Fig. 2. A glass platelet without Ag also shows ion tracks when ion irradiated at nitrogen temperature. However, they disappear when the same annealing procedure is applied. Thus, the small angle scattering confirms the arrangement and shape of the Ag metal clusters as induced by the ion irradiation and proves to be a very valuable complementary way to study such ion induced structures.

The authors are grateful to the HASYLAB staff at DESY, in particular to J. Wienold and E. Welter. We very much appreciate P. Szimkowiak's help in sample preparation. Special thanks are expressed to the colleagues from SF3, especially A. Hoell, who were jointly in charge of setting up the SAXS beamline with one of the authors (I.Z.).

- [1] K. L. Kelly et al., J. Phys. Chem. B **107**, 668 (2003)
- [2] A. Podlipensky et al., J. Phys. Chem. B **108**, 17699 (2004)
- [3] E. Valentin et al., Phys. Rev. Lett. **86**, 99 (2001)
- [4] G. Bataglin et al., Nucl. Instr. and Meth. in Phys. Res. B **200**, 185 (2003)
- [5] J. J. Penninkhof et al., Appl. Phys. Lett. **83**, 4137 (2003)
- [6] J. J. Rehr et al., J. Am. Chem. Soc. **113**, 5135 (1991)
- [7] E. A. Stern et al., Physica B **208** & **209**, 117 (1995)
- [8] M. Newville et al., Phys. Rev. B **47**, 14126 (1993)
- [9] H.-E. Mahnke et al., Nucl. Instr. and Meth. in Phys. Res. B **245**, 222 (2006)

#### Corresponding author:

H.-E. Mahnke  
mahnke@hmi.de

# Stochasticity in life: How microscopic fluctuations determine global behaviour of cells

M. Falcke, A. Skupin

■ HMI, SF5

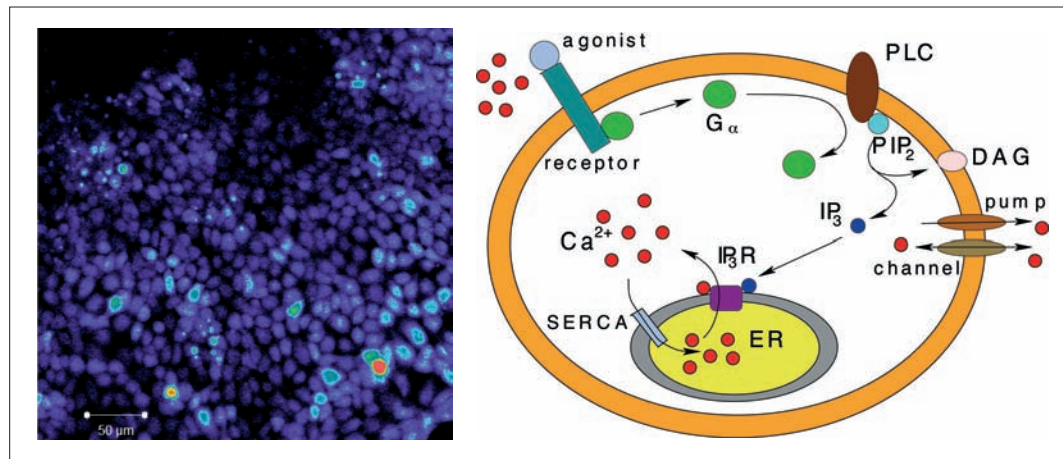


**Fig. 1:** Left panel: Microscopic fluorescence image of cultured astrocytes used in the investigation of calcium fluctuations in living cells. Red colour corresponds to high calcium concentration, blue to low concentrations. Right panel: Schematic illustration of a cell with the most important compartments for calcium oscillations: Calcium ( $\text{Ca}^{2+}$ ) can be released from the main calcium store, the endoplasmic reticulum (ER) (yellow), by ion channels. These channels are activated by calcium itself and  $\text{IP}_3$  (blue), which is produced by a G-protein ( $\text{G}_\alpha$ ) induced phospholipase C (PLC). Due to this mechanism, cells are connected to their environment by the activation of the G-protein by external stimuli, like hormones or calcium.

There are different kinds of repeated events: Sunrise will come tomorrow for sure, and the next summer will happen for sure, too. We do not know when the next big thunderstorm will come, but we do know it is unavoidable. Similarly, the next snow avalanche will go down a mountain side with certainty – we only do not know which day. However, here we know at least that another one will not follow immediately at the same spot because snow has to build up first again on the mountain top.

Repeated events are common in signaling with chemical messengers inside and between living cells. They are perceived as a repeated increase of the messenger concentrations and are usually called oscillations. Calcium ( $\text{Ca}^{2+}$ ) is probably the most ubiquitous second messenger, i.e. a messenger forwarding information arriving from outside within the cell [1]. It transmits its signal coded in the frequency of intracellular calcium concentration oscillations [2]. At the department Theoretical Physics (SF5), we investigate which type of repeated events these concentration peaks

during oscillations belong to: Are they real oscillations like the up and down of the sun, really random events like a storm or random events with minimal temporal separation like avalanches? Theoretical research of recent years [3] had predicted the last one: Random events with a minimal time lag – a minimal interspike interval ISI.

The generation of a spike is a random event. After the minimal ISI has passed, it occurs with a certain probability per time unit. If this probability is large, it will occur very soon after the minimal ISI elapsed and the sequence of spikes will be rather regular with the minimal ISI as period. If the probability for spike generation is small, it will take longer till the next event and the spike sequence will be more irregular. In fact, if the average ISI is long, the standard deviation of the ISI is a linear function of the average ISI since spike generation is a Poisson process.

In intracellular  $\text{Ca}^{2+}$  dynamics, intracellular storage compartments take up or  $\text{Ca}^{2+}$  into the bulk of the cell (the cytosol) or take it up from there [4].

Release is controlled by channels on the membrane of the compartment. If a channel opens,  $\text{Ca}^{2+}$  leaves the storage compartment and the concentration in the cytosol increases. The channels have the peculiar property that their open probability increases with the  $\text{Ca}^{2+}$  on the outside of the storage compartment. Consequently, if one channel opens,  $\text{Ca}^{2+}$  diffuses towards neighbouring channels and they open, too. Thus, release is a self amplifying process. This self amplification causes the individual spikes of the oscillations. The cell is in a refractory state after such a spike during which the opening probability of the channels is very low. The next spike may occur after recovery from inhibition. That sets the minimal ISI.

The opening of the first channel is a random event. Due to increased  $\text{Ca}^{2+}$  density, the neighbours of this first open channel are more likely to open as well, but they will not open with certainty. Hence, the probability per unit time for opening of a sufficient number of channels for a global event may become rather small. However, if sufficiently many channels open, release spreads through the whole cell – a wave is initiated. On the molecular level, channel opening corresponds to a binding event of a  $\text{Ca}^{2+}$  ion or  $\text{IP}_3$  molecule (Inositol triphosphate – another second messenger) at the cytosolic face of the channel. Hence, its randomness originates from the randomness of this binding event, i.e. thermal fluctuations. Typically, thermal fluctuations are averaged out, and on cellular level only deterministic behaviour is observed. The interesting property of intracellular  $\text{Ca}^{2+}$  dynamics is that fluctuations are carried through to the global level: The action of fluctuations can be read off the time series of global oscillations.

The most important prediction of recent theoretical investigations was that  $\text{Ca}^{2+}$  oscillations are repeated random events with a minimal ISI. That entails a linear dependence of the standard deviation of the ISI on the average ISI for large average ISI. We started a project in cooperation with several biochemistry laboratories: H. Kettenmann's laboratory at the Max-Delbrück-Centrum in Berlin-Buch, M. Wartenberg's laboratory at the GKSS outstation in Teltow outside Berlin, C. Taylor's laboratory at the University of Cambridge, and M. Bootman's laboratory at the Babraham Institute in Cambridge. The goal was to measure whether this theoretical prediction is verified by experimental data. Results from four different types of cells: astrocytes, micro glia, HEK cells (human embryonic kidney cells used in various experiments) and primitive endodermal cells confirm the theoretical prediction. Data from HEK cells are shown in Fig. 2. Clearly, the standard deviation  $\sigma$  increases with the average ISI.

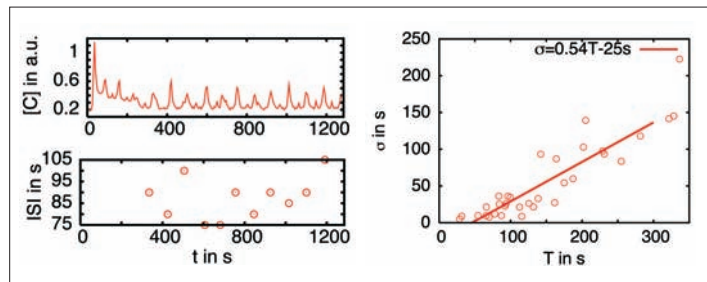


**Fig. 2:** A typical example of induced calcium oscillation in HEK cells (left top panel) and the corresponding inter spike intervals (ISI) (left bottom panel). By analyzing these oscillations, we derive a T-s-plot (right panel) showing the linear dependence of  $\sigma$  on T verifying our assumption of a stochastic process within the cell.

The experimental data confirm that repetitive wave initiation is the mechanism creating sequences of  $\text{Ca}^{2+}$  spikes. That mechanism replaces the idea of the  $\text{Ca}^{2+}$  handling inside cells being a deterministic oscillator. These two mechanisms are fundamentally different and entail different dependencies of oscillation characteristics on cell properties. The route to a comprehensive theory of intracellular  $\text{Ca}^{2+}$  oscillations is clear now with these fundamental results and we will follow it up.

Intracellular  $\text{Ca}^{2+}$  dynamics has already been known as a prototypical pattern forming system. Now, the appeal of intracellular  $\text{Ca}^{2+}$  dynamics to physicists has acquired another aspect with the experimental confirmation of the wave initiation hypothesis. We can study the statistics of microscopic fluctuations with macroscopic measurements.

- [1] Berridge, M.J., *Inositol trisphosphate and Calcium Signalling*, Nature **361**, 315–325 (1993)
- [2] Falcke, M., *Reading the patterns in living cells – the Physics of  $\text{Ca}^{2+}$  signaling*, Advances in Physics **53**, 255–440 (2004)
- [3] Falcke, M., *On the role of stochastic channel behavior in intracellular  $\text{Ca}^{2+}$  dynamics*, Biophys.J. **84**, 42–56 (2003)
- [4] Falcke, M., and D. Malchow, editors, *Understanding Calcium Dynamics – Experiments and Theory*, Lecture Notes in Physics, Vol. **623**, Springer, Berlin Heidelberg New York (2003)

#### Corresponding author:

M. Falcke  
falcke@hmi.de

# The biological role of arsenic in the rat

## Combined studies using tracer technique and biochemical methods

K. Bukalis, D. Alber, G. Bukalis, D. Behne, A. Kyriakopoulos

■ HMI, SF6

The human population of many countries such as India, Bangladesh, Thailand, Taiwan or China is chronically exposed to arsenic through consumption of the water containing arsenicals [1]. This leads to a variety of health effects, which depend strongly on the dose of exposure, age, health-status parameters, and nutrition and vary greatly among individuals [2].

In particular, an extremely high cancer rate is observed in this population. Thus there is a strong evidence for carcinogenicity of arsenic in humans, but only weak evidence in the case of animals – a unique scenario different from the situation found for other carcinogens. At present there are no

recognized models for the study of arsenic-induced carcinogenesis [3]. However, it has been convincingly established that arsenicosis (effect of chronic arsenic poisoning) is mediated through a modification of the gene expression, cell proliferation due to oxidative stress and other uncharacterized or poorly defined physiological aberrations or modifications [4]. The elucidation of such interactions might lead to the identification of sensitive subpopulations, provide cues for preventive or mitigation measures for arsenic intoxication, and suggest possible mechanism of toxicity.

Arsenic toxicity has been proposed to result from its affinity for the thiol groups of proteins. It has been reported that when arsenic is administered to cells it initially binds to cellular proteins before reduction or methylation can occur [5]. Therefore, the binding of arsenic to cellular proteins is a key determinate in arsenic metabolism. Although numerous studies have attempted to isolate arsenic-binding proteins, non proteins from mammalian tissues have been identified and demonstrated to bind arsenic. It is of great interest to analyze the arsenic-containing proteins present in the tissues of the rat and to get information on their subcellular distribution and their biological effects.

As arsenic is present in the organism in very small amounts (total arsenic content in the human body 3–4 mg), methods with extremely low limit of detection are needed in the investigation of the arsenic distribution among tissues and subcellular compartments and possible arsenic-containing proteins. For this purpose tracer methods, in which animals are labeled *in vivo* with  $^{73}\text{As}$ , are very suitable (a tracer is a substance containing a radioactive isotope; often used for monitoring the biological processes). With a half life of 80.3 days and a gamma energy in the range of 53 keV, this radionuclide is very well suited for tracer experiments. Because of the low detection limits of the tracer methods (below the femtogram range), only small amounts of the arsenic were used in experiments.

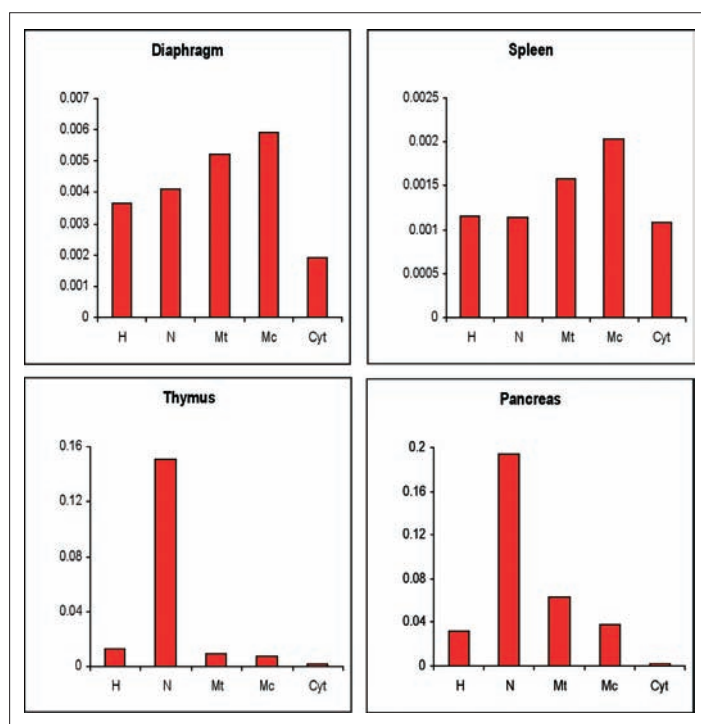


**Fig. 1:** Distribution of the  $^{73}\text{As}$  in the homogenates and subcellular fractions of the diaphragm, spleen, thymus and pancreas; homogenate (H), nuclei (N), mitochondria (Mt), microsomes (Mc) and cytosol (Cyt)

In order to obtain some information on arsenic sites of action and thus on its possible functions, the distribution of the tracer in the body compartments and their subcellular fractions was investigated. In this case rats were labeled *in vivo* by injection of 6 MBq  $^{73}\text{As}$  (130 ng arsenic) per animal. After 48 hours the tissues were dissected and the activity of the tracer was determined using a scintillation detector. The  $^{73}\text{As}$ -labelled tissues of the pancreas, thymus, spleen, liver, diaphragm, and lung were homogenized and then partitioned by differential centrifugation into nuclear, mitochondrial, microsomal and cytosolic fractions. The  $^{73}\text{As}$  activity was related to the protein concentration of those compartments. The arsenic-containing proteins present in the homogenates of these tissues have been studied by gel electrophoretic separation of the proteins and autoradiographic detection of the tracer.

Our results show that the arsenic was distributed inhomogeneously among the body compartments: the tissues varied strongly in the  $^{73}\text{As}$  content. The element was preferentially taken up by the thymus, pancreas and diaphragm. The tissues with the highest arsenic retention were homogenized and then partitioned by differential centrifugation. In the homogenates and subcellular fraction of these tissues differences in the  $^{73}\text{As}$  distribution were observed (see Fig. 1). The tracer was found to be incorporated differentially within the different cell compartments of the different tissues. It was mostly found in nuclei, but also in the cytosolic and microsomal fraction.

After combining tracer techniques with gel electrophoresis the arsenic-containing proteins could be detected in the homogenates of several rat tissues like spleen, adrenal gland, spermatic ducts, diaphragm, liver, thymus, trachea, brain, heart, lung, pancreas, testis, epididymis, small intestine and kidney. One of the autoradiograms is shown in Fig. 2. After evaluation of the autoradiograms several arsenic-binding proteins were distinguished. The protein labeled with  $^{73}\text{As}$  had relative molecular masses of >250 kDa, 75 kDa, 50 kDa, 37 kDa, 29–30 kDa, 25 kDa, 16 kDa and 15 kDa (Da=amu). There were remarkable differences in the characteristics of the arsenic-containing proteins between the tissues after SDS-PAGE (sodium dodecyl sulphate polyacrylamide gel electrophoresis). The  $^{73}\text{As}$ -binding bands with molecular masses of >250 kDa, 75 kDa, and 50 kDa were detected in all homogenates, whereas the bands of 37 kDa, 30–29 kDa, 25 kDa and 15 kDa were found only in some of them. The differences found in the distribution of the arsenic-binding proteins in the tissues indicate that the arsenic compounds may be involved in different intracellular processes. However nothing is known

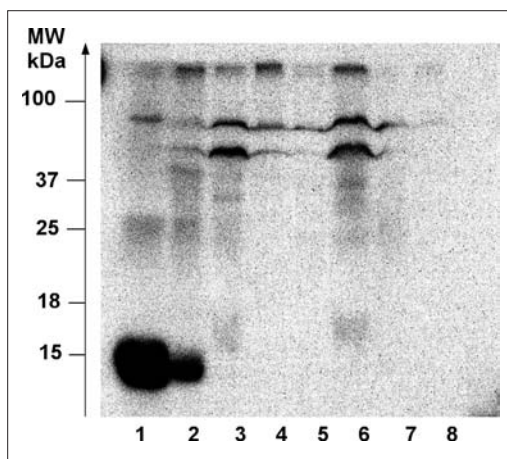


**Fig. 2:** Autoradiogram of the  $^{73}\text{As}$ -labeled proteins in the blood (1) and homogenates of spleen (2), adrenal gland (3), spermatic ducts (4), diaphragm (5), liver (6), thymus (7), trachea (8)

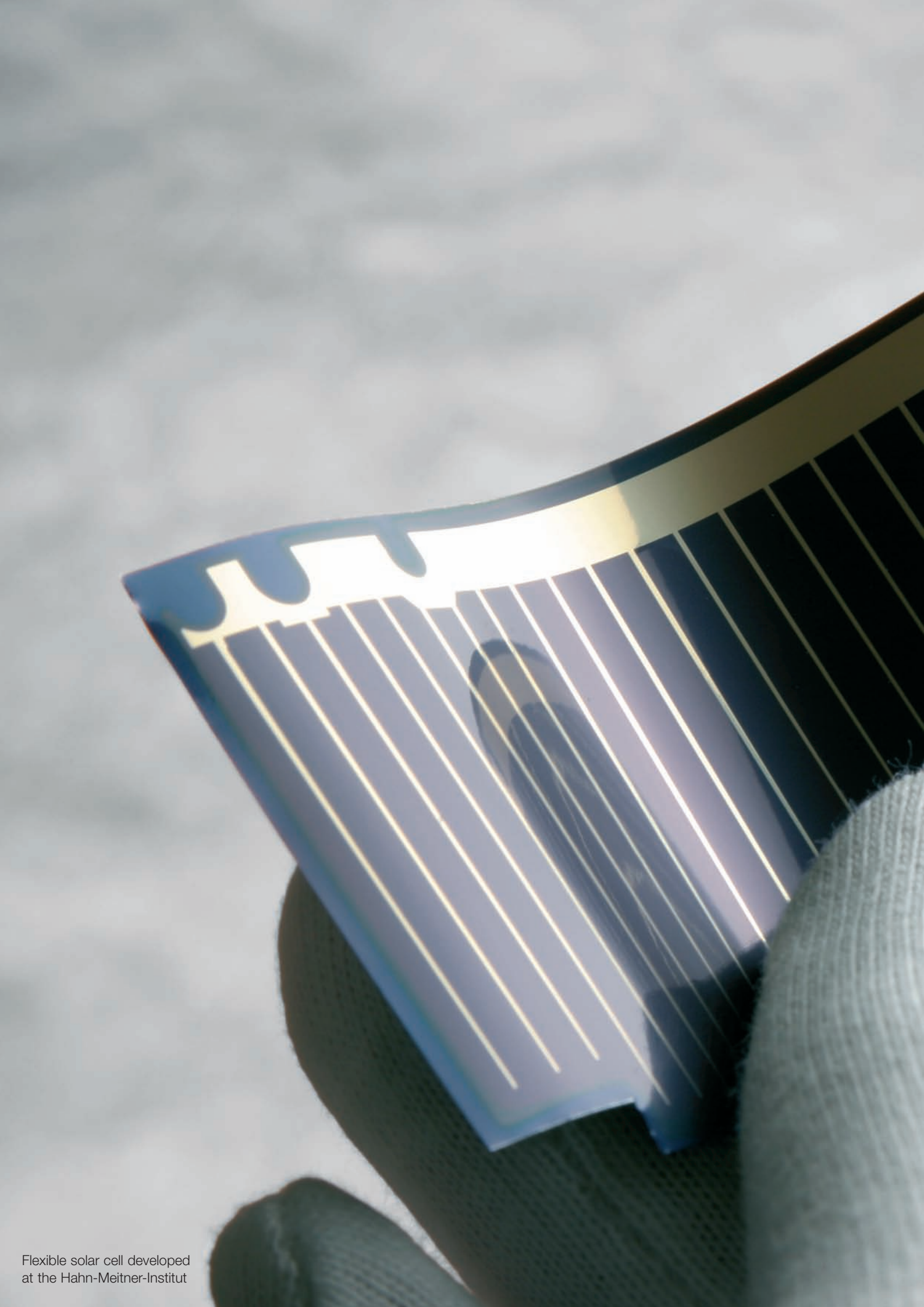
so far about these proteins, their structure, and function and how arsenic is incorporated into them. All elements which are incorporated non-covalently into the proteins are lost during the electrophoresis because it is a denaturing separation method, which causes the proteins to lose their native structure. In case when  $^{73}\text{As}$  remained in the proteins after SDS-PAGE the metalloid must be firmly bound, either covalently or as arsenosugar or one of the chemically active methylated compounds of trivalent arsenic.

The finding that arsenic is bound to proteins is of great interest. Therefore, further studies are being carried out in order to investigate more closely the biological functions of arsenic and especially the role of arsenic-containing proteins in different tissues.

- [1] Jolliffe, D.M., Budd, A.J., Gwilt, D.J., *Massive acute arsenic poisoning*, *Anaesthesia* **46** (4), 288–290 (1991)
- [2] Schoolmester, W.L., White, D.R., *Arsenic poisoning*, *Southern Med J* **73** (2), 198–208 (1980)
- [3] Chen, C.J., Chen, C.W., Wu, M.M., Kuo, T.L., *Cancer potential in liver, lung, bladder and kidney due to ingested inorganic arsenic in drinking water*, *Br J Cancer* **66**, 888–892 (1992)
- [4] Barchowsky, A., Dudek, E.J., Treadwell, M.D., Wetterhahn, K.E., *Arsenic induces oxidant stress and NF- $\kappa$ B activation in cultured aortic endothelial cells*, *Free Radic. Biol. Med.* **21**, 783–790 (1996)
- [5] Styblo, M., Thomas, D.J., *Binding of arsenicals to proteins in an *in vitro* methylation system*, *Toxicol Appl. Pharmacol.* **147**, 1–8 (1997)

#### Corresponding author:

K. Bukalis  
k.bukalis@hmi.de



Flexible solar cell developed  
at the Hahn-Meitner-Institut

A hand wearing a white knitted glove holds a solar cell. The solar cell has a dark surface with a grid of thin, light-colored lines. The background is a bright, slightly hazy sky. An orange banner is overlaid on the top right of the image, containing the title text.

## Scientific highlights Solar Energy Research 2005

SE1 Silicon Photovoltaics	68
SE2 Heterogeneous Material Systems	72
SE3 Technology	78
SE4 Dynamics of Interfacial Reactions	82
SE5 Solar Energetics	88
SE6 Electronic Structure of Semiconductor Interfaces	92

# Origin of preferential (100) orientation of poly-Si films made by aluminium-induced layer-exchange process

A. Sarikov<sup>1</sup>, J. Schneider<sup>2</sup>, J. Klein<sup>2</sup>, M. Muske<sup>2</sup>, S. Gall<sup>2</sup>, W. Fuhs<sup>2</sup>

■ 1 On leave from V. Lashkarev Institute of Semiconductor Physics NAS Ukraine, Kiev, Ukraine ■ 2 HMI, SE1

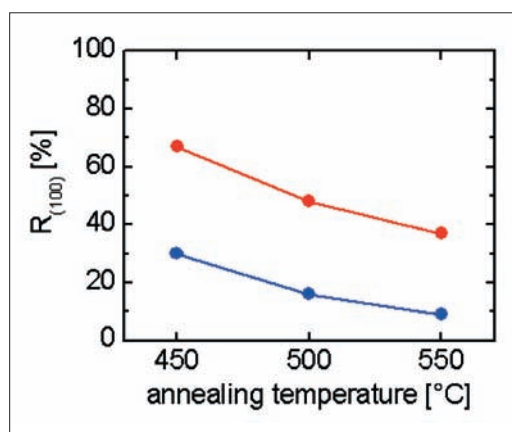


**Fig. 1:** Preferential (100) orientation  $R_{(100)}$  as a function of the annealing temperature,  $T_A$ , for samples with native oxide (red) and thermal oxide (blue) [4]. The definition of  $R_{(100)}$  is based on a 20° tilt with respect to the (100) orientation.

The formation of large-grained polycrystalline Si (poly-Si) seed layers on glass and the subsequent epitaxial thickening at low temperatures is a promising approach to create absorber layers of high electronic quality for poly-Si thin-film solar cells. The aluminium-induced layer-exchange (ALILE) process allows to form seed layers suitable for the subsequent epitaxial thickening at low temperatures (below 600°C). In the ALILE process, Al/amorphous silicon (a-Si) bi-layers on glass exchange their positions with a concurrent crystallization of the a-Si during annealing below the eutectic temperature of the Al/Si system (transformation of a glass/Al/a-Si structure into a glass/poly-Si/Al+Si structure) [1, 2]. The kinetics of this process is controlled by a thin  $\text{AlO}_x$  membrane between the initial Al and a-Si layers, obtained by oxidation of Al prior to a-Si deposition.

A characteristic feature of the poly-Si films prepared by the ALILE process is the preferential (100) grain orientation, which is very favourable for the epitaxial thickening at low temperatures [3]. The preferential (100) orientation,  $R_{(100)}$ , of the poly-Si layers made by the ALILE process is shown in Fig. 1, as obtained by electron back scattering diffraction (EBSD) [4] (the definition of  $R_{(100)}$  is based on a 20° tilt with respect to the (100) orientation). The preferential orientation is dependent upon the annealing temperature and the way the membrane has been formed (native oxide (Fig. 1, red) and thermal oxide (Fig. 1, blue)). Lower annealing temperatures result in higher degree of  $R_{(100)}$ , while annealing at higher temperatures leads to more Si grains featuring other orientations.

We have proposed a simple model for the formation of the preferential (100) orientation of Si grains during the ALILE process [5], which starts from the assumption of a preferential nucleation. The nucleation of Si grains during the ALILE process occurs heterogeneously at the interface between the membrane and the grain boundaries of polycrystalline Al. We have assumed a double pyramid shape of the Si nucleus in Al, formed by {111} planes, due to the lowest surface energy of this plane [6], and considered the formation of a Si nucleus obtained by sectioning the double Si pyramid by the Al/ $\text{AlO}_x$  membrane interface. The orientation of the sectioning plane was determined by two angles,  $\varphi$  and  $\theta$ , the rotation angle of the horizontal projection of plane normal, and the tilt angle from the vertical axes ([100] direction). The model structure is shown in Fig. 2. The formation of the critical nucleus is determined by the change of the Gibbs energy  $\Delta G$ :

$$\Delta G = \sigma_{\text{Al,Si}} S_{\text{Al,Si}} + \sigma_{\text{AlO}_x,\text{Si}} S_{\text{AlO}_x,\text{Si}} - \gamma V$$

Here,  $\sigma_{Al,Si}$  and  $\sigma_{AlO_x,Si}$  are the specific interface energies of Si with the Al and the  $AlO_x$  membrane, respectively,  $S_{Al,Si}(\varphi, \theta)$  and  $S_{AlO_x,Si}(\varphi, \theta)$  are the respective interface areas,  $\gamma$  is the specific volume energy of Si, and  $V(\varphi, \theta)$  is the nucleus volume. The first two terms describe the increase of the Gibbs energy due to the formation of the interface between Si and Al or  $AlO_x$  membrane, respectively. The third term describes the decrease of the Gibbs energy due to the Si bulk formation. The critical size of a nucleus and the corresponding critical Gibbs energy associated with nucleation,  $\Delta G_{cr}(\varphi, \theta)$ , at a fixed nucleus orientation relative to the Al/ $AlO_x$  membrane interface plane are determined by the maximum of the change of the Gibbs energy.

Si nuclei with minimum critical Gibbs energy are formed preferentially. Therefore, the preferential orientation of the poly-Si films is determined by the orientation of these nuclei. In Fig.3, the dependence of the critical Gibbs energy on the tilting angle,  $\theta$ , is shown for tilting in two directions, (110) ( $\varphi=0$ ) and (111) ( $\varphi=\pi/4$ ). The calculations have been made using  $\gamma=3.5 \times 10^8 \text{ J/m}^3$ , which corresponds to two times oversaturation of Al with Si,  $\sigma_{Al,Si}=0.2 \text{ J/m}^2$ , which corresponds approximately to the interface energy of 0.1 eV/atom of the solid phase crystallisation of amorphous Si [6], and  $\sigma_{AlO_x,Si}=0.5 \times \sigma_{Al,Si}$ . The value of the interface energy between the Si and the  $AlO_x$  membrane was taken arbitrary, only taking into account that it should be smaller than the  $\sigma_{Al,Si}$  value, to enable heterogeneous nucleation. This is justified since other values of  $\sigma_{AlO_x,Si}$  have an effect on only quantitative and not qualitative results.

It can be seen from Fig.3 that the energy barrier for nucleus formation,  $\Delta G_{cr}$ , is the smaller the closer is the nucleus orientation to (100). Therefore, the probability of formation of (100) oriented nuclei is larger compared to any other orientation. Especially this is true for the lower temperatures of annealing. At higher temperatures, the probability of nuclei to have orientation different from (100) increases, which can explain the experimentally observed temperature dependence of the preferential orientations of poly-Si films made by the ALILE process.

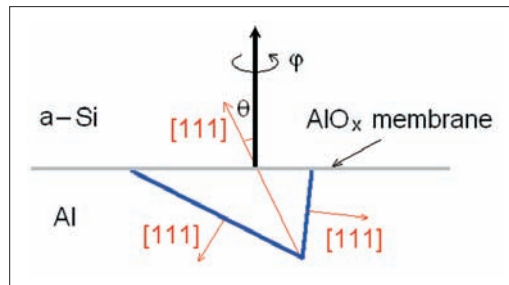


**Fig. 2:** Sketch of tilted pyramid. The orientation of the pyramid is determined by angles  $\varphi$  and  $\theta$ . The picture is shown for  $\varphi=45^\circ$ .

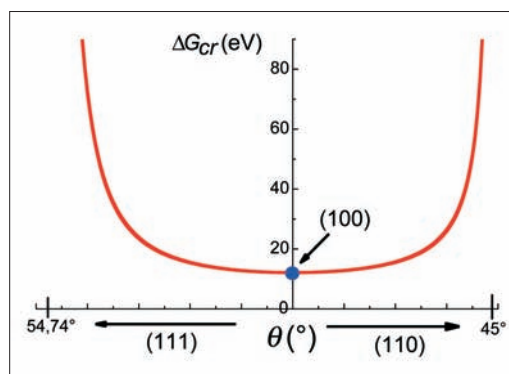


**Fig. 3:** Calculated critical Gibbs energy,  $\Delta G_{cr}$ , as a function of the tilt angle,  $\theta$ , from (100) towards (110) and (111) orientation

- [1] O. Nast, S.R. Wenham, J. Appl. Phys. **88** (1), 124 (2000)
- [2] J. Schneider, et al., Mater. Res. Soc. Symp. Proc. **862**, A 2.2 (2005)
- [3] B. Rau, et al., J. Cryst. Growth **270**, 396 (2004)
- [4] S. Gall et al., Thin Solid Films **511–512**, 7 (2006)
- [5] J. Schneider et al., J. Cryst. Growth **287**, 423 (2006)
- [6] C. Spinella, et al., J. Appl. Phys. **84** (10), 5383 (1998)

**Corresponding author:**

A. Sarikov  
andrey.sarikov@hmi.de

# Structural defects in crystalline silicon epitaxially grown at temperatures below 600°C

K. Petter<sup>1</sup>, B. Rau<sup>1</sup>, I. Sieber<sup>1</sup>, D. Eyidi<sup>2</sup>, M. Stöger-Pollach<sup>2</sup>, S. Gall<sup>1</sup>, K. Lips<sup>1</sup>, W. Fuhs<sup>1</sup>

■ 1 HMI, SE1 ■ 2 Technische Universität Wien, Vienna, Austria

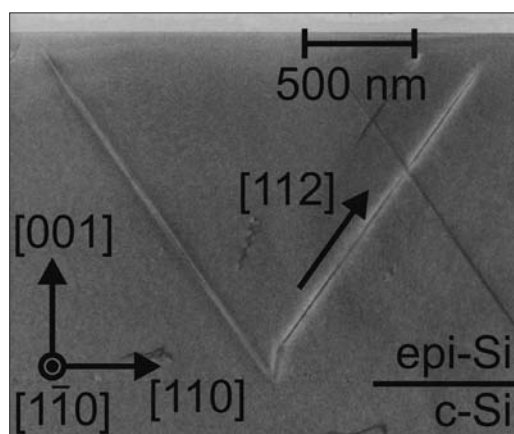


**Fig. 1:** TEM cross-section image of an epi-Si layer on top of a c-Si wafer revealing the V-shaped defect E2 that originates at the epi-Si/c-Si interface

En route to the realisation of large-grained polycrystalline silicon thin-film solar cells on glass, deposition methods are required that enable epitaxial growth on appropriate seed layers at temperatures below the softening point of the glass substrate ( $\sim 600^\circ\text{C}$ ). For the solar cell concept of the department such seed layers are produced from aluminium-induced crystallisation of amorphous silicon which are then epitaxially thickened by Electron-Cyclotron Resonance Chemical-Vapour Deposition (ECRCVD) [1]. This method enables low-temperature epitaxy by increasing the adatom mobility at the growth front due to low energy ion bombardment. However, a general problem is the formation of defects in the epitaxially grown silicon (epi-Si) layers. Depending on their density and electrical activity, recombination of charge carriers at such defects may severely lower the minority carrier lifetime and degrade the performance of a solar cell produced from this material. Therefore, it is most important to identify the relevant defects in epi-Si, understand their mechanism of formation and point out procedures to minimise their density.

In this work we present an investigation on line defects that develop during epitaxial growth with ECRCVD. In order to minimise influences of the non-ideal seed layer, the best possible substrate was used for epitaxy, namely a (100) oriented monocrystalline silicon (c-Si) wafer. Epi-Si layers deposited in the temperature range of  $560\text{--}600^\circ\text{C}$  are macroscopically of good crystalline quality and cannot be distinguished from perfect crystals using methods like Rutherford Backscattering or Raman investigations. However, using transmission electron microscopy (TEM) a variety of extended defects can be observed [2]. Fig. 1 exemplary shows a TEM cross section image of a V-shaped defect, called E2, that is created at the epi-Si/c-Si interface and grows in the [112] direction. Further analysis revealed that also two other types of line defects, labelled E1 and D, are present in the epi-Si layers [2]. Models of the line defects identified in epi-Si are presented in Fig. 2. Defects D and E2 are pairs of partial dislocations confining stacking faults (shaded region) with line directions of [314] and [112], respectively. Note that both start to grow at the epi-Si/c-Si interface. With secondary ion mass spectroscopy (SIMS) we revealed that there is a high oxygen concentration at the epi-Si/c-Si interface, which is probably due to a contamination of the wafer surface before deposition. Such an oxygen contamination is known to lead to the formation of dislocations in epi-Si layers [4]. In contrast to D and E2, the E1 defects have a different structure with their origin lying in the layer itself. Additional analysis using photoluminescence showed [2], that these defects are presumably so called “line interstitial defects”. These defects build up by agglomeration of self-interstitials, which are introduced into the epi-Si layers due to the low-energy ion bombardment during the growth.

In silicon solar cells, the density of extended defects in the absorber layer strongly determines device performance. A determination of defect densities in the epi-Si layers can, in principle, be accomplished by TEM. This, however, is connected with high preparative and analytical efforts. A more suitable method is defect etching, that makes use of the strained crystal region, which is always present around structural defects. Etch solutions like the so called "Secco Etch" have an anisotropic etch rate depending on the strain in the crystal. Etching the surface of the epitaxial layers therefore leads to etch pits where structural defects penetrate the surface. A scanning electron microscopy (SEM) image of the etched surface of a typical epi-Si film is shown in Fig. 3. An analysis of the form and crystallographic orientation of the etch pits makes it possible to relate the etch pits to the structural defects observed by TEM [2]. The etch pits are marked and named according to the classification shown in Fig. 2. With this identification the density of the different line defect can easily be determined.

With this procedure, we determined the dislocation density,  $N_D$ , of  $2\ \mu\text{m}$  thick boron-doped epi-Si layers on (100) c-Si substrate to be  $4 \times 10^6\ \text{cm}^{-2}$ . An as-grown solar cell prepared from these epi-Si layers had an efficiency of 4.2% and a short circuit current of  $13.0\ \text{mA cm}^{-2}$ , which is predicted for such a high value of  $N_D$  [3]. This leads us to the conclusion that the dislocations present in the epi-Si solar cell absorber are one major factor limiting the efficiency. Simulations show, that a reduction of  $N_D$  to  $10^6\ \text{cm}^{-2}$  should be sufficient to solve this problem [3]. In future work, we will therefore further investigate how the density of defects or their electrical activity can be reduced. Beside post deposition treatments like rapid thermal annealing and hydrogen passivation we will further optimize the wafer pre-treatments, since a reduction of the surface oxygen contamination by a factor of 10 should be sufficient to lower  $N_D$  by a factor of 100 [4].

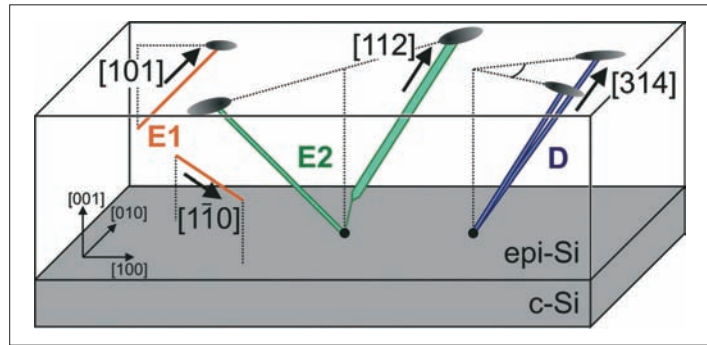


**Fig. 2:** Models of line defects in epi-Si layers. E1 defects are so called "line interstitial defects", E2 and D are pairs of partial dislocations with line directions of [112] and [314], respectively.

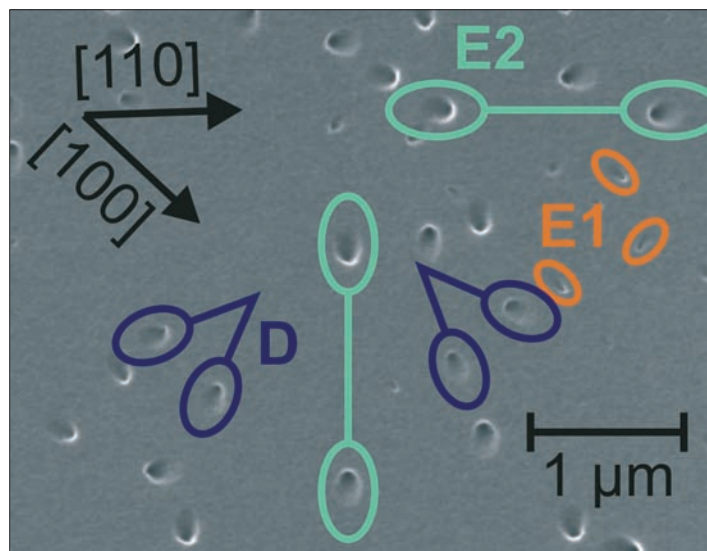


**Fig. 3:** Etch pits observed after treating the surface of the epi-Si layer with a defect etch. The etch pits could be assigned to the defects whose models are shown in Fig. 2.

- [1] B. Rau, I. Sieber, J. Schneider, M. Muske, M. Stöger-Pollach, P. Schattschneider, S. Gall, W. Fuhs, *J. Crystal Growth* **270**, 396 (2004)
- [2] K. Petter, D. Eyidi, M. Stöger-Pollach, I. Sieber, P. Schubert-Bischoff, B. Rau, A. T. Tham, P. Schattschneider, S. Gall, K. Lips, W. Fuhs, *Physica B* **376–377**, 117 (2006)
- [3] M. Imaizumi, T. Ito, M. Yamaguchi, K. Kaneko, *J. Appl. Phys.* **81**, 7635 (1997)
- [4] M. Tejwani, P. Ronsheim, *Mat. Res. Soc. Symp. Proc.* **259**, 467 (1992)

# Progress in Taking the CdS Layer out of Thin-Film Polycrystalline CuInS<sub>2</sub> Solar Cells

A. Ennaoui<sup>1</sup>, M. Bär<sup>1,3</sup>, J. Klaer<sup>2</sup>, T. Kropp<sup>1</sup>, R. Sáez-Araoz<sup>1</sup>, H.-W. Schock<sup>2</sup>, M.C. Lux-Steiner<sup>1</sup>

■ 1 HMI, SE 2 ■ 2 HMI, SE 3 ■ 3 Current address: University of Nevada, Las Vegas, USA

## Introduction

At the Hahn-Meitner-Institut (HMI), the two departments SE2 and SE3 cooperate in a joint effort with the aim to eliminate the CdS window layer commonly used in CuInS<sub>2</sub> solar cell devices. This is motivated by the potential to enhance the spectral response in the blue wavelength region by the use of materials with wider band-gap than CdS ( $E_g \sim 2.4$  eV). Furthermore, CdS as a heavy metal compound should be avoided in the final solar modules as well as in their production processes. Thus chalcopyrite photovoltaic industry should not be listed in the future as a source of cadmium emission to the environment. In this work we present recent progress in Cd-free CuInS<sub>2</sub> with Zn(S,O) ( $E_g \sim 3.6$ – $3.8$  eV) buffer layers prepared by a solution growth method known as Chemical Bath Deposition (CBD).

phur [1] and allow the formation of Zn(S,O) layer with high growth rate.

XPS analysis of Zn(S,O) on CIS:

We focused on the interface formation during the growth of the ZnS buffer onto the CIS substrate. The approach for the investigation of the CBD-ZnS/CIS interface is described in ref. [2,3]. A set of samples was characterized by X-ray Photoelectron Spectroscopy (XPS) and X-ray Auger Electron Spectroscopy (XAES) using an Mg K $\alpha$  x-ray source (1253.6 eV). The buffer layer was deposited onto (KCN-etched) CIS substrates within different deposition times. The evaluation of XPS spectra in the Zn3d and In4d region reveals a complete coverage of the CIS absorber layer after 13,5 min of buffer deposition. The evaluation of the Zn L<sub>3</sub>M<sub>45</sub>M<sub>45</sub> XAES signal for the Zn(S,O)/CIS sample series (Fig. 1, right) shows that in the early stages of the CBD process (up to 6 min deposition time) a thin (up to 0.6 nm) ZnS layer is formed on the CIS, whereas in the second half of the CBD ("9 min" and "13.5 min" sample) Zn(S,O) is deposited with a greatly increased growth rate. This is supported by the comparison of the Zn L<sub>3</sub>M<sub>45</sub>M<sub>45</sub> XAES measured spectra with Zn L<sub>3</sub>M<sub>45</sub>M<sub>45</sub> (G) Auger peak of Zn-compounds possibly formed in the chemical bath (e.g., ZnO, ZnS, Zn(OH)<sub>2</sub>) [4]. Fig. 1 (left) shows the normalized XPS photoemission signals of the CIS substrate and Zn(S,O) buffers. The attenuated substrate intensities (In 3d<sub>3/2</sub>, In 4d<sub>3/2</sub>, Cu 2p<sub>3/2</sub>, Cu 3p<sub>1/2</sub>) are normalized to the value of the uncovered substrate: "0 min" and the intensity of the attenuating Zn(S,O) top-layer (Zn 2p<sub>3/2</sub> and Zn 3d<sub>3/2</sub>) XPS peaks are normalized to the value of a complete substrate coverage: "13.5 min".

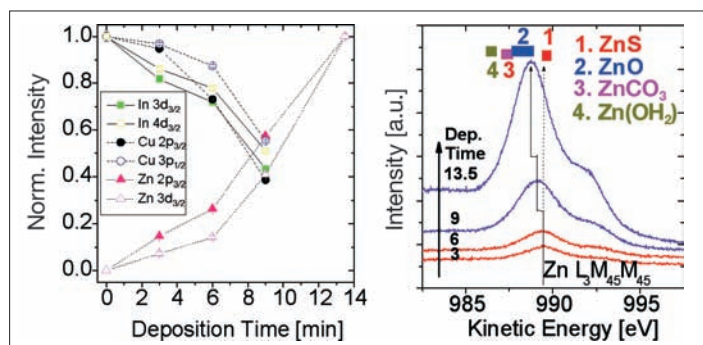


**Fig. 1:** left: Normalized XPS intensities signal from the attenuated substrate and attenuating Zn(S,O) top-layer. right: Zn L<sub>3</sub>M<sub>45</sub>M<sub>45</sub> Auger peak for different coverage with Zn(S,O) buffer. The regions of different Zn-compounds from the literature are indicated in bars.

## CBD-Zn(S,O) growth on CIS

Background of CBD-Zn(S,O):

A typical CBD of ZnS uses ammonia (NH<sub>3</sub>), Zn-salt (ZnSO<sub>4</sub>) and thiourea (SC(NH<sub>2</sub>)<sub>2</sub>) in an aqueous solution. SC(NH<sub>2</sub>)<sub>2</sub> is known to provide S<sup>2-</sup> ions. NH<sub>3</sub>, usually described as a cation complexing agent, plays an important role in controlling the formation of metal hydroxide and increases the rate of thiourea hydrolysis. We have originally conceived a new CBD process where SC(NH<sub>2</sub>)<sub>2</sub> and Zn-salt form [Zn(SC(NH<sub>2</sub>)<sub>2</sub>)<sub>n</sub>]<sup>2+</sup> complexes. The new complexes act as a source of zinc and sul-

The intensities of the substrate photoemission signals decrease with increasing deposition time, simultaneously the intensities of the top-layer-related Zn XPS peaks increase. Interestingly, the photoemission signals ascribed to In are more strongly attenuated by the Zn(S,O) top-layer as the ones ascribed to Cu in the initial stages of the chemical bath deposition. This finding gets even more pronounced if one takes the inelastic mean free path (IMFP) of the corresponding photoelectrons into account (according to the universal curve the IMFPs of the Cu 3p and Cu 2p photo-

electrons are smaller than those of the In4d and In3d photoelectrons, respectively). The thickness calculated from the attenuation of the In (In3d<sub>3/2</sub> and In4d) photoemission lines is bigger than the one determined from the intensity behavior of the Cu (Cu2p<sub>3/2</sub> and Cu3p) XPS signals. Since a larger Zn(S,O) layer “thickness” is determined for Indium, this can be interpreted as an In migration away from the buffer/absorber interface during ZnS/Zn(S,O) deposition, a Cu migration towards the hetero-contact or even a Cu “diffusion” out of the CIS into the deposited buffer layer. The detail for this issue will be developed in Ref. [5].

### Solar cell devices

All samples were prepared according to the preparation conditions described in ref. [2, 3]. Table 1 summarizes the device performance with Zn(S,O) buffer. The efficiencies are compared with the corresponding CBD-CdS reference cells. All the results are supported by significant statistical data. Annealing in air at approx. 200°C has positive effects on the device performance.

Buffer	Type	V <sub>oc</sub> [mV]	J <sub>sc</sub> [mA/cm <sup>2</sup> ]	FF [%]	η [%]
Zn(S,O)	Cell	700.4	700.4	65.8	10.4
CdS		705.7	705.7	66.8	10.2
CdS	Module	671.6	671.6	66.9	9.07
Zn(S,O)		700	700	64.0	10.1

**Table 1:** Performance of cells and modules with CBD-Zn(O,S) buffer layer compared to CdS base line under standard conditions for AM1.5 irradiation

As expected, the CIS solar cell with alternative Zn(S,O) buffer benefits from its increased window transparency in the short-wavelength region compared to the device with CdS buffer as indicated by the higher J<sub>sc</sub>. This conclusion is also supported by external quantum efficiency measurements of corresponding solar cells with Zn(S,O) and CdS buffers, respectively, which are shown in Fig. 2. The higher transparency of the Zn(S,O) buffer layer in the short-wavelength region in comparison to that of the CdS layer can clearly be seen. The difference between the respective QEs (QE<sub>Zn(S,O)}</sub> – QE<sub>CdS</sub>) is also given at the bottom of Fig. 2. The area below this curve related to the solar spectrum AM1.5 is indicative of the respective difference in J<sub>sc</sub>, which is determined here to be approx. 1 mA/cm<sup>2</sup>.

This improvement of J<sub>sc</sub> of the devices with a Zn(S,O) buffer in comparison to the CdS buffered reference is obviously sufficient to compensate losses from V<sub>oc</sub> and FF, which are still a little lower than those of solar cells with CBD-CdS buffer, resulting in a comparable efficiency. In order to determi-

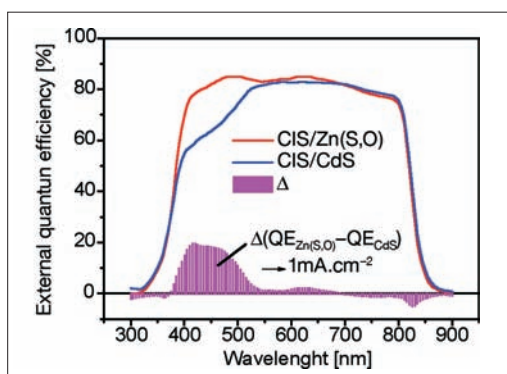


**Fig. 2:** External quantum efficiencies of CIS-based solar cells with Zn(S,O) and CdS buffer, respectively. The difference  $\Delta$  between the two QEs is indicated.

ne the active area efficiency of the CIS-based device with Zn(S,O) buffer the J<sub>sc</sub> (24.5 mA/cm<sup>2</sup>) extracted from corresponding QE measurements was used. In this way active area was calculated to 11.3%, which is to our knowledge the (up to now) highest reported efficiency of Cd-free CuInS<sub>2</sub>-based thin film solar cells with Zn-compound buffer layers.

### Final remarks

The new CBD process originally conceived allowed the formation of Zn(S,O) based buffer layers on CIS absorber with high growth rate and demonstrate the potential of being as good as the conventional used CdS buffers for CIS solar cell devices. For the first time, Cd free CIS-based mini-modules yield active area (17.2 cm<sup>2</sup>) efficiency up to 10%. The following issues are currently investigated: CBD control of oxygen to sulfur ratio, intermixing at CIS/Zn(S,O) interface and valence band offset, the impact of intermixing on the devices performances and scaling up the CBD process to large area 10 × 10 cm<sup>2</sup>.

- [1] German Patent pending: 10 2004 040 546.8-33.
- [2] A. Ennaoui, M. Bär, J. Klaer, T. Kropp, R. Sáez-Araoz, and M.C. Lux-Steiner, Proc. 20<sup>th</sup> European Photovoltaic Solar Energy Conference (EPVSEC-20), Barcelona, Spain, (2005) 1882
- [3] A. Ennaoui, M. Bär, J. Klaer, T. Kropp, R. Sáez-Araoz, and M.C. Lux-Steiner, Prog. Photovolt. In press
- [4] M. Bär, A. Ennaoui, J. Klaer, T. Kropp, R. Sáez-Araoz, N. Allsop, I. Lauermann, H.-W. Schock, and M.C. Lux-Steiner, J. Appl. Phys., submitted.
- [5] M. Bär, A. Ennaoui, J. Klaer, T. Kropp, R. Sáez-Araoz, S. Lehmann, A. Grimm, I. Lauermann, Ch. Loreck, St. Sokoll, Ch. Jung, H.-W. Schock, Ch.-H. Fischer and M.C. Lux-Stein J. Appl. Phys. In preparation

### Corresponding author:

A. Ennaoui  
ennaoui@hmi.de

# Optimising the interface between zinc-phthalocyanine films and the transparent indium-tin oxide anode in organic solar cells

M. Vogel, B. Johnev, M. Rusu, F. Streicher, S. Sadewasser, T. Mete, Ch. Breyer, M. Ch. Lux-Steiner, K. Fostiropoulos

■ HMI, SE2

Organic solar cells are regarded as a potentially low cost technology and may play a crucial role in the photovoltaic evolution of the coming decades [1]. Scientific knowledge in this field however is much less extensive than in the case of inorganic technology. Among the most important issues for the optimisation of photovoltaic devices range the interfaces between inorganic electrodes and organic photoactive films. To ensure loss free transport of charge carriers across these interfaces, the formation of uniform, ohmic contacts without traps or defects are required.

In the following we focus on the interface between the transparent Indium-tin oxide (ITO) electrode and a zinc-phthalocyanine (ZnPc) film. In organic solar cells based on ZnPc and  $C_{60}$  holes need to be conducted across this interface. Judging from the work function of solvent cleaned ITO of 4.2 eV [2] and the ionization energy of ZnPc of 5.3 eV [3], a mismatch between highest occupied molecular orbital (HOMO) of ZnPc and the Fermi level in the ITO conduction band of 1.1 eV is expected. To reduce this mismatch and thus improve hole transport the work function of ITO can be increased by surface treatments, i.e. dipping ITO substrates into phosphoric acid [4]. This treatment induces the formation of a surface dipole layer and in consequence an increase of the work function by  $0.6 \pm 0.1$  eV [2]. Solar cell performance was thus improved by up to 40% [5].

To provide a better understanding of this effect, the interface was characterised using photoelectron spectroscopy (PES) and ultra high vacuum Kelvin probe force microscopy (UHV-KPFM). As in standard solar cell preparation [5] ITO substrates were coated with ZnPc by thermal vacuum deposition. The samples were then transferred in vacuum to the ultra high vacuum PES system and analysed by ultraviolet photoelectron spectroscopy (UPS). By fabricating a series of extremely thin (0–64 Å) ZnPc films, the UPS results yielded a detailed picture of the electronic transition from ITO to ZnPc. The resulting energy diagrams for the ITO reference sample (solvent cleaned commercial substrates) and for phosphoric acid dipped ITO are plotted in Fig. 1.

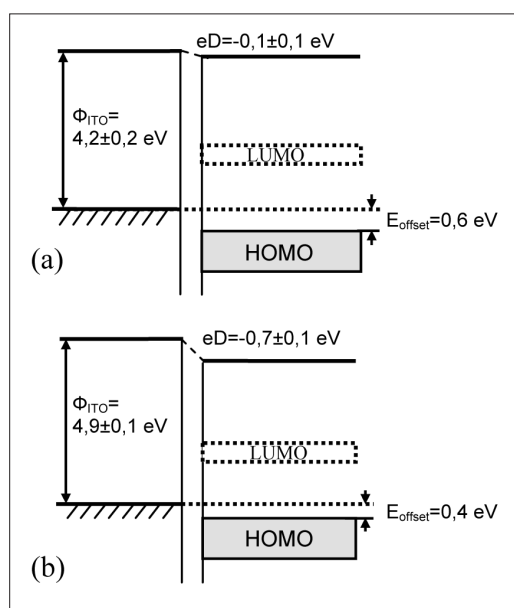


**Fig. 1:** Energy diagrams of ZnPc on solvent cleaned ITO (a) and of ZnPc on phosphoric acid treated ITO.  $\phi$ : work function,  $eD$ : dipole, LUMO: lowest unoccupied molecular orbital.

The results of the UPS measurements lead to a number of interesting conclusions. They show that the offset between HOMO of ZnPc and Fermi level of ITO is nearly the same for solvent cleaned and phosphoric acid treated ITO. It is important to note that within the accuracy of the measurement ( $\pm 0,1$  eV) no band bending was observed in the phthalocyanine film. However the results imply the formation of a dipole within the first monolayer of ZnPc. This dipole is about equal in magnitude and opposite in direction compared to the surface dipole of ITO induced by the acid treatment. In consequence the improvement in efficiency of solar cells produced with acid treated ITO cannot be attributed to a reduced offset at the interface. Another mechanism must be responsible for the beneficial effects of ITO acid treatment. Several hints suggest that these effects are due to the formation of a uniform interface with little defects between acid treated ITO and ZnPc: X-ray PES measurements have shown that the treatment with phosphoric acid causes a chemical reaction of acid ions with the ITO surface [2]. The resulting chemically bound monolayer proved to be very stable. UHV-KPFM measurements of phosphoric acid treated ITO yield the locally resolved work function of the sample. The resulting image is presented in Fig. 2. It confirms the work function values found by PES and in addition shows that the acid treatment leads to a very homogeneous work function with a standard deviation of only 0.019 eV.

To further optimise the ITO-ZnPc interface the approach of chemical modification of the ITO anode is continued. Currently examinations on modified, soluble ZnPc molecules with four phosphoric acid groups are in progress. The aim is to maintain the benefits of a chemically bound monolayer on ITO while at the same time establishing close contact of phthalocyanine molecules with the surface. First measurements indicate a strong increase in work function and enhanced crystallinity of ZnPc-films on thus treated ITO substrates.

- [1] C. J. Brabec, Sol. Energy Mater. Sol. Cells **83**, 273 (2004)
- [2] M. Vogel, Dissertation Freie Universität Berlin 2005
- [3] W. Gao, A. Kahn, Organic Electronics **3**, 53 (2002)
- [4] F. Nüesch, L. J. Rothberg, E. W. Forsythe, Q. T. Le, Y. Gao, Appl. Phys. Lett. **74**, 880 (1999)
- [5] B. Johnev, M. Vogel, K. Fostiropoulos, B. Mertesacker, M. Rusu, M.-C. Lux-Steiner, A. Weidinger, Thin Solid Films **488**, 270 (2005)

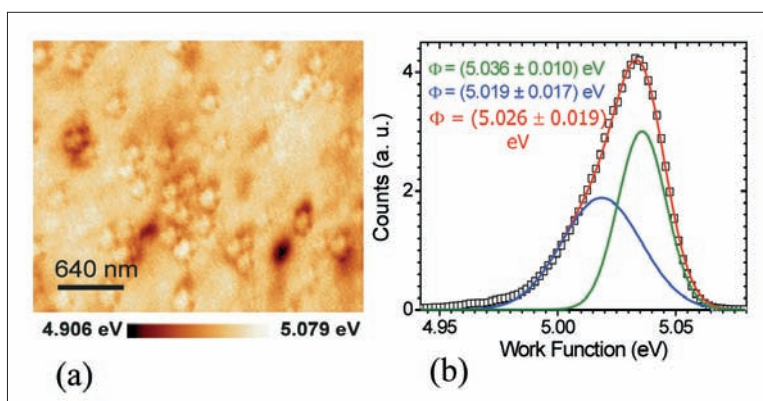


**Fig. 2:** (a) UHV-KPFM work function image of a phosphoric acid treated ITO surface (b) the respective histogram (b)

# On the $\text{CuGaSe}_2$ - $\text{CuGa}_3\text{Se}_5$ solid state transition in CCSVT-grown $\text{CuGa}_x\text{Se}_y$ thin films

S. Lehmann<sup>1</sup>, M. Bär<sup>1,2</sup>, D. Fuertes Marrón<sup>1</sup>, P. Pistor<sup>1</sup>, S. Wiesner<sup>1</sup>, M. Rusu<sup>1</sup>, I. Kötschau<sup>1</sup>, I. Lauer<sup>1</sup>, A. Grimm<sup>1</sup>, S. Sokoll<sup>1</sup>, Ch. Jung<sup>3</sup>, Ch.-H. Fischer<sup>1,4</sup>, Th. Schedel-Niedrig<sup>1</sup>, M.Ch. Lux-Steiner<sup>1,4</sup>

■ 1 HMI, SE2 ■ 2 Department of Chemistry, University of Nevada, Las Vegas, USA ■ 3 BESSY Berlin, Germany  
 ■ 4 Freie Universität Berlin, Germany

Cu-poor  $\text{Cu}(\text{In}_{1-x}\text{Ga}_x)\text{Se}_2$   $x \approx 0.3$  films used for high performance devices reaching efficiencies of almost 20% show a surface composition resembling to that of a 1:3:5 compound. A well established model states that a Cu-depleted surface region has beneficial effects on complete cells due to band gap widening and n-type inversion. Experimental evidence of a 1:3:5 surface composition was found in device quality

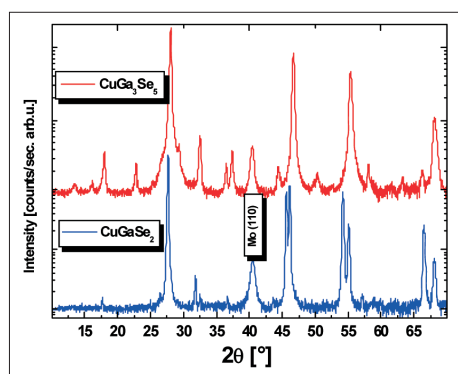


**Fig. 1:** XRD scans of a chalcopyrite single phase CCVT-grown  $\text{CuGaSe}_2$  thin film (bottom/blue) and of an ODC single phase CCVT-grown  $\text{CuGa}_3\text{Se}_5$  thin film (top/red) (measured in a Bruker D8 Advance setup with  $\text{Cu-K}\alpha_{1,2}$ -radiation)

$\text{CuGaSe}_2$  films [1]. However, it still remains unclear whether the presence of such a surface region has a similar positive impact on wide gap  $\text{CuGaSe}_2$ , as compared to its low gap counterparts. To elucidate this problem we carried out a systematic study of the impact of Cu-depletion in  $\text{CuGaSe}_2$  films.

Non-vacuum chemical close spaced vapour transport (CCSVT) was used for the growth of thin polycrystalline films by exposure of metallic Cu-precursors deposited on Mo-coated plain soda lime glass substrates to a  $\text{GaCl}_x/\text{H}_2\text{Se}$  atmosphere [2]. The final film composition can be controlled, ranging from single phase 1:1:2 up to 1:3:5 by adjusting the process parameters.  $\text{CuGa}_x\text{Se}_y$  thin films were grown in a compositional range of  $1 < x < 3$ . This was performed by a variation of deposition times. For analysis of the absorber backside a glass substrate was glued with silver-epoxy on the top side of selected samples. Afterwards the absorber layer was lifted-off [3] under inert  $\text{N}_2$ -atmosphere, peeling the  $\text{CuGa}_x\text{Se}_y$  from the Mo back contact making the absorber backside accessible for characterization.

X-ray diffraction (XRD) spectra were recorded at a Bruker D8 Advance setup in grazing incident geometry for incident angles  $\vartheta_1 = 0.5^\circ - 2.0^\circ$ , yielding surface and bulk sensitive structural information which is strongly depth-correlated (for  $\vartheta_1 = 0.5^\circ \rightarrow$  information depth,  $a = 1 \text{ mm}$  and for  $\vartheta_1 = 2.0^\circ \rightarrow a = 4 \text{ mm}$ ) [4, 5]. Both phases, the chalcopyrite (CCP) and the 1:3:5 ordered defect compound (ODC) can easily be distinguished from their XRD pattern (see Fig. 1), resulting from different space-group symmetries,  $I\bar{4}2d$  for CCP and (proposed)  $I42m$  for  $\text{CuIn}_3\text{Se}_5$  [6].

An analysis of the (112) reflexion detected under grazing incident conditions of  $\vartheta_1 = 0.5^\circ$  up to  $2.0^\circ$  is shown in Fig. 2. By comparison of the measurements of the absorbers' front- and backside it can be clearly shown that the ODC phase is mainly located at the surface of the thin film structure (Fig. 2).

Compositional data on the  $[\text{Ga}]/[\text{Cu}]$ -ratio in the  $\text{CuGa}_x\text{Se}_y$  thin films were collected by using surface sensitive X-ray emission spectroscopy (XES) (performed at CISSY/BESSY 2-U41PGM,  $h\nu = 1200 \text{ eV}$ ) and bulk sensitive X-ray fluorescence (XRF) (measured with a standard Philipps MagiX-Pro X-ray fluorescence system). While the integral composition provided by the XRF measurements was based on the analysis of the  $\text{K}\alpha$ -fluorescence radiation of the relevant elements, the surface sensitive XES measurement used the  $\text{L}_{2,3}$ -fluorescence radiation of Ga and Cu. The latter detection mode has an information depth of about  $900 \text{ nm}$  [4, 5] for Ga-rich samples and for both used emission lines (Ga and  $\text{Cu L}_3$ ).

The comparison of the Cu- and Ga- $\text{L}_3$  emission lines from the XES spectra taken for two (in terms of integral composition) different samples at their front- and backsides reveals (see Fig. 3):

- The front- is Cu-poorer/Ga-richer than the backside,
- The Ga-signal for the backsides of both samples is in the same range whereas for the corresponding front sides it is significantly higher.

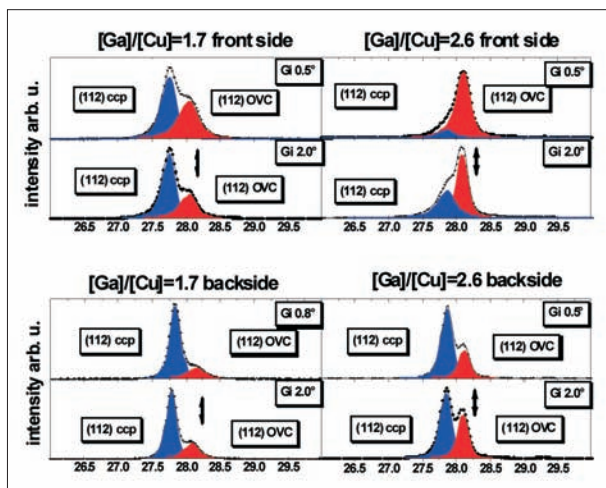


**Fig. 2:** Detailed XRD-scans showing the (112) reflexions of chalcopyrite (blue) as well as ODC structure (red) in grazing incident geometry for surface sensitivity [ $\theta_1=0.5/0.8^\circ$ ] and bulk sensitivity [ $\theta_1=2.0^\circ$ ]. Both were carried out for front- (top) and backsides (bottom) of CCSVT-grown  $\text{CuGa}_x\text{Se}_y$  thin films with integral  $[\text{Ga}]/[\text{Cu}]=1.7$  (left) and  $[\text{Ga}]/[\text{Cu}]=2.6$  (right) (measured with a Bruker D8 Advance setup with  $\text{Cu-K}\alpha_{1,2}$ -radiation).

iii.) The Ga-signal, which is simulated for the measured integral composition indicates that the sample with  $[\text{Ga}]/[\text{Cu}]\approx 2.6$  consists of nearly equal amounts of both phases (ODC on CCP), whereas for the sample with  $[\text{Ga}]/[\text{Cu}]\approx 1.7$  a thick CCP layer is covered by a relatively thin ODC layer.

Additionally, we have carried out photoelectron emission spectroscopy measurements (PES, not shown) that give information on the first few nanometres of the sample surface. This PES data always reveal a Cu-poor (surface) composition compared to that calculated from the XES data. This leads to the conclusion that the surface of all thin films, even that of a single phase ODC layer, is copper-depleted.

Based on our results, we propose a model for the  $\text{CuGa}_3\text{Se}_5$  solid state phase formation for Ga-rich  $\text{CuGa}_x\text{Se}_y$  CCSVT-grown thin films:

The transition from  $\text{CuGaSe}_2$  to  $\text{CuGa}_3\text{Se}_5$  starts with an almost stoichiometric  $\text{CuGaSe}_2$  thin film where copper-depletion occurs only in the first few nanometres of the sample. Successive Ga- and Se-enrichment leads to an integral composition of the film of  $[\text{Ga}]/[\text{Cu}]\approx 1.5$ . At this point the integral composition of the film crosses the coexistence line for the CCP single phase and the CCP/ODC two-phase region. Beyond this composition  $1.5 < [\text{Ga}]/[\text{Cu}] < 3.0$  an ODC phase is formed on top of the CCP film (i.e., the ODC becomes that thick that its – compared to the samples' integral – Cu-poorer composition cannot only be revealed

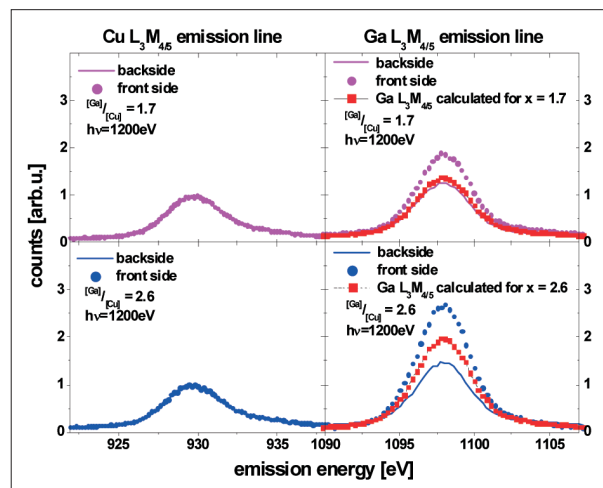


**Fig. 3:** XES detail spectra of  $\text{Cu L}_3$  (left) and  $\text{Ga L}_3$  (right) emission lines of CCSVT-grown  $\text{CuGa}_x\text{Se}_y$  thin films with integral  $[\text{Ga}]/[\text{Cu}]=1.7$  (top) and  $[\text{Ga}]/[\text{Cu}]=2.6$  (bottom) (recorded at CISSY/BESSY-U41-PGM,  $h\nu=1200\text{eV}$ ). The spectra were normalized to the intensity of the  $\text{Cu L}_3$  emission line.

by PES but also by XES measurements) and grows both inward and outward, as the total film thickness increases.

This process takes place until the complete layer consists of a single phase ODC, which nevertheless still shows hints for a further Cu-depletion in its near surface region.

- [1] A. Meeder, L. Weinhardt, R. Stresing, D. Fuertes Marrón, R. Würz, S.M. Babu, Th. Schedel-Niedrig, M. Ch. Lux-Steiner, C. Heske, E. Umbach, *J. Phys. Chem. Solids* **64**, 1553 (2003)
- [2] M. Rusu, S. Wiesner, D. Fuertes Marrón, A. Meeder, S. Doka, W. Bohne, S. Lindner, Th. Schedel-Niedrig, CH. Giesen, M. Heuken and M. Ch. Lux-Steiner, *Thin Solid Films* **451–452**, 556 (2004)
- [3] D. Fuertes Marrón, A. Meeder, S. Sade-wasser, R. Würz, C.A. Kaufmann, Th. Glatzel, Th. Schedel-Niedrig and M. Ch. Lux-Steiner, *Journ. Appl. Physics* **97**, 094915-1 (2005)
- [4] Lawrence Berkeley Laboratories internet [http://www-cxro.lbl.gov/optical\\_constants](http://www-cxro.lbl.gov/optical_constants)
- [5] National Institute of Standards and Technology, <http://physics.nist.gov/PhysRefData/>
- [6] T. Hanada, A. Yamana, Y. Nakamura, O. Nittono and T. Wada, *Jpn. J. Appl. Phys.* **36**, L1494–L1497 (1997)

**Corresponding author:**

S. Lehmann  
sebastian.lehmann@hmi.de

# Studying interdiffusion of $\text{CuInS}_2$ and $\text{CuGaS}_2$ by *in situ* diffraction

I.M. Kötschau, A. Weber, H.-W. Schock

■ HMI, SE3

In order to better understand the growth of chalcopyrite compounds for solar cell applications it is very useful to study the film formation *in situ* by energy dispersive x-ray diffraction (EDXRD). Apart from the basic understanding of  $\text{CuInS}_2$  growth [1,2] mechanism using metallic Cu/In precursors it was shown that EDXRD in conjunction with diffuse laser light scattering (LLS) helps to establish new methods for industrial process control [3]. In this report we further extend the capabilities of EDXRD to study the interdiffusion of  $\text{CuInS}_2$  and  $\text{CuGaS}_2$ .

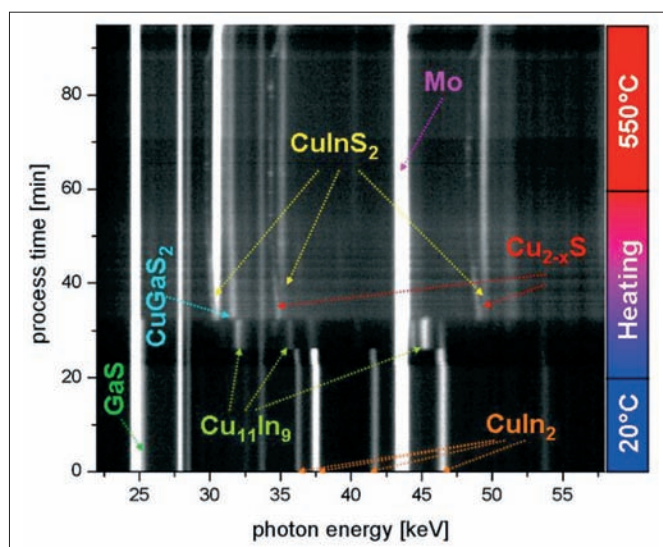


**Fig. 1:** EDXRD spectra as function of process time. The intensity of the peaks is provided by the grey scale. Brighter areas signify higher intensities.

The partial replacement of In by Ga in the chalcopyrite structure widens the band gap of the material [4]. Thereby the open circuit voltage of corresponding devices can be significantly enhanced [5]. In order to monitor the Ga incorporation in the a quaternary  $\text{Cu(In,Ga)S}_2$  alloy we studied the phase transformations of  $\text{Ga}_x\text{S}_y$ -(Cu,In) thin film stacks annealed in sulfur vapour by *in-situ* EDXRD at the F3 beamline at Hasylab (DESY). The Ga was supplied by a crystalline ( $\text{Ga}_x\text{S}_y$ )-layer, deposited by thermal evaporation of  $\text{Ga}_2\text{S}_3$  before sputtering elemental Cu and In precursor layers. The sulfuri-

zation was carried out in specially designed growth chamber compatible for installation at the EDXRD beamline. Typical annealing temperatures were  $550^\circ\text{C}$ . High resolution spectra acquired with 15 sec. integration time allow tracking of fast structural changes. Fig. 1 shows the EDXRD spectra as a function of process time. Brighter areas correspond to higher intensities. The temperature profile of the substrate is indicated by the colour code at the right axis. In the beginning of the heating phase we observe intermetallic phase transformations of the (Cu,In)-precursor. At about  $260^\circ\text{C}$  the diffraction signals of the  $\text{Cu}_{11}\text{In}_9$  phase disappear. At the same time we observe the almost simultaneous formation of a secondary  $\text{Cu}_{2-x}\text{S}$  phase and a  $\text{CuInS}_2$  phase stacked on top of a  $\text{CuGaS}_2$  phase. A very interesting finding is, that time evolution of the phases is significantly different when amorphous  $\text{Ga}_x\text{S}_y$  precursors are used. For longer annealing times (of crystalline  $\text{Ga}_x\text{S}_y$ ) the EDXRD-spectra show the appearance of a third, intermediate  $\text{Cu(In,Ga)S}_2$  phase and the diffusion of Ga into the  $\text{CuInS}_2$ . The diffusion process can be monitored by comparison of the lattice parameters as function of time during the annealing phase. Therefore the (110) diffraction signal of the sputtered Mo substrate with its known thermal expansion coefficient allows a precise conversion of all other energy positions into the corresponding lattice parameters. For better comparison the lattice parameters were converted to  $2\theta$  Bragg angles for chalcopyrite phases, the temperature profiles of the substrate and the LLS transient as a function of process time. The intensity of the diffraction signal is colour coded. Low intensity corresponds to dark blue and high intensities to saturated red as indicated by the colour scale. During the heating phase the thermal expansion leads to decreasing scattering angles for all three phases. Upon cooling the effect is reversed. However during the annealing phase the temperature is fixed, so that changes in the lattice constant (scattering angle) can be interpreted in terms of interdiffusion processes. The model for the fitting algorithm required to fix the lattice parameter of the intermediate, more Ga-rich,  $\text{Cu(In,Ga)S}_2$  phase in the center of the stronger signals of the  $\text{CuGaS}_2$  and  $\text{CuInS}_2$  phases. During the annealing phase we observe a mode-

rate increase of the  $\text{CuInS}_2$  scattering angle while the position of the  $\text{CuGaS}_2$  signal remains nearly constant. This can be interpreted in terms of an interdiffusion process since Ga incorporation reduces the lattice parameter of pure  $\text{CuInS}_2$ . As Ga diffuses upwards to the top of the film, the top-most part of the  $\text{CuGaS}_2$  layer is converted to a quaternary  $\text{Cu(In,Ga)}\text{S}_2$  layer with high Ga content and the  $\text{CuInS}_2$  on top is transformed into a  $\text{Cu(In,Ga)}\text{S}_2$  alloy with low Ga content. The shift of the  $\text{CuInS}_2$  peak is still small. However, the overall amount of Ga was limited to yield a homogeneous  $\text{Ga}/(\text{Ga}+\text{In})$  ratio of 0.15. Fig. 3 depicts schematically a preliminary summary of the phase transformations the  $\text{Ga}_x\text{S}_y$ -(Cu,In) precursor annealed in S atmosphere using crystalline  $\text{Ga}_x\text{S}_y$  layers. The findings serve as input for the preparation of quaternary  $\text{Cu(In,Ga)}\text{S}_2$  alloys by reactive annealing.

- [1] HMI Annual Report 2003  
 [2] E. Rudigier, J. Djordjevic J., C. von Klopmann, B. Barcones, A. Pérez-Rodríguez and R. Scheer, Journal of Physics and Chemistry of Solids **66**, 1954–1960 (2005)  
 [2] HMI Annual Report 2001  
 [3] M. Turcu, I.M. Kötschau and U. Rau, J. Appl. Phys. **91**, 1391–1399 (2002)  
 [4] A. Neisser, PhD Thesis, Freie Universität Berlin (2002)

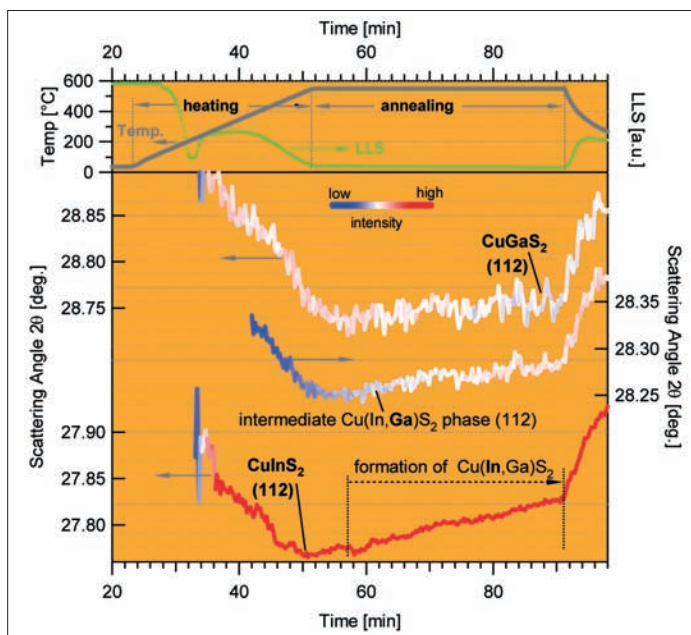


**Fig. 2:** Calculated peak positions for  $\text{Cu-K}\alpha$  wavelength, substrate temperature and LLS transient as a function of process time.  $\text{CuGaS}_2$  has a higher scattering angle and thus a smaller lattice parameter as  $\text{CuInS}_2$ . The increasing scattering angle of the  $\text{CuInS}_2$  signal during the annealing phase indicates therefore an interdiffusion process of Ga into  $\text{CuInS}_2$  to form a quaternary  $\text{Cu(In,Ga)}\text{S}_2$  alloy. The relative intensity of the phases is provided by the colour code.

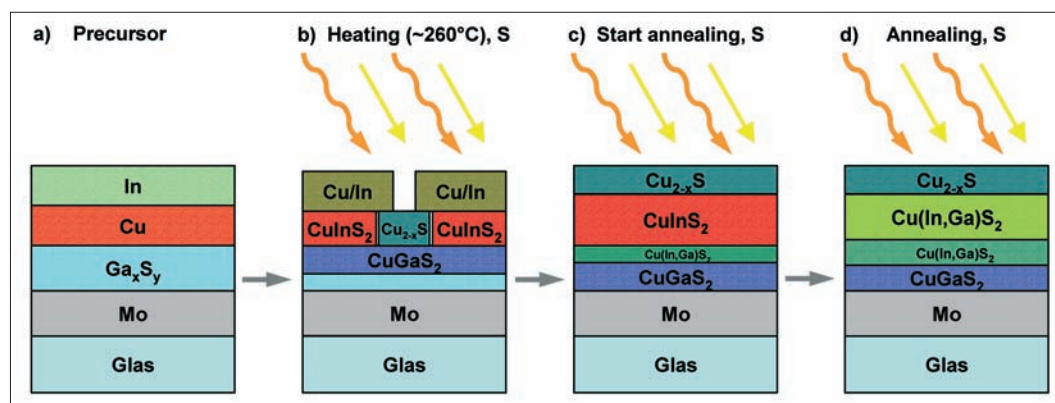


**Fig. 3:** Schematic representation of the phase transformation during Annealing of  $\text{Ga}_x\text{S}_y$ -(Cu/In) precursor layers in S vapour. **a)** Precursor as deposited. **b)** During the heating phase after the first  $\text{CuGaS}_2$ ,  $\text{CuInS}_2$  formation. The secondary and quasi-liquid  $\text{Cu}_{2-x}\text{S}$  phase supports a fast chalcogen- and metal transport. **c)** During the annealing phase the part of the  $\text{CuGaS}_2$  phase is transformed into an intermediate Ga-rich  $\text{Cu(In,Ga)}\text{S}_2$  alloy. **d)** For longer annealing times the Ga diffuses into the  $\text{CuInS}_2$  and forms a Ga-poor quaternary  $\text{Cu(In,Ga)}\text{S}_2$  alloy.

# A flexible, $\text{Cu}(\text{In,Ga})\text{Se}_2$ based, thin film solar cell module

C.A. Kaufmann<sup>1</sup>, A. Neisser<sup>1</sup>, K. Sakurai<sup>1</sup>, P. Körber<sup>1</sup>, H.-W. Schock<sup>1</sup>, R. Klenk<sup>2</sup>, M.C. Lux-Steiner<sup>2</sup>

■ 1 HMI, SE3 ■ 2 HMI, SE2

In the past few years space industry has shown increased interest in flexible  $\text{Cu}(\text{In,Ga})\text{Se}_2$  (CIGSe) thin film solar cells due to the specific advantages that devices of this type offer. Space applications require a technology that, above all, has a high specific power, i.e. it needs to be light and at the same time has to show a high efficiency. Furthermore it needs to be tolerant to space radiation in order to ensure minimum degradation while on orbit. Flexible thin film solar cells seem to have the potential to fulfill all these criteria. Still, they are not only of interest for space applications but wherever mobile generation of electrical power is required and weight is an issue. An efficient, robust, cheap, light, flexible and thus unbreakable, solar generator would immensely broaden the range of applicability of solar power generators across all types of applications. Therefore the HMI is currently working on the development of high efficiency  $\text{Cu}(\text{In,Ga})\text{Se}_2$  thin film modules on Ti-foil substrates. Our aim is to demonstrate that high efficiency flexible modules present an attractive technology for wide terrestrial use.

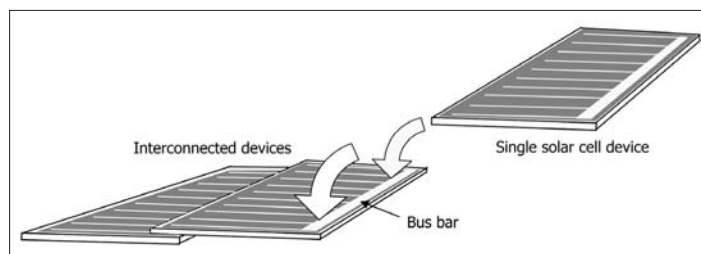


**Fig. 1:** Schematic for illustration of shingle-like interconnection of single cells for module integration

A primary reason for the choice of titanium as substrate material for CIGSe thin film solar cells is that the thermal expansion coefficient of titanium matches that of CIGSe [1]. Hence stress within the multi-layered device structure is kept low, even in extreme thermal environments and in particular also during fabrication. The conductivity of the substrate enables a roof-tile-like interconnection of large area, single devices as a method for module fabrication. A schematic for shingle-like interconnection of single cells for module integration is shown in Fig. 1. The bus bar of the lower

device is connected to the back of the top device using a simple soldering process with indium as the filler metal. Shingle-like interconnection is an alternative to monolithic integration, an elegant interconnection technique that uses the inherent advantage of the multi-layered structure of the thin film device but which, on conductive substrates, would require an additional insulation layer between device and substrate. Insulating flexible substrates, as for example polyimide foil, on the one hand ideal for monolithic integration, are on the other hand not stable at the process temperatures that are necessary in order to produce a high quality absorber.

Fabrication processes for established high efficiency thin film devices are not easily transferred from the rigid glass substrate to the flexible titanium foil. Nevertheless, for small area devices, the transfer is achieved without efficiency loss [2,3]. In addition to that, activities to manufacture high quality flexible devices with a larger area have been successful [3,4]. The single, flexible CIGSe thin film solar cell devices presented here are prepared on a  $25\ \mu\text{m}$  thick titanium foil, and consist of a stacked layer sequence in the order Mo/CIGSe/CdS/i-ZnO/ZnO:Ga. The transparent front and the back contact are both sputtered, the CdS buffer layer is deposited by chemical bath deposition and the CIGSe absorber layer is deposited using a 3 step co-evaporation process. Prior to the absorber layer deposition a sodium containing precursor is evaporated onto the Mo back contact. In addition to that a Ni/Al grid is evaporated onto the finished devices in order to facilitate current collection. Laser light scattering (LLS) is used as an in-situ process control during the PVD process [5].

Due to the fact that after shingle-like interconnection the bus bar is completely shaded by the active part of the top device, its area is not taken into account for the determination of the total area of the single cell device of  $27.1\text{cm}^2$ . A string of 4 cells with a total module area of  $130\text{cm}^2$  thus has an aperture area of  $108.4\text{cm}^2$ . Fig. 2 shows a fully assembled module after encapsulation.

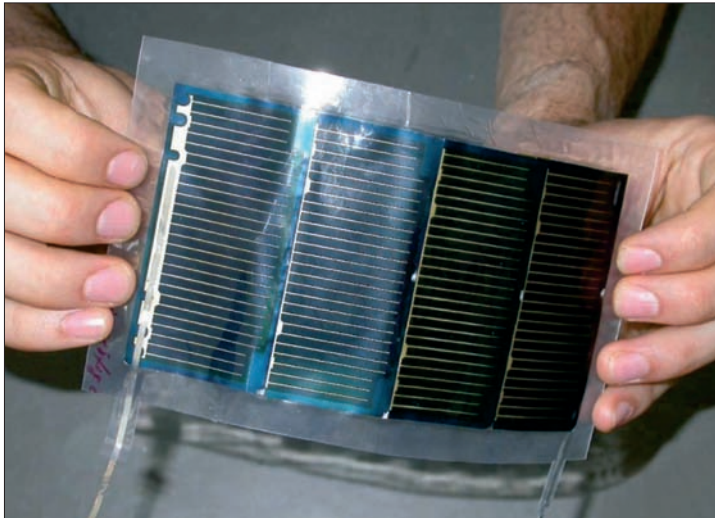


**Fig. 2:** Encapsulated, flexible CIGSe thin film solar cell module; total area  $130\text{ cm}^2$  and aperture area  $108.4\text{ cm}^2$

In order to achieve the technology transfer from the rigid glass to the flexible titanium foil substrate, several issues had to be resolved [3]. For example, localized leakage currents were initially observed to limit the flexible device's performance by reducing the parallel resistance  $R_p$ .  $R_p$  is generally determined via  $I$ - $V$ -measurements in the dark. These leakage currents were found to originate from defects of the surface of the titanium foil substrate. Having introduced a conditioning step for the foil surface onto which the solar cell is to be deposited, parallel resistances of  $>1\text{ k}\Omega\text{ cm}^2$  could be reached on large area devices. Nevertheless a parallel resistance as low as  $100\Omega\text{ cm}^2$  has in many cases been proven to be sufficient in order to reach efficiencies  $>10\%$  under standard AM 1.5 conditions.

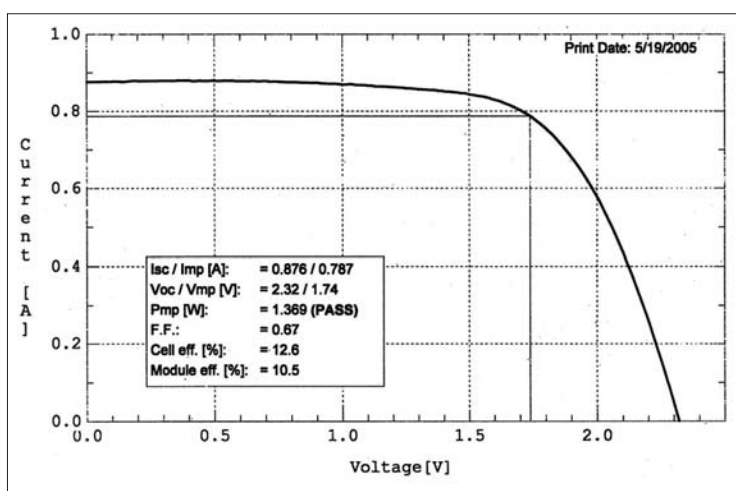


**Fig. 2:**  $I$ - $V$ -characteristic of  $130\text{ cm}^2$  flexible CIGSe module

When scaling up the device from a small lab size, loss mechanisms such as the series resistance of the front grid, lateral inhomogeneities of device parameters due to material non-uniformities and last but not least an increased probability for localized leakage currents due to defects incorporated into the device come into play [6]. So far, a maximum efficiency of 15.0% (AM 1.5) has been measured at the HMI for a flexible CIGSe thin film device with  $27.1\text{ cm}^2$  total area [3]. Using roof-tile-like interconnection, a module was fabricated with 4 single cell connected in series and showed an efficiency of 10.5% ( $130\text{ cm}^2$ ), measured before

encapsulation. This correlates with a specific power of  $\sim 500\text{ W/kg}$  (without encapsulation) and an aperture area efficiency of 12.6%. Fig. 3 shows the corresponding  $I$ - $V$ -characteristic and related parameters. In conclusion we have shown that the flexible  $\text{Cu}(\text{In,Ga})\text{Se}_2$  thin film solar cell technology represents a viable future option to enhance power supply technologies for mobile outdoor applications.

- [1] M. Hartmann, M. Schmidt, A. Jasenek et. al.; Proc. 28<sup>th</sup> IEEE PVSC **638**, Anchorage (2000)
- [2] C.A. Kaufmann, A. Neisser, R. Klenk, R. Scheer; Thin Solid Films **480–481**, 515 (2005)
- [3] A. Neisser, C.A. Kaufmann, R. Klenk et al.; Proc. 7<sup>th</sup> EPSC, Stresa (2005)
- [4] C.A. Kaufmann, A. Neisser, R. Klenk et al.; Proc. MRS Spring Meeting, San Francisco (2005)
- [5] K. Sakurai, R. Hunger, R. Scheer et al.; Prog. in Photovoltaic: Res. & Appl. **12**, 219 (2004)
- [6] A. Neisser, C.A. Kaufmann, R. Klenk et al.; Proc. 31<sup>st</sup> IEEE PVSC, Florida (2005)

# Low band gap InP-based multi-junction solar cells

U. Seidel, H. J. Schimper, U. Bloeck, K. Schwarzburg, T. Hannappel

■ HMI, SE4

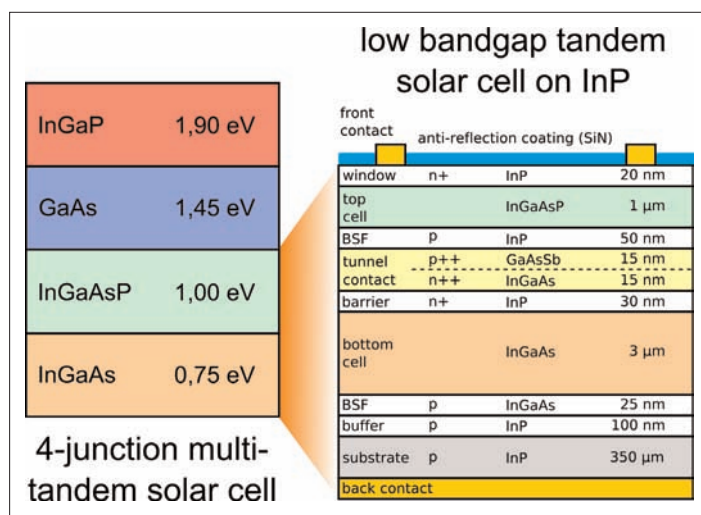


**Fig. 1:** The solar spectrum could be exploited more efficiently than in the current GaAs-based world record triple solar cell when combining a GaAs-based top cell with higher band gaps and an InP-based tandem bottom cell with lower band gaps

Three junction devices grown lattice-matched to GaAs on an Ge-based bottom cell have recently shown world record conversion efficiencies of around 39% under concentrated sunlight [1]. Even higher efficiencies are expected when employing more than 3 junctions. However, cell concepts with more than 3 junctions are in demand for an absorber material with a band gap around 1 eV. Extensive studies have been conducted to use N-containing III-V material lattice-matched to GaAs. Unfortunately, the diffusion lengths in these delicate dilute semiconductor compounds remain far too low. In an alternative approach compounds with different lattice constants can be combined either by mechanical stacking, grading techniques, wafer bonding [2] or via separation of the optical spectrum [3]. However, much less efforts have been made to develop low band gap, InP-based multi-junction solar cells (MJSC) so far. Our idea aims at an interconnection of two MJSC on different lattice constants, i.e. a well-established, GaAs-based high band MJSC ( $E_{\text{gap}} > 1.4 \text{ eV}$ ) and a low band gap MJSC prepared on the lattice constant of InP. Fig. 1 shows our idea of a 4-junction MJSC

design: The bottom cell is a tandem consisting of InGaAs and InGaAsP pn-junctions grown lattice-matched to InP. The upper tandem consists of GaAs and InGaP subcells. Here, we report on preliminary results obtained with a newly designed low band gap tandem structure. Once optimized, the complete cell shown in Fig. 1 is expected to give well above 40% efficiency under concentrated sunlight. Extending the concept to 5 or 6 junctions, surpassing the 50% efficiency limit seems possible.

III-V materials were grown by MOCVD in an Aixtron AIX-200 reactor using non-gaseous precursors that are much less toxic and more economical than conventional gaseous precursors. Fig. 2 shows the internal quantum yield of an InP cell grown with tertiarybutyl-phosphine (TBP) and trimethyl-indium (TMIIn) (red curve) in comparison to the best InP cell reported in the literature (blue curve) [4]. While earlier attempts with non-gaseous precursors were less successful (green curve) [5], our result demonstrates that very good results can indeed be obtained with these advantageous precursors. Fig. 3 shows the quantum efficiency of single pn-junction cells made of the absorber materials employed in our low band gap tandem. The red curve in Fig. 1 shows the signal for the material with the lowest

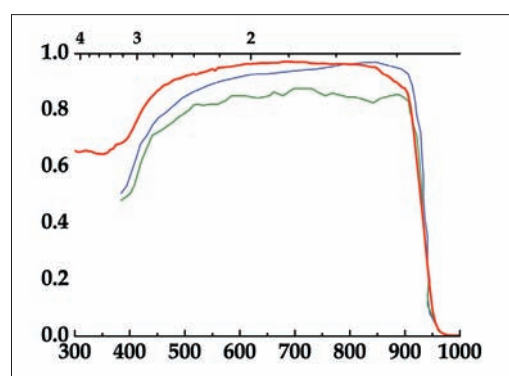


**Fig. 2:** Internal quantum efficiency (IQE) of an InP n/p solar cell (red) [5] compared to the IQE of the best InP cell reported in the literature (blue) [3] and the formerly best InP cell prepared with TBP (green) [4]

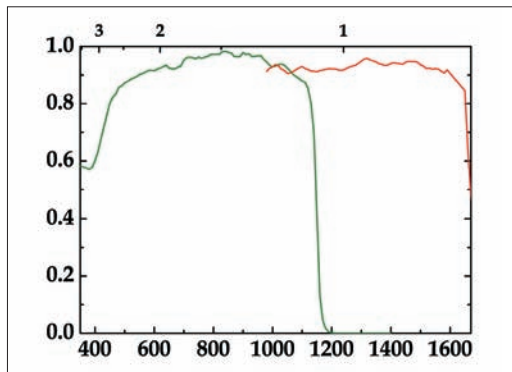


**Fig. 3:** Internal quantum efficiency (IQE) of an InGaAs cell (red) with an absorber layer thickness of  $2\ \mu\text{m}$  and IQE of an InGaAsP cell (green)

band gap, InGaAs ( $E_g = 0.75\ \text{eV}$ ), grown on p-InP(100). The green curve in Fig. 3 shows the result for the quaternary '1 eV material', i.e.  $\text{In}_x\text{Ga}_{1-x}\text{As}_y\text{P}_{1-y}$  ( $E_{\text{gap}} = 1.08\ \text{eV}$ ,  $x = 0.83$ ,  $y = 0.37$ ). Different single junction cells with virtually the same band gaps were prepared with GaAsSb ( $E_{\text{gap}} = 0.75\ \text{eV}$ ) and InAlGaAs ( $E_{\text{gap}} = 1.1\ \text{eV}$ ) [6]. Although the performance of these less explored materials was promising [6], more optimization is needed before they would be employed equivalently in our multi-junction structure.

The low band gap tandem solar cell of Fig. 1 was grown monolithically on a p-InP(100) substrate. In this structure the subcells are connected via a hetero tunneling structure consisting of thin layers of p-GaAsSb and n-InGaAs. This asymmetric material combination was used because of the favorable band offsets. The GaAsSb layer of the tunnel junction was grown at  $T = 500^\circ\text{C}$  to achieve best layer quality. All other layers of the solar cell were grown at a temperature of  $T = 600^\circ\text{C}$ . After processing a SiN antireflective coating was deposited on top. The influence of different preparation procedures on the critical GaAsSb-InP hetero-interface and on the cell performance was investigated in detail, in particular by reflectance difference/anisotropy spectroscopy (RDS/RAS). First results with this low band gap tandem solar cell are represented in Fig. 4. It shows the I-V characteristic under full AM1.5g spectrum (blue) and in addition the response to filtered AM1.5g illumination. For the latter measurement a RG850 (Schott) filter was used to simulate the operation below a GaAs top cell. An open circuit voltage of  $694\ \text{mV}$ , a short circuit current density of  $15.2\ \text{mA}/\text{cm}^2$ , a fill factor of 76%, and a solar conversion efficiency exceeding 8% was in-house measured underneath the GaAs-adequate filter. Measurements were carried out with the in-house solar simulator (SE2). This is already a

significant improvement of the performance of a Ge-based bottom cell ( $\eta < 5\%$ ) that is employed in the Ge-based world record triple cell [7]. Further improvement of our low band gap tandem seems possible and under concentrated sunlight the efficiency would be even higher either way. Thus, the potential to enhance the conversion efficiency of a complete 4-junction cell as illustrated in Fig. 1 well above 40% appears obvious. The band gap of InGaAsP can be tuned in a wide range between  $0.75\ \text{eV}$  and  $1.4\ \text{eV}$  while maintaining the lattice match to InP [6]. This gives the opportunity to further improve the efficiency by using a 3 junction low bandgap cell.

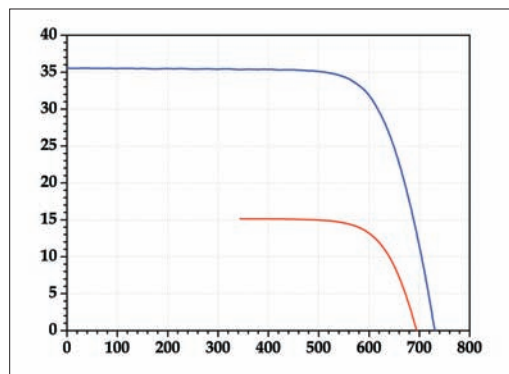


**Fig. 4:** I-V characteristic of an InGaAs/InGaAsP tandem solar cell measured under a full (blue curve) and a filtered (red curve, RG850) AM1.5g spectrum

- [1] R. R. King et. al., Conference Proceedings, 20<sup>th</sup> European Photovoltaic Solar Energy Conference, Barcelona, 118–123 (2005)
- [2] J. M. Zahler, A. Fontcuberta i Morral, Chang-Geun Ahn, H. A. Atwater, M. W. Wanlass et al., Ncpv and solar program review meeting proceedings, 723 (2003)
- [3] L. Fraas, J. Avery, H. Huang, E. Shifman, K. Edmondson et al., 20<sup>th</sup> european photovoltaic solar energy conference and exhibition, 476 (2005)
- [4] C. J. Keavney, V. E. Haven, S. M. Vernon, Proc. 21<sup>st</sup> IEEE PV Specialists Conf. IEEE, Kissimmee, FL, USA, 141 (1990)
- [5] R. W. Hoffman, N. S. Fatemi, D. M. Wilt, P. P. Jenkins, D. Brinker, D. A. Scheiman, Proc. 24<sup>th</sup> IEEE PV Specialists Conf., IEEE, Waikoloa, HI, USA, 1882 (1994)
- [6] H.-J. Schimper, Z. Kollonitsch, K. Möller, U. Seidel, U. Bloeck, K. Schwarzburg, F. Willig, T. Hannappel, J. Cryst. Growth (2005) online available, DOI: 10.1016/j.jcrysgro.2005.10.121
- [7] C. Baur, M. Meusel, F. Dimroth, A. W. Bett, Conference Record of the 31<sup>st</sup> IEEE PV Specialists Conf., IEEE, Piscataway, NJ, USA, 675 (2005)

#### Corresponding author:

T. Hannappel  
hannappel@hmi.de

# Binding geometry of phosphonic and carboxylic acid groups on rutile TiO<sub>2</sub>

L. Gundlach, R. Ernstorfer, R. Eichberger, S. Felber, F. Willig

■ 1 HMI, SE4

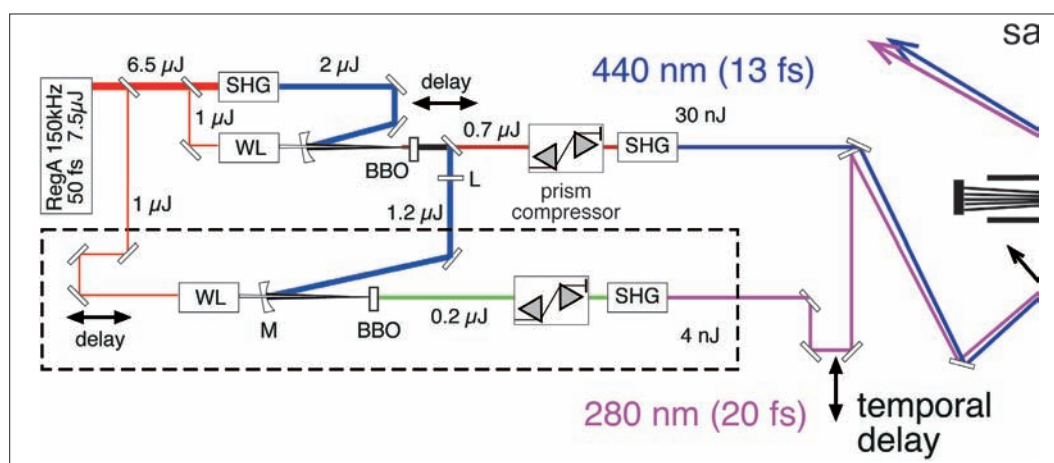


**Fig. 1:** Experimental setup consisting of two 150 kHz NOPAs both pumped with a 400 nm SHG pulse illustrated (left hand side) and a UHV chamber equipped with a time of flight spectrometer (right hand side)

The exact knowledge of the binding geometry of adsorbates bound chemically to metal or semiconductor surfaces is of crucial importance for understanding most relevant processes like electron transfer and photocatalytic reactions. Heterogeneous electron transfer is the first step of the charge separation in dye-sensitized solar cells (DSSC) like the Grätzel cell [1]. A detailed investigation of the binding geometry of adsorbed molecules requires a well ordered sample, unless single molecules are investigated.

Here we report on a model system for DSSC, i.e. rutile single crystal TiO<sub>2</sub> sensitized with a specially tailored perylene dye. This model system was selected because of its favourable spectroscopic properties and extensively investigated in our group mainly with transient absorption spectroscopy and time-resolved two-photon photoemission spectroscopy (TR-2PPE) for investigating the charge transfer and transport processes at these interfaces. For measuring the adsorption geometry angular resolved 2PPE was used. 2PPE is a pump-probe technique where a first ultrashort laser pulse excites an electron to a normally unoccupied state and a second ultrashort probe pulse lifts the electron above the vacuum energy of the sample. The emitted electron is detected in a time of flight detector (TOF).

To get angular resolution the sample was rotated in front of the electron analyzer. The position on the sample where the electron spectra were taken consequently changed slightly with changing the angle. Therefore, spectra with s- and p-polarized pump pulse were recorded and subtracted assuming that background emission is not polarisation dependent. A prerequisite to determine the adsorption geometry with this method is the knowledge of the direction of the transition dipole moment for the molecular excitation step. For perylene this is along the long molecular axis. Consequently, molecules that stand upright on the surface, e.g. perylene-carboxylic acid, can not be excited with s-polarized pump pulses and yielded no 2PPE signal originating from the molecule. The resulting 2PPE yield  $W$  versus rotation angle  $\theta$  is proportional to the electric field of the pump pulse at the surface  $E_z^{pump}$  projected onto the transition dipole moment  $\mu_z^{ion}$  (for details see [2]):

$$W \propto |E_z^{pump} \mu_z^{ion}|^2 \times W^{ion} \quad \text{Eq. 1}$$

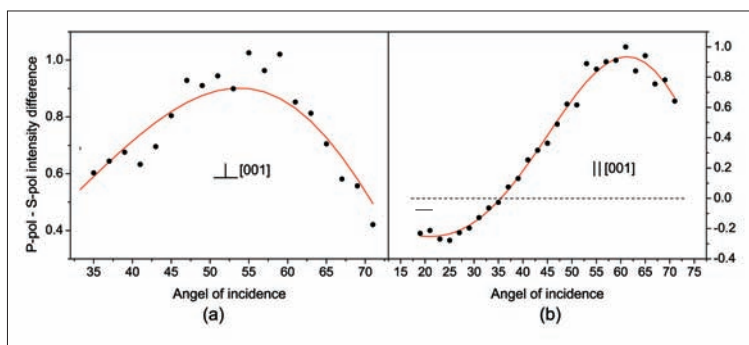


**Fig. 2:** Peak height of the 2PPE difference signal between p- and s-polarized pump pulse as a function of the angle of incidence for Pe'-rod on rutile (black), measured with the plane of incidence perpendicular (a) and parallel (b) to [001]. Red Curve: Calculated response (Eq. 2).

Upright bonding geometry could be verified for three different dyes with different spacer groups attached to the (110) surface of rutile via carboxylic acid groups. Latter result is in very good agreement with the reported bridging geometry of formate on the (110) surface of rutile resulting in a  $p(2 \times 1)$  LEED pattern [3].

The same measurements were performed on a perylene derivative (4-{4-[4-(8,11-Di-tert-butyl-perylen-3-yl)-phenyl]-bicyclo[2.2.2]oct-1-yl)-benzyl)-phosphonic acid) equipped with an other anchor group extensively investigated in our group, i.e. phosphonic acid (Fig. 2). Phosphonic acid can bind via three oxygen atoms in a triangular conformation, but considering the surface structure of  $\text{TiO}_2$  (110) the five-coordinated  $\text{Ti}_{4+}$  atoms are arranged in rows. Nilsing et al. performed DFT calculations to study the binding geometry of phosphonic acid on anatase (101) surfaces [4]. They have reported that a monodentate geometry with two hydrogen bonds and one metal-oxygen bond is the strongest configuration. Accordingly, one would expect a tilted configuration with the tilt angle perpendicular to the the [001] axis (c.f. Fig. 3). In this case the expected 2PPE yield reads:

$$W_{\infty} \left( \frac{|E_z^{\text{pump}} \mu_x^{\text{ex}} + E_z^{\text{pump}} \mu_x^{\text{ex}|2} - |E_y^{\text{pump}} \mu_y^{\text{ex}|2}}{|E_z^{\text{pump}} \mu_x^{\text{ex}} + E_z^{\text{pump}} \mu_x^{\text{ex}|2}} \right) \times \quad \text{Eq. 2}$$

It should be mentioned that, because of the lack of knowledge concerning the exact direction of the transition dipole moment for the ionization step with respect to the main axis of the molecule and the alignment of the molecular plane with respect to the surface, the rotation angle of the ionization dipole moment is not well defined. However, for the sample with the plane of incidence parallel to [001] (see Fig. 2 (b)) the tilt angle

of the long molecular axis with respect to the surface normal can be measured quite reliable because the pole of Eq. 2 depends only on the excitation step.

In summary, from the angular-resolved measurement the bonding geometry of the perylene dye bound via a phosphonic acid group to the  $\text{TiO}_2$  rutile (110) surface could be deduced. The long molecular axis is tilted against [110] with an angle of around  $58^\circ$  in the direction perpendicular to the

oxygen rows. This configuration is compatible with a bi- as well as a monodentate binding geometry with one or two hydrogen bonds, respectively. A balls and sticks model for the perylene dye bound with a bidentate configuration onto the  $\text{TiO}_2$  surface is shown in Fig. 3.

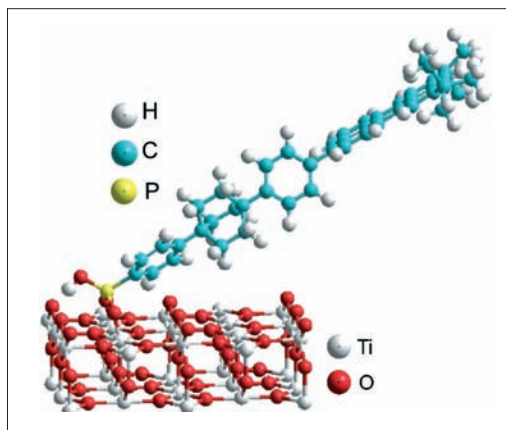


**Fig. 3:** Geometry of bidentate adsorbed DTB-Pe-rod on rutile (110)  $\text{TiO}_2$  deduced from our 2PPE measurements

- [1] B. O. Regan and M. Grätzel, *Nature* **353**, 737 (1991)
- [2] L. Gundlach, PhD thesis, Freie Universität Berlin (2005)
- [3] H. Onishi, T. Aruga, C. Egawa, Y. Iwasawa, *Surf. Sci.* **193**, 33–46 (1988)
- [4] M. Nilsing, S. Lunell, P. Persson, L. Ojamäe, *Surf. Sci.* **582**, 49 (2005)

#### Corresponding author:

F. Willig  
willig@hmi.de

# Ultrafast electron transfer via a bridge-extended donor orbital

R. Ernstorfer, L. Gundlach, R. Eichberger, S. Felber, F. Willig

■ HMI, SE4

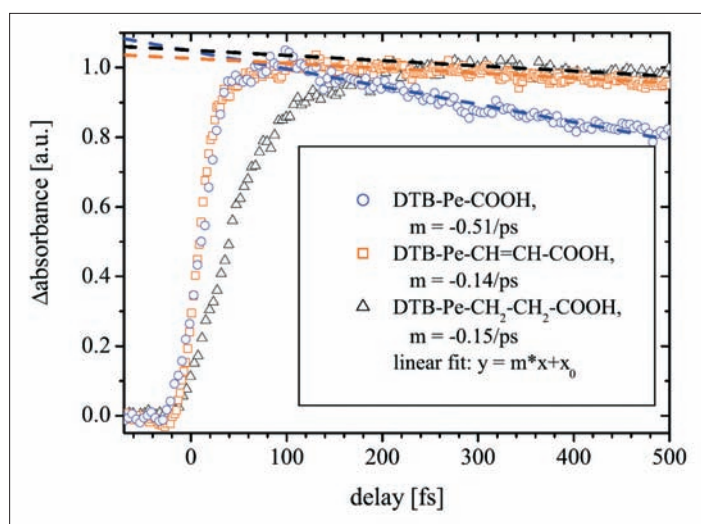


**Fig. 1:** Rise and early decay of the absorption of the product state of heterogeneous electron transfer, i.e. the cation of perylene, for DTB-perylene attached to  $\text{TiO}_2$  via different bridge-anchor units. The fit to the pump-probe signals showed an injection time of 10 fs for  $-\text{CH}=\text{CH}-\text{COOH}$ , of 57 fs for  $-\text{CH}-\text{CH}-\text{COOH}$ , and of 13 fs for  $-\text{COOH}$ . Recombination rate as shown in the figure.

Transport of electrons through molecular bridges (wires) of different chemical nature is an important topic for the postulated field of molecular electronics [1] and may be of high relevance for improving dye sensitized/organic solar cells. We report here on transient absorption experiments probing electron transfer via different molecular bridges in UHV. Electron transfer occurred from the excited singlet state of the aromatic chromophore perylene to nano-sized particles of anatase  $\text{TiO}_2$ . The chromophore was linked covalently to a carboxylic group, which binds to surface Ti atoms and thus functions as the anchor group. Optionally, bridge groups were inserted in-between the perylene backbone and the anchor group. Three different experimental systems were compared: firstly, no bridge, secondly a conjugated  $-\text{CH}=\text{CH}-$  bridge unit, and thirdly a saturated  $-\text{CH}_2-\text{CH}_2-$  unit. Bulky side groups were attached to the perylene chromophore (2,5-bitertiary-butyl-perylene-9-yl, DTB-Pe) to prevent the formation of dimers by neighboring perylene chromophores on the surface. A particularly attractive feature of the perylene/ $\text{TiO}_2$  system is the validity of the so called “wide band limit”, which is realized if the molecular donor level is energetically far above the conduction band minimum compared to the width of the electron transfer spectrum [2]. In this regime the electron transfer time is controlled by the strength of the electronic coupling and not by the magnitude of individual Franck-Condon factors [2]. UPS measurements revealed that for all three investigated systems the donor level is at least 700 meV above the conduction band minimum. The electron transfer time was determined from the time-resolved rise of the absorption signal of the ionized perylene at around 570 nm, i.e. the molecular product state of electron transfer. Our group has shown before that the absorption spectra for the ground state, the excited singlet state, and the cationic state of the chromophore perylene are spectrally well separated from each other. The laser pump (central wavelength 435 nm) and probe (central wavelength typically at 570 nm) pulses were generated with two NOPAs at a repetition rate of 150 kHz and the crosscorrelation (FWHM) was typically in the range of 25 to 30 fs.

Fig. 1 shows the time-dependent absorption of the perylene cation for the three investigated systems. There are characteristic differences in the rise (electron injection) and decay (recombination) for the two different bridge units. Electron injection via the carboxyl anchor group alone gave a time constant of 13 fs, whereas 10 fs were determined when the  $-\text{CH}=\text{CH}-$  bridge unit was inserted. In contrast, electron transfer in the presence of the  $-\text{CH}_2-\text{CH}_2-$  bridge unit was found to be much slower with a time constant of 57 fs. The spatial separation of the perylene ring structure from the  $\text{TiO}_2$  surface was most likely comparable for the conjugated and the saturated bridge units and the recombination rate observed in this early time window is almost identical for both bridges. The extension of the donor orbital onto the conjugated bridge can be seen in Fig. 2 (center) as derived from a semi-empirical calculation. The perylene  $S_0-S_1$  transition has strong HOMO-LUMO character [3] so that the LUMO wavefunction can be considered a good approximation to the excited state wavefunction. Fig. 2 refers to the free molecule, whereas in the actual system the molecule was attached to the surface of  $\text{TiO}_2$ . The proximity of empty isoenergetic electronic states in the  $\text{TiO}_2$  conduction band can lead to a further extension of the excited state donor orbital right into the electronic states of the solid. Thus, a direct optical charge transfer contribution appears possible that is not included in the picture derived for the donor orbital of the isolated neutral molecule shown in Fig. 2. Nevertheless, the very different extensions of the chromophore's donor orbital, i.e. onto the conjugated bridge but not onto the saturated bridge, are clearly borne out by the different chemical structure of the bridge units. For electron injection the latter functioned as insulator whereas the conjugated bridge as conducting molecular wire. The lower part in Fig. 2 shows the LUMOs of the oxidized dye molecules, which are the relevant electronic states in view of the recombination reaction. The striking difference compared to the excited states of the neutral molecules is the missing extension onto the bridge (marked with an arrow). Thus the conjugated and saturated bridge result in a very similar recombination rate (Fig. 1) that is dictated by the distance between the donor and acceptor. Expressed in the fancy language of molecular electronics, the  $\text{sp}^2$ -hybridized bridge is wire-like in one direction of ET and insulator-like in the opposite, i.e. it has some character of a molecular rectifier.

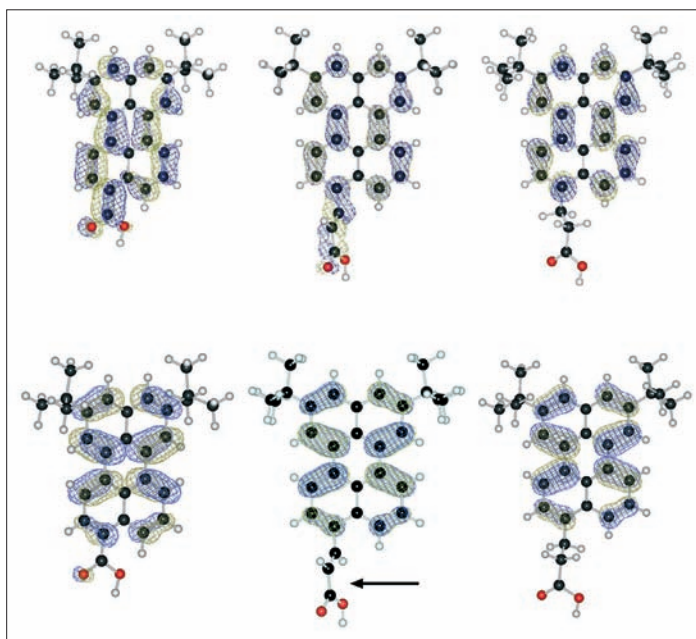


**Fig. 2:** Upper part: LUMOs of DTB-Perylene with three different bridge-anchor groups:  $-\text{COOH}$  (left),  $-\text{CH}=\text{CH}-\text{COOH}$  (center), and  $-\text{CH}_2-\text{CH}_2-\text{COOH}$  (right). The energy of the LUMO for the neutral molecule is sufficiently close to that of the conjugated bridge and has pure  $\pi^*$  character. The orbital representing the donor wavefunction extends onto the  $\text{sp}^2$ -hybridized conjugated bridge unit (center) but not onto the saturated bridge unit (right). Lower part:  $\beta$ -LUMOs of the oxidized DTB-perylene compounds. In contrast to the LUMO of the neutral dye, the conjugated bridge is not involved in the MO. Wavefunctions calculated with ZINDO/S on a ZINDO/1 optimized geometry.

- [1] Molecular Electronics, Edited by J. Jortner and M. A. Ratner, Blackwell Science, Oxford (1997)
- [2] S. Ramakrishna, F. Willig, V. May, A. Knorr, *J. Phys. Chem. B* **107**, 607 (2003); S. Ramakrishna, F. Willig, V. May, *Phys. Rev. B* **62**, R16330 (2000)
- [3] T. M. Halasinski, J. L. Weisman, R. Ruitkamp, T. J. Lee, F. Salama, M. Head-Gordon, *J. Phys. Chem. A* **107**, 3660 (2003)

Corresponding author:

F. Willig  
willig@hmi.de

# Photocurrent injection into $\text{TiO}_2$ nano particles utilizing $\text{WS}_2$ quantum sheets

H. Tributsch, M. Thomalla

■ HMI, SE5

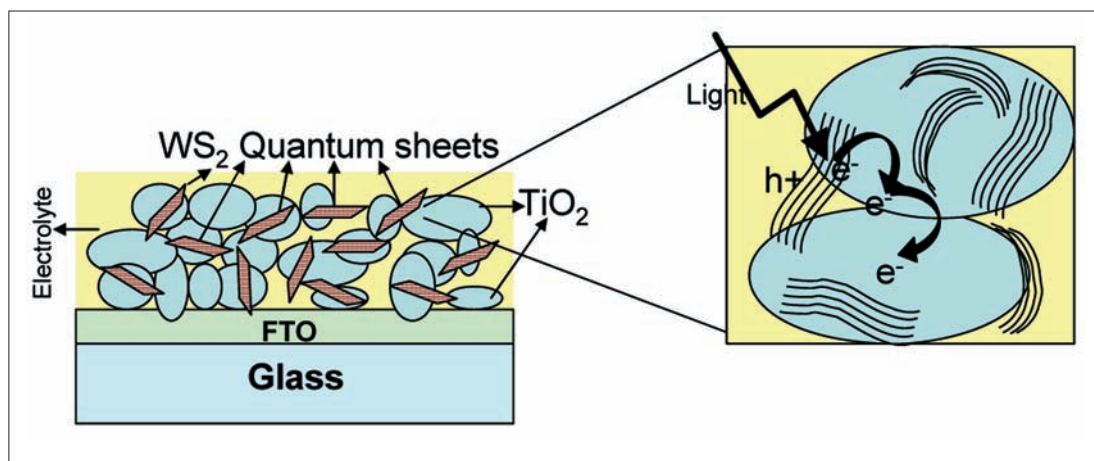


Fig. 1: Scheme of the  $\text{TiO}_2/\text{WS}_2$  nano composite solar cell

Significant efforts have recently been undertaken to develop nano composite solar cells. They do not need well crystallized materials and rely on chemical kinetic mechanisms for current rectification.

In particular, the solar cell developed by Grätzel and his group with its high solar energy conversion of up to 11% has increased the research efforts in this field [1]. A main problem with experimental nano composite solar cells up to now, both for dye solar cell and polymer/fullerene composite solar cell has been the long term stability. Unfortunately the original  $\text{cis-RuL}_2(\text{SCN})_2$  with  $\text{L} = 2,2'$ -bipyridyl-4,4'-dicarboxylatoacid (bpca) dye has not the desirable stability of 20 years [2, 3] and in addition the iodine/iodide redox system, the volatile solvent and its confinement pose problems.

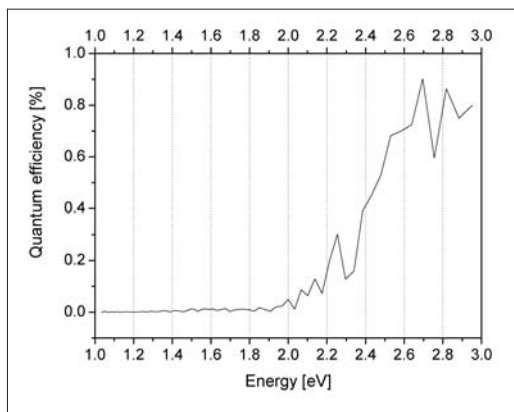


Fig. 2: Quantum efficiency of  $\text{WS}_2/\text{TiO}_2$  cell

An interesting approach is to replace the organic dye with inorganic semiconductor quantum dots. Semiconductor quantum dots have several advantages. Firstly their band gap can be easily adjusted by changing the size of the particle to match the solar spectrum and the band gap of  $\text{TiO}_2$ . Secondly, they may be selected to possess a high absorption coefficient, which allows to produce very thin absorbers and to reduce the amount of materials. And most important, it may be possible to apply a metallically conducting nano-contact as they are used in traditional solid state solar cells. In the presented work tungsten disulfide, which, due to its electronic structure, has been demonstrated to be a photochemically stable nano particle, has been investigated in a nano composite solar cell. The aim of this project is to sensitize porous, nanostructured  $\text{TiO}_2$  (150 nm) with  $\text{WX}_2/\text{MoX}_2$  ( $X = \text{S}, \text{Se}$ ) quantum sheets ( $\sim 5$  nm) with the help of various chemical deposition methods. These substances have high absorption indexes (up to  $3 \times 10^5 \text{ cm}^{-1}$ ) and single crystal  $\text{WSe}_2$  photoelectrochemical solar cells gave efficiencies of 17% in iodine-iodide electrolyte [4]. The absorber has been characterized with help of EDX, TEM, REM, Raman spectroscopy and light absorption measurements. The photosensitization has been confirmed via electrochemical measurements. The surface of  $\text{TiO}_2$  has been modified by a thin  $\text{Al}_2\text{O}_3$  film, which significantly enhanced the photocurrent density, at solar light intensity, to  $0.1\text{--}0.4 \text{ mA/cm}^2$ . Moiré-patterns suggest that the S-W-S layers of  $\text{WS}_2$  are not perfectly aligned in direction of c-axis, emphasizing the role of lateral electron transfer.

It is suggested, that  $\text{WS}_2$  is deposited in the porous  $\text{TiO}_2$  matrix as is shown in Fig. 1. The picture also visualises, how the electrolyte ( $\text{I}^-/\text{I}_3^-$ ) regenerates the  $\text{WS}_2$  sheets after photo induced electron injection into  $\text{TiO}_2$  nano particle. When the  $\text{WS}_2$  treated  $\text{TiO}_2$  nano layer is exposed to an  $\text{I}^-/\text{I}_3^-$  solution (propylene carbonate) and illuminated, photocurrents are indeed observed.

The spectrally resolved quantum efficiency of the  $\text{WS}_2$  sample in LiI electrolyte is shown in Fig. 2. A clear contribution of visible light, confirming the photosensitization of  $\text{TiO}_2$  by  $\text{WS}_2$  nano layer, is observed. The onset of the photocurrent is at 1.8 eV, which corresponds to the direct band gap of  $\text{WS}_2$  and also agrees with optical measurements.  $\text{WS}_2$  induced photocurrents are observed in a solar cell arrangement but systematic research will be needed to better understand the mechanism and to achieve a significant improvement of efficiency.

- [1] B. O'Reagan, M. Grätzel, *Nature* **353**, 737 (1991)
- [2] Helena Greijer Agrell, Jan Lindgren, Anders Hagfeldt *Solar Energy*, Volume 75, Issue 2, 169–180 (2003)
- [3] M. Thomalla H. Tributsch *IPS 15*, Paris, *Comptes rendus Chimie*, in press
- [4] O. Srivastava, G. Prasad, *J. Phys. D: Appl. Phys.* **21**, 1028–1030 (1998)

# Self-organized nanostructures on silicon for photovoltaic applications

H. J. Lewerenz, S. Skorupska, M. Aggour, M. Kanis, M. Lublow, H. Jungblut

■ HMI, SE5

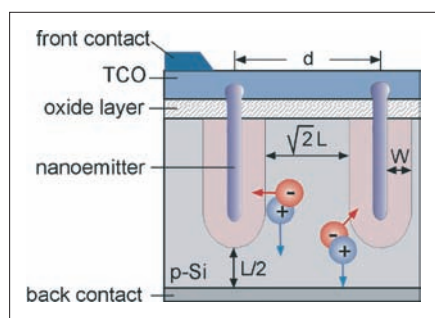


**Fig. 1:** Schematic of a Schottky-type nano-emitter solar cell;  $d$ , distance between pores;  $L$ , diffusion length;  $W$ , space charge layer width

Self organization allows large area preparation of surface features with sizes well below the limits of present lithographic methods. (Photo)electrochemical self organization occurs at low temperature under well defined conditions, such as applied potential, charge and current flow, illumination level, wavelength and solution composition that enable reproducible fabrication of micro- and nanopopographic patterns. Although regular topographies with micrometer dimensions could be prepared [1], analogous achievements in the nanometre domain have not yet been realized. They necessitate (i) empirical research, (ii) detailed knowledge of the silicon (photo)electrochemistry and (iii) analysis of results for possible applications. A schematic of an envisaged solar device is shown in Fig. 1: excess minority carrier collection occurs through nanometer-sized Schottky contacts, spaced in relation to the minority carrier diffusion length that are contacted to the front TCO [2]. Schottky nanoemitters can be fabricated by metal deposition into nanopores.

Spontaneous initiation and subsequent propagation of nanopores has been observed in series of fundamental studies of Si dissolution in acidic and alkaline electrolytes [3]: on (1×1) H-terminated Si(111), first nanopitting is seen at the re-entrant sites of the structure (Fig. 2a). Pore initiation is attributed to local electric fields between Si and counter ions, immobilized at specific sites above the surface, determined by DLVO and non-DLVO interactions [4]. The focussing effect of the electric field leads to minority carrier deflection to these sites, local oxidation of Si atoms and dissolution (Fig. 2b).

Corresponding deconvoluted SRPES (synchrotron radiation photoelectron spectroscopy) data (Fig. 3) reveal postulated dissolution reaction intermediates and a signal for the higher oxidized fully coordinated Si at the pit formation site ( $\Delta E_b = 3.6 \text{ eV}$ ).

Pore propagation is facilitated for Si(001) where pore walls perpendicular to the surface are  $\langle 110 \rangle$  oriented. Electrolytic (1×1) H-termination results in stable pore side walls and nanopores of rectangular shape. In a combined photoelectrochemical and chemical experiment, such nanopores have been prepared: first, Si(001) was made to oscillate at high anodic potentials in acidic electrolyte. The surface is then covered by a  $\sim 10 \text{ nm}$  thick oxide that exhibits tiny cracks and pores (Fig. 4a). In KOH, the Si substrate is locally etched where the pores connect electrolytically. A subsequent HF dip removes the oxide layer leaving the imprint of the beginning nanopore propagation on the Si surface (Fig. 4b).

For efficient solar cell preparation, the pores should penetrate deeper into the absorber according to Fig. 1. Then, (photo)electro-deposition of a Schottky barrier metal into the pores produces the nanoemitter wires. The average pore distance can be controlled via the current phase at emersion. Such cell can be prepared self-organized at low temperature with three successive solution treatments. Generally, the nanopore distance allows usage of low diffusion length material. Recombination processes at the Si/metal and Si/SiO<sub>2</sub> interface, however, have to be controlled.

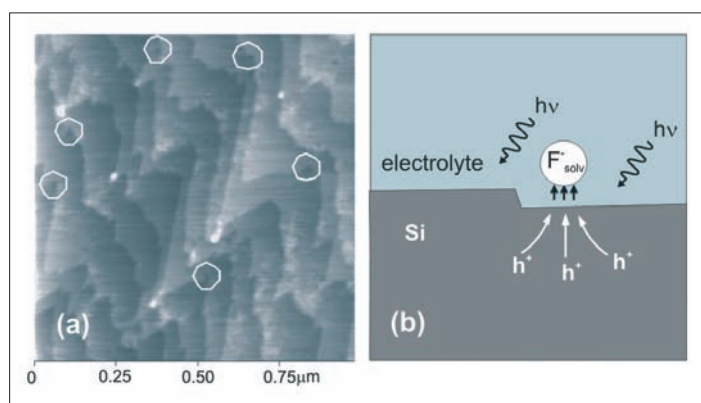


**Fig. 2:** Nanopore initiation at re-entrant sites on Si(111) obtained by CM AFM (a) and schematic of localized oxidation (b)

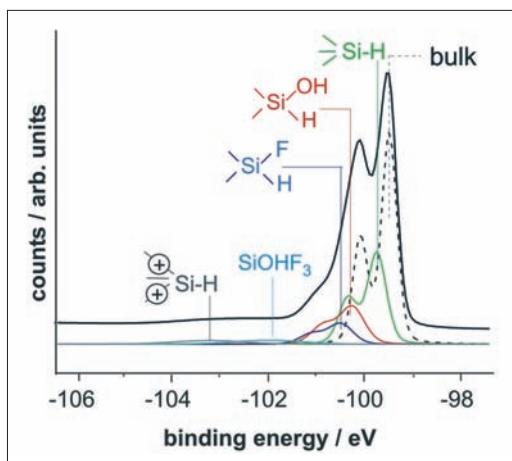


**Fig. 3:** SRPES of Si(111) after divalent photo-dissolution in ammonium fluoride electrolyte

This can be done by oxidation prior to metal deposition into the pores and by oxide annealing, respectively.

At cathodic potential, so-called step bunching is observed in alkaline solution. Up to 5 nm high terraces are formed on n-Si(111) [5]. SRPES shows that the surface is in accumulation, forming a two-dimensional electron gas (2DEG) without front contact material. The Si 2p core level binding energy shift of 0.2 eV with increasing photon energy can be reproduced by calculation of the Thomas-Fermi screening potential for an electron concentration of  $3 \times 10^{18} \text{ cm}^{-3}$  [5]. The AFM image in Fig. 5 shows the structure. Similar to the pore structures, the topography is of fundamental interest w.r.t. light coupling properties, which we investigate by Brewster angle analysis [6]. Also, relevant aspects of resistance quantization of 2DEGs at low temperature can be investigated [7].

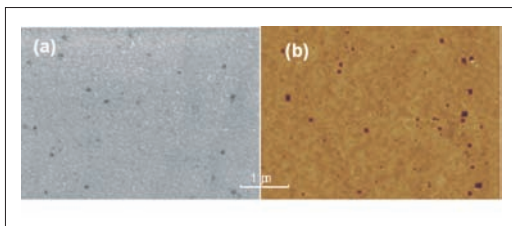


**Fig. 4:** Nanopore propagation experiments; (a) HRSEM image of pores in heterogeneous oxide after current oscillations; (b) AFM image of pore growth into Si in alkaline medium by three-step soft solution technique

Regular oxide patterns with nanometre dimensions have been obtained in the region of negative resistance of the photocurrent-voltage characteristics of Si(111) in dilute acidic HF containing electrolyte. A typical image is shown in Fig. 6 after saturation oxidation on air. Regular, brick-type features are spread across the surface that can be comparably easily removed by an AFM tip, allowing regular oxide and bare silicon patterning.

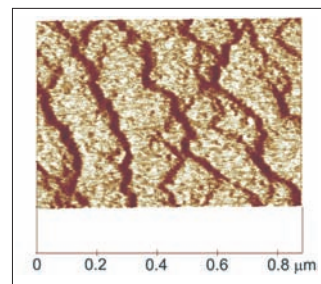


**Fig. 5:** CM-AFM image of a step-bunched Si(111) surface

Finally, it should be noted that the produced patterns are also important for immobilization of biological molecules, such as enzymes (proteins). Very little is known about protein-semiconductor junctions or interactions, and research in this area can lead to substantial advances in the field of proteomics.

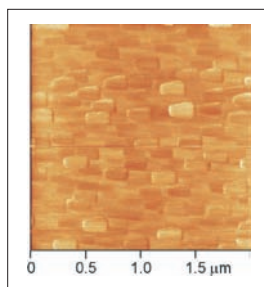


**Fig. 6:** AFM image of anodic oxide patterns after photoelectrochemical conditioning in 0.1M NH<sub>4</sub>F

- [1] V. Lehmann, U. Gösele, Appl. Phys. Lett. **58**, 856 (1991)
- [2] H. J. Lewerenz, Patent application DE, Az 103 47 401.3 (2003)
- [3] H. J. Lewerenz et al., J. Electrochem. Soc. **150**, E185 (2003); K. Skorupska et al., Electrochem. Commun. **7**, 1077 (2005)
- [4] B. V. Derjaguin, L. Landau, Acta Physicochimica (USSR) **14**, 633 (1941); E. J. Verwey, J. Th. G. Overbeek, Theory of the Stability of Lyophobic Colloids, Amsterdam, Elsevier (1948)
- [5] M. Krčmar et al., Phys. Rev. B **61**, 13821 (2000)
- [6] K. Skorupska et al., Appl. Phys. Lett. **87**, 262101 (2005)
- [7] M. Lublow, H. J. Lewerenz, Transactions of the Institute of Metal Finishing **83**, 238–247 (2005)
- [8] K. von Klitzing et al., Phys. Rev. Lett. **45**, 494 (1980)

#### Corresponding author:

H.-J. Lewerenz  
lewerenz@hmi.de

# Electronic structure of epitaxial ZnO thin films grown by MOMBE

S. Andres, C. Pettenkofer

■ HMI, SE6

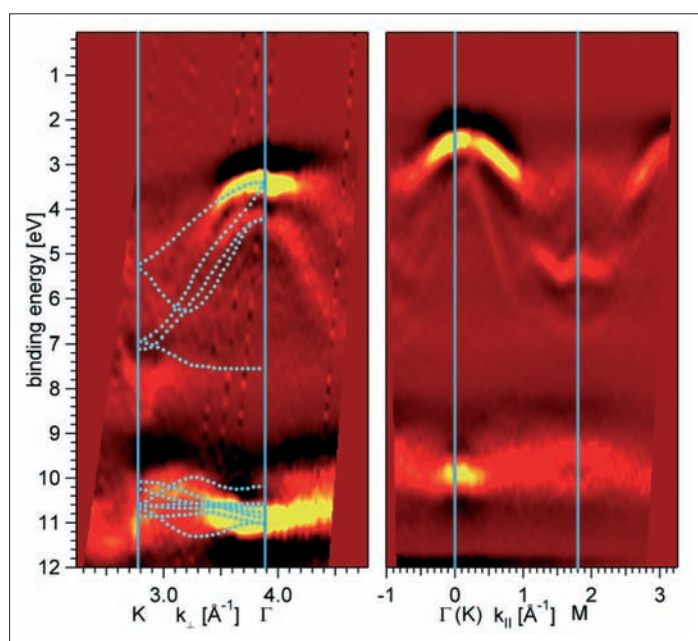


**Fig. 1:** ARUPS data of an annealed ZnO(11-20) film grown on r-plane sapphire. Dotted lines indicate a theoretical band calculation after Vogel et al.[1], which has been adapted to our measured data.

Optically transparent semiconductor compounds such as ZnO have gained considerable interest lately due to a variety of possible applications in the field of laser diodes, displays and solar cells. Molecular beam epitaxy is the growth method of choice for producing well-defined high quality monocrystalline layers. While the bulk electronic structure of ZnO was investigated in the past, a firm understanding of the surface and interface electronic properties is still an issue in ongoing research. In this report, we focus on the deposition of ZnO thin films on sapphire ( $\text{Al}_2\text{O}_3$ ) as well as on SiC.

ZnO films were deposited in a UHV-MOMBE system from the organic precursor diethylzinc and water at growth pressures in the 10–5 mbar range at a deposition temperature of 450°C. As substrates, the r-plane of the  $\text{Al}_2\text{O}_3$  single crystal and n-type 6H-SiC(0001) were chosen.

Samples were grown and characterized in situ by photoelectron spectroscopy (UPS, XPS) and low energy electron diffraction (LEED) without breaking the vacuum.

On the r-plane of  $\text{Al}_2\text{O}_3$  ZnO grows epitaxially exhibiting the (11-20) surface. Especially the glide plane symmetry of the substrate is transferred to the growing film, as could be observed in the LEED patterns. Thus, an existence of different domains in these films can be ruled out. Concerning the chemical analysis, XPS data show no residuals of carbon in the film, which proves a clean reaction of the precursor substances. In the O1s spectra an admixture of about 5–10% hydroxide is found which can be removed by annealing to 600°C. Valence band spectroscopy (UPS) reveals a change in the O2p band upon annealing such that the resulting spectra resemble those of a clean bulk crystal surface. Since this change is more predominant in the more surface sensitive Hell spectra we conclude that the as-grown films incorporate hydroxide at the topmost layers. Atomic force microscopy (AFM) scans of the surfaces obtained ex-situ show a film surface roughness of 2 nm which reduces to 1.5 nm after annealing. The carrier concentration  $n$  is found to be below  $10^{19} \text{ cm}^{-3}$  with mobilities above  $13 \text{ cm}^2/\text{Vs}$ .

Fig. 1 displays angular resolved UPS data of an annealed ZnO(11-20) film. The spectra show a dispersion of the upper bands which are assigned to O2p derivatives. The dominant emission at a binding energy of about 11 eV corresponds to Zn3d bands showing weak but nevertheless considerable dispersion. A valence band splitting into 3 subbands is clearly visible for the  $k_{||}$  series (right hand side of Fig. 1). This can be explained by the hexagonal symmetry of the crystal field and the spin-orbit-interaction. For comparison, we have adapted a theoretical band calculation from the literature [1] to our data. The calculation exhibits an offset of about 2 eV for the Zn3d bands in comparison with our data. Consequently, in Fig. 1 we adapted these band calculations to the measured data.

In a second experiment we deposited ZnO on 6H-SiC (0001). The substrates were prepared by thermal annealing above 1000°C in hydrogen atmosphere and were transferred into the Integrated System under N<sub>2</sub>. Here, a ZnO film was grown in consecutive steps in order to allow for an in-situ analysis of the changings in the interfacial properties (band bending, band offset) by XPS/UPS as well as the crystalline quality (LEED). Fig.2 depicts the evolution of the substrate (Si2p emission), the film (Zn2p as well as O1s emission) and the valence bands. From the development of the corelevel lines in the course of deposition and the UPS spectra we obtained the band alignment at the interface ZnO(0001)/SiC(0001). Fig.3 sketches the energetic offsets and displays the determined offset values.

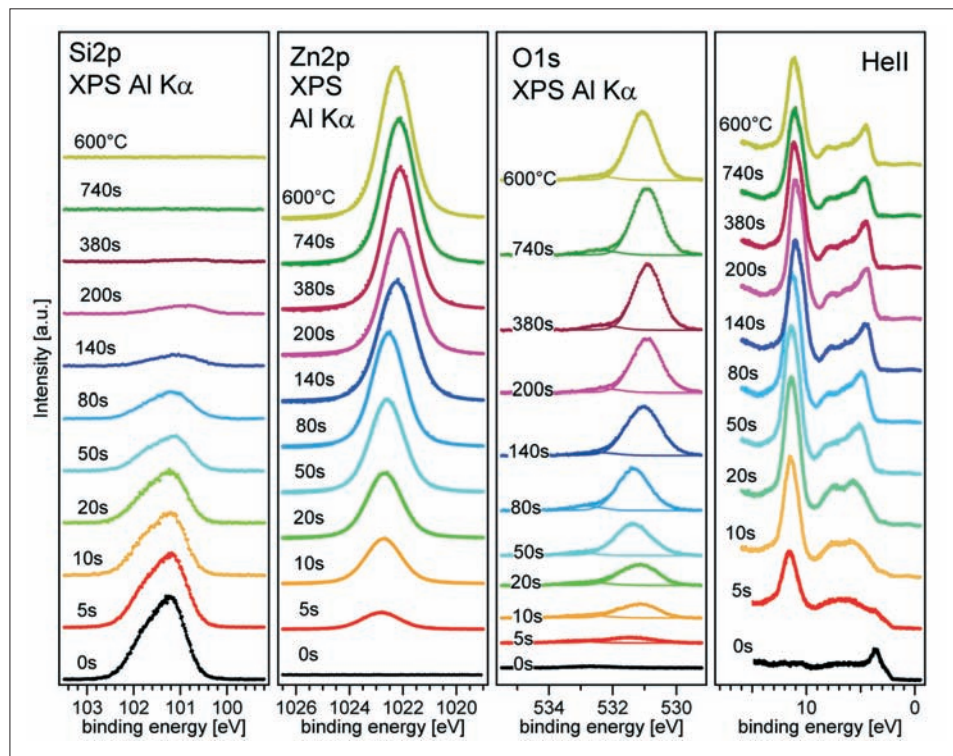


**Fig. 2:** Development of selected photoemission spectra with respect to stepwise deposition of ZnO on SiC(0001)

In conclusion, we have deposited well-defined monocrystalline ZnO films on sapphire and SiC using diethylzinc and water as precursors in our MOMBE system. The quality of the films is sufficient to obtain angular resolved photoemission data, which can provide a comparison with the electronic structure of bulk crystal surfaces. Using a stepwise deposition procedure in our integrated system we were able to determine the band alignment of the ZnO/SiC interface.

[1] D. Vogel, P. Krüger, and J. Pollmann, Phys. Rev. B **54**, 5495 (1996)

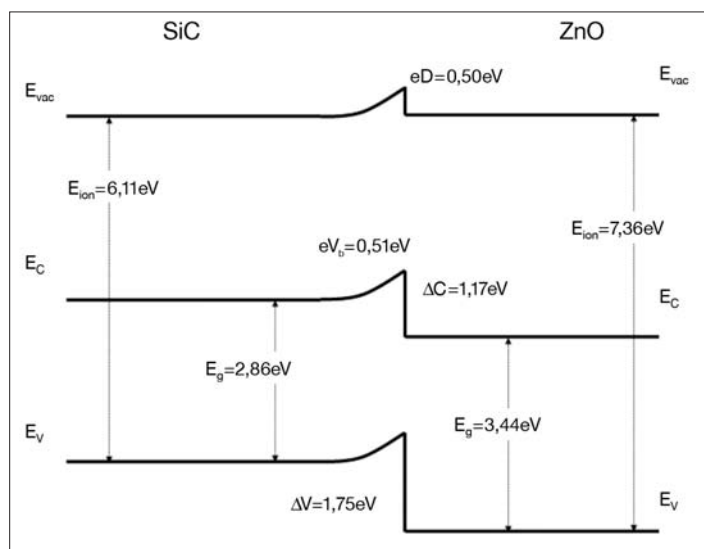


**Fig. 3:** Band alignment of the ZnO(0001)/SiC(0001) interface as determined from the photoemission spectra (cf. Fig. 2)

**Corresponding author:**  
C. Pettenkofer  
pettenkofer@hmi.de

# HMI – Scientific Departments



1. Edition  
June 2006

**Annual Report 2005**  
**Selected Results**  
**HMI-B 608**

**Published by**

Hahn-Meitner-Institut Berlin GmbH  
Glienicke Str. 100  
14109 Berlin  
Germany

[info@hmi.de](mailto:info@hmi.de)

<http://www.hmi.de>

Phone: (+49) (0) 30-8062-0

Fax: (+49) (0) 30-8062-2181

Member of the Helmholtz Association

**Concept and Coordinating Editor**

Dr. Paul Piwnicki

[piwnicki@hmi.de](mailto:piwnicki@hmi.de)

**Coordination Solar Energy**

Erik Zürn

[erik.zuern@hmi.de](mailto:erik.zuern@hmi.de)

**Book Design**

Frenkelson Werbeagentur, Potsdam

[www.frenkelson.de](http://www.frenkelson.de)

**Printing**

Druckerei Format, Berlin

[www.formatdruck.de](http://www.formatdruck.de)

© 2006 Hahn-Meitner-Institut

